R.L. Myklebust
National Bureau of Standards

ELECTRON PROBE ANALYSIS

SOCIETY of AMERICA

THIRD NATIONAL CONFERENCE

on

ELECTRON MICROPROBE ANALYSIS

CHICAGO, ILLINOIS

JULY 31—AUGUST 2, 1968

THIRD NATIONAL CONFERENCE ON ELECTRON MICROPROBE ANALYSIS

PRESENTED BY

THE ELECTRON PROBE ANALYSIS SOCIETY OF AMERICA

JULY 31 THROUGH AUGUST 2, 1968

PICK-CONGRESS HOTEL

CHICAGO, ILLINOIS

THE ELECTRON PROBE ANALYSIS SOCIETY OF AMERICA

INCORPORATED ON JANUARY 1, 1968

— NATIONAL OFFICERS - 1968 —

PRESIDENT

L. S. Birks
Naval Research Laboratory

PRESIDENT-ELECT

K. F. J. Heinrich
National Bureau of Standards

SECRETARY

T. O. Ziebold
Massachusetts Institute of Technology

TREASURER

A. A. Chodos
California Institute of Technology

MEMBER AT LARGE (3 YEARS)

H. Yakowitz
National Bureau of Standards

MEMBER AT LARGE (2 YEARS)

C. A. Andersen
Applied Research Laboratories

MEMBER AT LARGE (1 YEAR)

S. H. Moll
Advanced Metals Research Corp.

THE ELECTRON PROBE ANALYSIS SOCIETY OF AMERICA

— SUSTAINING MEMBERS —

Applied Research Laboratories
Glendale, California

Consolidated Electrodynamics Corporation
Monrovia, California

Corning Glass Works
Corning, New York

Engis Equipment Company
Morton Grove, Illinois

Materials Analysis Company
Palo Alto, California

Perkin-Elmer Corporation
Norwalk, Connecticut

Philips Electronic Instruments
Mount Vernon, New York

THIRD NATIONAL CONFERENCE ON ELECTRON MICROPROBE ANALYSIS

— INVITED SPEAKERS —

New Methods and Instrumentation

K. F. J. HEINRICH

National Bureau of Standards
Washington, D. C.

Quantitative Analysis and the Principles of Electron Scattering and X-ray Generation

S. J. B. REED

British Museum of Natural History
London, England

Data Collection and Evaluation

T. O. ZIEBOLD

Massachusetts Institute of Technology
Cambridge, Massachusetts

THIRD NATIONAL CONFERENCE ON ELECTRON MICROPROBE ANALYSIS

—GENERAL PROGRAM—

TUESDAY, JULY 30, 1968

5:00 p.m.	Registration in the Rendezvous East Room until 9:00 p.m.
5:00	Exhibits open in the Rendezvous Room.

WEDNESDAY, JULY 31, 1968

8:00 a.m.	Registration in the Rendezvous East Room.
8:50	Conference opening by General Chairman, J. V. Smith.
9:00	Address by EPASA President, L. S. Birks.
9:20	Invited paper by S. J. B. Reed.
10:20	Technical session: Quantitative Electron Microprobe Analysis.
2:20 p.m.	Technical session: Metallurgical Research.
5:00	EPASA Business meeting: L. S. Birks presiding.
6:30	Reception in the Gold Room.

THURSDAY, AUGUST 1, 1968

9:00 a.m.	Invited paper by K. F. J. Heinrich.
10:00	Technical session: New Methods and Instrumentation.
1:50 p.m.	Technical session: Scanning Electron Microscopy.
3:30	Technical session: The Ion Microprobe Analyzer.
4:30	Technical session: Soft X-ray Emission and Microanalysis.
7:30	Banquet in the Gold Room.

FRIDAY, AUGUST 2, 1968

9:00 a.m.	Invited paper by T. O. Ziebold.
10:00	Technical session: Data Collection and Evaluation.
12:45 p.m.	Technical session: Microanalysis of Glasses, Semiconductors, Nuclear Materials, Papers and Paints.
2:40	Technical session: Biological and Geological Research.
5:00	Technical session: Report by Probe User Groups.
5:40	Conference closing.

THIRD NATIONAL CONFERENCE ON ELECTRON MICROPROBE ANALYSIS

— ACKNOWLEDGEMENT —

In addition to the committee chairmen, many other persons and organizations helped in the planning of this Conference. It is only through the tireless efforts and dedication of Miss Lynna Bamberger that these transactions have been completed. She has helped with the Conference organization in so many ways that it is not possible to enumerate them here.

The University of Chicago, The Dow Chemical Company and Illinois Institute of Technology Research Institute have provided considerable encouragement and support for the Conference by permitting members of their organizations to spend considerable time in Conference planning.

The following organizations, through financial support, made it possible for several distinguished foreign scientists to attend the Conference: Argonne National Laboratory, Bendix, Consolidated Electrodynamics Corporation, Ford Motor Company, Inland Steel, International Business Machines, Mobil Oil Research and Development Corporation and the University of Iowa.

The exhibitors, listed elsewhere, through their payments for exhibition space, provided financial support for the Conference. Funds for the coffee breaks were provided by JEOLCO, Philips Electronic Instruments, Siemens America, Perkin-Elmer and Princeton Gamma-Tech.

We must thank all the members of the Midwest Electron Probe Users Group for their enthusiastic support and assistance. In particular, thanks are due the Steering Committee of that group which served as the Organizing Committee for the National Conference: D. Beaman, F. Borile, H. Diehl, E. Eichen, C. Hudgens, M. Ingram, C. Knowles, J. Lenke, B. Ostrofsky and T. Schreiber.

Last of all and certainly not least, we must acknowledge the advice and assistance provided by the organizers of the Second National Conference without which our task would have been considerably more difficult. We are particularly indebted to Dr. T. O. Ziebold.

THIRD NATIONAL CONFERENCE ON ELECTRON MICROPROBE ANALYSIS

— CONFERENCE ORGANIZERS —

GENERAL CHAIRMAN . . . . J. V. SMITH, University of Chicago

ARRANGEMENTS CHAIRMAN . . C. R. KNOWLES, University of Chicago*

PROGRAM CHAIRMAN . . . . D. R. BEAMAN, The Dow Chemical Company

The committees were made up of members of the Midwest Electron Probe Users Group.

Hotel	J. W. Lenke
Exhibitors	B. Ostrofsky
Audio-Visual . . .	D. O'Boyle
Registration . . .	G. Hallerman
Entertainment . .	J. Isasi
Ladies Program . .	M. Hallerman
Signs	M. J. Ingram
Public Relations .	E. Eichen
Secretary	H. A. Diehl
Transactions . . .	D. R. Beaman

TRANSACTIONS COMMITTEES

F. Borile (chairman)	E. Bottkol, E. Eichen, T. P. Schreiber, N. Stalica
C. Hudgens (chairman) . . .	E. Glover, L. Gray, J. Isasi, T. P. Schreiber
M. J. Ingram (chairman) . .	H. Diehl, A. Hogben
C. Knowles (chairman) . . .	A. Ganguli, E. Glover, J. V. Smith
T. P. Schreiber (chairman) .	L. Gray, D. O'Boyle, D. Solum

TYPING

L. Bamberger (chairman) . .	S. Dunham, C. Gestwicki, D. Hathaway, I. Henry, V. Thompson, E. Wagner

* Now at the M. D. Anderson Hospital and Tumor Institute

THIRD NATIONAL CONFERENCE ON ELECTRON MICROPROBE ANALYSIS

— PROGRAM —

TUESDAY, JULY 30

5:00 p.m. Registration begins in the Rendezvous East Room and will continue until 9:00 p.m.

5:00 Exhibits open in the Rendezvous Room. There will be fourteen exhibits.

8:30 Executive Committee of the Electron Probe Analysis Society of America meets in the Shelby Room.

WEDNESDAY, JULY 31

8:00 a.m. Registration in the Rendezvous East Room.

All technical presentations will be held in the Great Hall.

8:50 Welcome by General Chairman, J. V. Smith.

9:00 Address by the President of the Electron Probe Analysis Society of America, L. S. Birks.

9:20 INVITED PAPER BY S. J. B. REED

Quantitative Analysis and the Principles of Electron Scattering and X-ray Generation

TECHNICAL SESSION

Quantitative Electron Microprobe Analysis
Chairman D. R. Beaman

10:20 Quantitative Microanalysis of Intermetallic Compounds; J. A. Belk.

10:40 Estimation of Detection Limits in Electron Probe Microanalysis; H. S. de Ben.

11:00 Absorption Correction in Quantitative Microanalysis of Refractory Metal Carbides; L. J. Gray.

11:20	Interpretation of Thin Film Microanalysis Data From an Electron Microscope-Microprobe; G. Judd and G. S. Ansell.
11:40	The Effect of Microstructure and Intensity Correction Factors on the Use of Multiphase Alloys as Calibration Standards; S. H. Moll and G. W. Bruno.
12:00	A Computer Program for Electron Probe Microanalysis in the Fields of Metallurgy and Geology; J. I. Goldstein.
12:20 p.m.	A Computer Program with Simplified Input to Convert Microprobe Relative Intensity to Alloy Composition; L. R. Woodyatt and R. J. Henry.
12:40	Lunch
12:45	Luncheon meeting of representatives from seven users groups to discuss affiliation with the National Society in the Shelby Room.

TECHNICAL SESSION

Metallurgical Research with the Electron Microprobe
Chairman T. P. Schreiber

2:20	The Use of the Electron Probe in Corrosion Research; A. P. von Rosenstiel and P. J. Berg.
2:40	Electron Probe Microanalysis of Inhomogeneities in Some Aluminum Alloys; W. A. Sipes.
3:00	Microprobe Investigation of Tin Plate Surface Defects; H. Nikkel and J. W. Lodge.
3:20	Coffee break sponsored by JEOLCO.
3:40	Diffusion of Copper in Beta Titanium; O. Caloni, A. Ferrari and P. Strocchi.
4:00	Electron Microprobe Analysis of Nickel-Iron-Cobalt Thin Film Wire Memory Elements; A. A. Chodos.
4:20	Enhanced Diffusion During Low Temperature Fatigue; W. L. Bradley and M. A. Wilkov.
4:40	Determination of the Solid Solubility of Mercury in Aluminum; D. R. Beaman.

5:00 BUSINESS MEETING

The Electron Probe Analysis Society of America
L. S. Birks presiding

6:30 RECEPTION

Gold Room

THURSDAY, AUGUST 1

8:00 a.m. Registration in the Rendezvous East Room.

9:00 INVITED PAPER BY K. F. J. HEINRICH

New Methods and Instrumentation

TECHNICAL SESSION

New Methods and Instrumentation in Electron Microprobe Analysis
Chairman C. R. Hudgens

10:00 Electron Probe Multicolor Scanning Images; J. F. Ficca, Jr.

10:20 Composite Microprobe Scanning Images in Color; H. Yakowitz, K. F. J. Heinrich and D. L. Vieth.

10:40 Stabilization of Gain Shift in Proportional Counters; W. T. Kane.

11:00 A Combined Scanning Electron Microscope-Microprobe Analyzer; V. G. Macres, O. Preston, N. C. Yew and R. Buchanan.

11:20 Reduction of Contamination Effects in Electron Microprobe Analysis; H. Neuhaus.

11:40 The "ELMISONDE" a Universal Combination of Electron Probe, Scanning Electron Microscope and High Resolution Transmission Electron Microscope; K. Toegel and J. Hellgardt.

12:00 A New Quantitative Phase Analyzer; M. Tong, C. Conty and R. Lewis.

12:20 p.m. Lunch

12:25 Luncheon meeting for authors, invited speakers and session chairmen in the Plaza Room.

TECHNICAL SESSION

Scanning Electron Microscopy
Chairman P. Lublin

1:50 High Resolution Cathodoluminescence with the Scanning Electron Microscope; L. H. Pruden, E. J. Korda, D. P. Smith and J. P. Williams.

2:10 Detection of Secondary Electrons with a Channel Electron Multiplier; P. S. Ong.

2:30 Improved Microprobe Performance Through a New Scanning Display System; W. Morris, E. Lifshin and R. Bolon.

2:50 Metallography with the Scanning Electron Microscope; O. Johari, J. W. Lenke, I. Corvin and R. F. Dragen.

3:10 Coffee break sponsored by Philips Electronic Instruments.

TECHNICAL SESSION

The Ion Microprobe Analyzer
Chairman E. Eichen

3:30 New Developments in the Ion Microprobe Mass Analyzer; C. F. Robinson, H. J. Liebl and C. A. Andersen.

3:50 Progress in Analytic Methods for the Ion Microprobe Mass Analyzer; C. A. Andersen.

4:10 A Secondary Ion Emission Microanalyzer; J. M. Rouberol, J. Guernet, P. Deschamps, J. P. Dagnot, J. M. Guyon de la Berge and C. M. Judson.

TECHNICAL SESSION

Soft X-ray Emission and Microanalysis
Chairman F. Borile

4:30 Thin Film and Light Element Analysis; I. B. Borovskii.

4:50 Beryllium Determination in Microprobe Analysis; S. Kimoto, H. Hashimoto and H. Uchiyama.

5:10 The Use of Blazed Gratings in the Electron Microprobe; J. B. Nicholson.

5:30 Improvement of the "Built-up Analyzing Crystal"; H. Okano, K. Hara and T. Tomura.

6:00 Bar facilities set up in the Gold Room Foyer.

7:00 BANQUET

Gold Room

FRIDAY, AUGUST 2

8:00 a.m. Registration in the Rendezvous East Room.

9:00 INVITED PAPER BY T. O. ZIEBOLD

Data Collection and Evaluation

TECHNICAL SESSION

Data Collection and Evaluation
Chairman B. Ostrofsky

10:00 Correction for Coincidence Losses and Determination of Deadtime in the Electron Probe X-ray Microanalyzer; F. Borile, M. A. Short and J. Tabock.

10:20 A Statistical Evaluation of the X-ray Intensity Measurements from an Electron Microprobe Analyzer; J. P. Smith and J. E. Pedigo.

10:40 Further Studies on Mechanism of Gain Shift in Flow Proportional Counters; N. Spielberg.

11:00 Additional Diffracting Planes in EDDT Crystals; R. D. Wantman and G. A. Hutchins.

11:20 Lunch

TECHNICAL SESSION

Electron Probe Microanalysis of Glasses, Semiconductors, Nuclear Materials, Papers and Paints
Chairman C. R. Knowles

12:45 p.m. Electron Probe Microanalysis of Paper and Paint Films; J. F. Ficca, Jr.

1:05 Electron Beam Microprobe Technique to Measure Phosphosilicate Glass Thickness and Composition; J. J. Gniewek and N. G. Koopman.

1:25 Cathodoluminescence as a Routine Analytical Method for the Semiconductor Industry; J. P. Smith.

1:45 Distribution of Plutonium and Uranium in a Mixed Oxide Fuel Irradiated in a Fast Neutron Flux; N. R. Stalica and C. A. Seils.

2:05 Electron Probe Microanalysis of Alkali Metals in Glasses; L. F. Vassamillet and V. E. Caldwell.

2:25 Coffee break sponsored by Siemens America.

TECHNICAL SESSION

Biological and Geological Research with the Electron Microprobe
Chairman A. Hogben

2:40 New Applications of Electron Microprobe Analysis in Renal Pathology; P. Galle, J. P. Berry and J. Stuve.

3:00 Observations on Human Blood Cells; K. G. Carroll and J. L. Tullis.

3:20 An Electron Probe and Electron Microscope Investigation of Asbestos Bodies in Lung Sputum; A. P. von Rosenstiel and H. B. Zeedijk.

3:40 Electron Microprobe Analysis of the Silver Amalgam--Tooth Interface; S. H. Y. Wei and M. J. Ingram.

4:00 A Study of High Temperature Reactions in Strontium Zirconate by Cathodoluminescence; N. A. Richard and D. I. Phalen.

4:20 New Data on Natural Phases in the System Ag-Te; E. F. Stumpfl and J. Rucklidge.

4:40 Quantitative Analysis with a Newly Designed Electron Probe; F. W. Warnaars.

TECHNICAL SESSION

Reports by Probe User Groups
Chairman J. Lenke

5:00 Report on the Activities of the New York Metropolitan Probe Users Group; H. Schreiber, Jr. and G. L. Fisher.

5:20 Report on the Activities of the Midwest Electron Probe Users Group; D. R. Beaman and T. P. Schreiber.

5:40 Closing remarks by J. V. Smith.

Conference closes.

THIRD NATIONAL CONFERENCE ON ELECTRON MICROPROBE ANALYSIS

— LIST OF EXHIBITORS —

Applied Research Laboratories, P. O. Box 1710, Glendale, California 91209.

Buehler, Ltd., 2120 Greenwood Street, P. O. Box 830, Evanston, Illinois 60204.

Consolidated Electrodynamics Corporation, 1500 S. Shamrock, Monrovia, California 91017.

Engis Equipment Company, 8035 Austin Avenue, Morton Grove, Illinois 60063.

The Harshaw Chemical Company, 1945 E. 97th Street, Cleveland, Ohio 44106.

Isomet Corporation, 433 Commercial Avenue, Palisades Park, New Jersey 07650.

Jarrell-Ash Company, 590 Lincoln Street at Route 128, Waltham, Massachusetts 02154.

JEOLCO (U.S.A.), Inc., 477 Riverside Avenue, Medford, Massachusetts 02155.

Materials Analysis Company, 1060 East Meadow Circle, Palo Alto, California 94303.

Ortec, Inc., 100 Midland Road, Oak Ridge, Tennessee 37830.

The Perkin-Elmer Corp., Norwalk, Connecticut 06852.

Philips Electronic Instruments, 750 South Fulton Avenue, Mount Vernon, New York 10550.

Princeton Gamma-Tech., Inc., Box 641, Princeton, New Jersey.

Siemens America, Inc., Empire State Building, 350 Fifth Avenue, New York, New York 10001.

SUMMARIES
OF
PAPERS

An index of authors and their affiliations follows these papers.

QUANTITATIVE MICROANALYSIS OF INTERMETALLIC COMPOUNDS

J. A. BELK

Intermetallic compounds have been studied as the chances of getting large concentrations homogeneously distributed are much greater than with solid solutions. Two particular compounds were chosen and analysed in a completely different schedule. One was investigated in detail in one laboratory under various experimental conditions and using both K and L radiation for one of the elements. The other was circulated to a series of fourteen laboratories for a comparative study of quantitative analyses. As nine of the laboratories had substantially similar instruments it was possible to compare data at all stages including the choice of correction procedures.

A copper zirconium compound was studied in detail both because its composition was in some doubt and because Zr K_α and Zr L_α radiation could be used. The atomic number correction is similar for both radiations but the absorption correction very different. Experimental determinations were made at various accelerating voltages. A number of different correction procedures were used, the Philibert formula for absorption with the σ modified by Duncumb and other workers being used together with atomic number corrections based on the work of Bethe, Duncumb and Shields and Belk. The effectiveness of the various combinations of corrections in covering all the accelerating voltages and wavelengths is displayed and discussed, and the importance of choice of mass absorption coefficients indicated. The compound is identified as Cu_3Zr with a slight departure from stoichiometry.

The specimen that was circulated was nominally $FeAl_3$ and it was analyzed by fourteen laboratories at three specified accelerating voltages. For uniformity and ease of comparison of results a set of mass absorption coefficients due to Heinrich was used.

The results are tabulated as count ratios, correction factors and corrected results obtained at the three different voltages. Mean value and standard deviation are quoted for each comparable set of values and in the case of the corrected results an overall mean and standard deviation for all results is included.

The count ratios for aluminium decrease with increasing accelerating voltage and the corrected results exhibit the same trend, whereas the iron results vary in the opposite way. For the nine laboratories using the same instrument it is possible to analyze the relationship between the count ratios, correction factors and corrected results. The standard deviation of the count ratios expressed as a percentage relative scatter was 4.8 and the variation in the correction factors expressed in the same way is 7.3. If there had been a

random combination of experimental results and correction factors this would have led to a final relative scatter of 8.75 in the corrected results. The actual scatter was 6.2 clearly indicating a selection of suitable correction factors for the various experimental results.

Finally the average experimental count ratios from the nine similar instruments were taken as the best experimental values and these were corrected by the various methods outlined for the copper-zirconium compound. The importance of a suitable choice of mass absorption coefficients and absorption and atomic number correction procedures is obvious for the aluminium results. The iron results are much less sensitive to correction parameters.

In conclusion it is found that the formula

$$\sigma = \frac{5.28 \times 10^5}{E_o^{1.7} - E_c^{1.7}}$$

compensates well for variations in accelerating voltage and that this combined with an atomic number correction based on Bethe's formula with the mean ionization potential proportional to the atomic number and the Heinrich mass absorption coefficients gives the most satisfactory results.

SUMMARY OF RESULTS

Standard deviations given in parenthesis.

COUNT RATIOS
Microscans - 9 instruments

	15 kV	20 kV	25 kV
Al	.373 (.013)	.296 (.015)	.242 (.014)
Fe	.357 (.017)	.359 (.011)	.371 (.017)

A.E.I. S.E.M. 2 - 3 instruments

	15 kV	20 kV	25 kV
Al	.414 (.017)	.344 (.011)	.303 (.021)
Fe	.373 (.002)	.377 (.008)	.383 (.016)

CORRECTION FACTORS
Microscans

	15 kV	20 kV	25 kV
Al	1.691 (.118)	2.045 (.164)	2.461 (.171)
Fe	1.045 (.053)	1.042 (.056)	1.063 (.051)

A.E.I. S.E.M. 2

	15 kV	20 kV	25 kV
Al	1.486 (.091)	1.754 (.100)	2.055 (.088)
Fe	1.025 (.036)	1.027 (.033)	1.031 (.034)

CORRECTED RESULTS

	15 kV	20 kV	25 kV
Al	.640 (.036)	.626 (.040)	.612 (.040)
Fe	.372 (.025)	.371 (.013)	.384 (.018)

Chemical Analysis: - Al 61.3 wt%
Fe 38.6 wt%

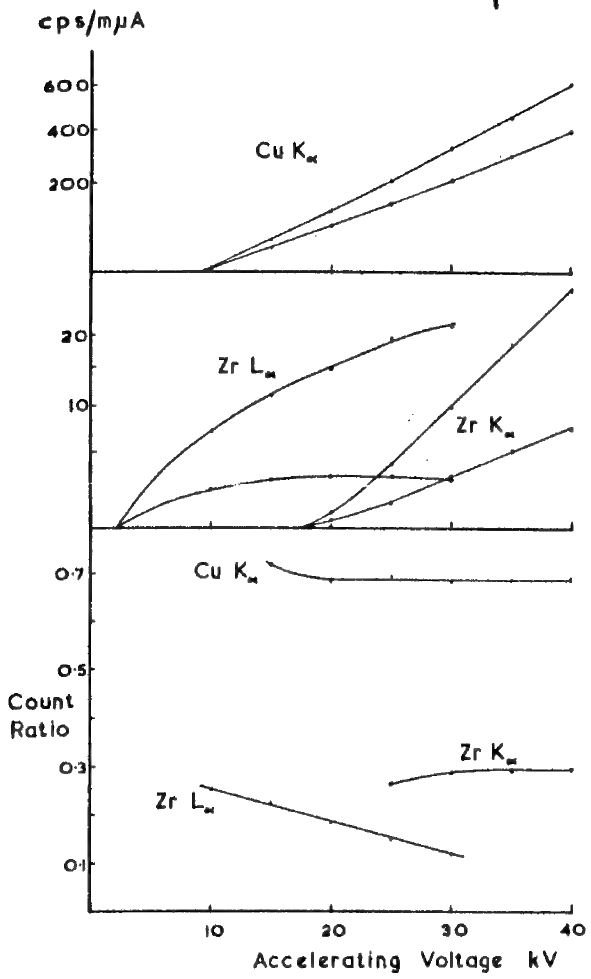

Fig. 1. X-ray intensities from standards and alloys and count ratios all vs. accelerating voltage for copper zirconium compound.

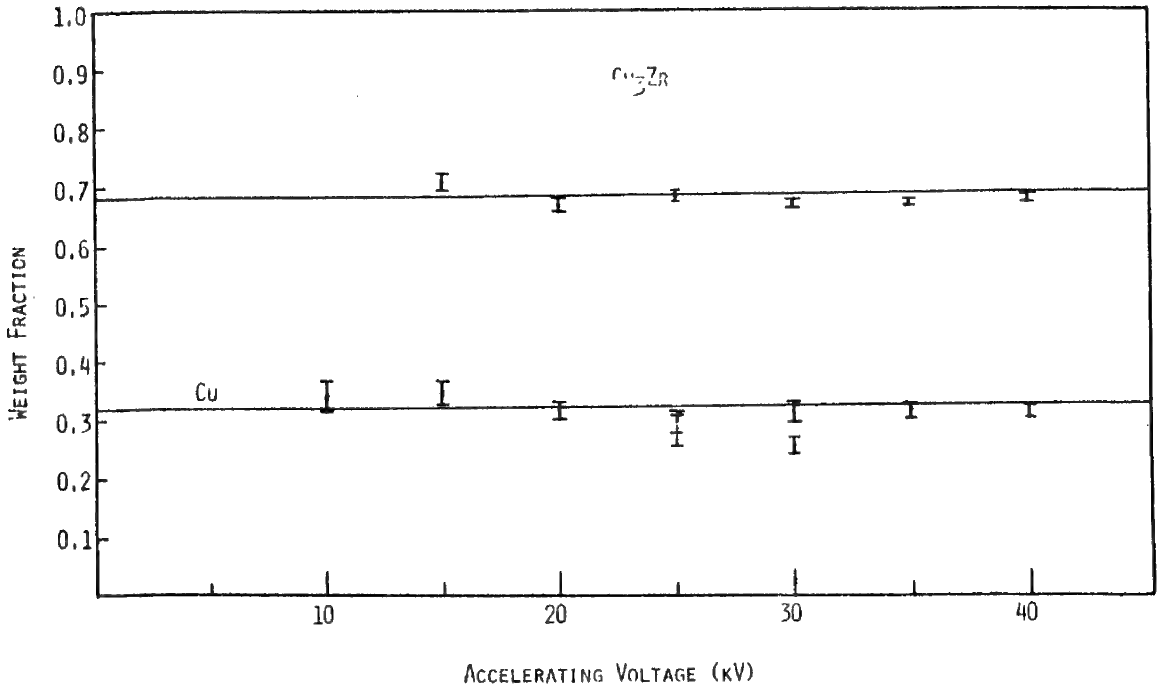

Fig. 2. Corrected quantitative analyses on copper zirconium compound.

ESTIMATION OF DETECTION LIMITS IN ELECTRON PROBE MICROANALYSIS

H. C. de Ben

The measurement of trace quantities of one element in another on a microscopic spatial scale has become increasingly important. However, there are few published experimental results on electron probe detection limits. It was therefore decided to measure detection limits of several different elements in a variety of matrices using a constant accelerating potential of 30 kV and normal operating conditions. A Philips electron probe was used with the usual continuously bent mica crystal spectrometer.

The method involved measuring the intensity from a certified standard of low but known content of the element of interest and relating it to the detection limit by a linear extrapolation to the weight fraction corresponding to the minimum statistically significant net intensity above background. This statement is embodied in Equation 15 of Reference 1 which orginated with Theisen(2).

Alloy standards were selected which would lead most efficaciously to a mapping of detection limits for a wide spread of excited and matrix elements. Each alloy generally contained a small percentage of one or more of the elements to be measured in the matrix of interest.

The detector electronics were operated in the integral mode. Each intensity was determined by five measurements of 20 seconds each. Background was obtained on a pure element standard of the matrix element without disturbing the spectrometer. To average out the effects of sample inhomogeneity, the beam was scanned in a line 200 microns long and parallel to the spectrometer axis while measuring intensities from the alloy standards. Other intensity measurements were made with a stationary beam. The two methods were shown to give comparable results.

The average background counts, $\bar{N}_b$, and alloy standard counts, $\bar{N}_s$, were first normalized to 0.1μa beam current. The weight fraction detection limit, C_{DL}, was then calculated from the relation:

$$C_{DL} = \frac{1.47 \sqrt{\bar{N}_b}}{\bar{N}_s - \bar{N}_b} C_s$$

where C_s is the weight fraction of the excited element in the alloy standards. This value of C_{DL} represents the minimum detectable weight fraction to be

expected with greater than 80% confidence where random photon fluctuations are the only deviations from the mean and where the beam current is 0.1μa. This definition is one which assures that all the data are consistent.

The values of C_{DL} thus obtained from $K\alpha_1$ and $L\alpha_1$ lines were plotted vs. the matrix atomic numbers Z_B separately on logarithmic graphs (Figs. 1 and 2). The curves were obtained after first smoothing the points with straight lines on a C_{DL} versus Z_B^3 graph. The justification for this is traced to the fact that absorption in the matrix is the overwhelming influence on C_{DL}.

The experimental standard deviations for $\bar{N}_s$ and $\bar{N}_b$ varied from 1 to 10 percent and compared well with the theoretical values $\bar{N}_s^{-\frac{1}{2}}$ and $\bar{N}_b^{-\frac{1}{2}}$ with a few exceptions in the case of $\bar{N}_s$. The main reason for these exceptions was shown to be nonuniformity in the distributions of certain excited elements.

The experimental points were used to establish contours of constant C_{DL} on a logarithmic graph of Z_B vs. the excited element atomic number, Z_A (Fig. 3). On the same graph, regions had been previously outlined which represented areas in which the relative positions of matrix absorption edge energies and excited element spectral line energies were the same. The logarithmic representation permitted these regions to be defined by nearly linear boundaries because of the power law dependence of such energies on atomic numbers (Moseley's Law).

Before this extrapolation of the results was made, two points were demonstrated. First, it was shown that C_{DL} is a continuous function of Z_A over finite intervals. (In the present case, the detection limits from different odd order reflections of mica are approximately equivalent.) Secondly, from established theoretical concepts, an analytical expression was found for an extrapolation function. This expression may be written:

$$Z_B = Z_A \left(p\, Z_A^4 + q\, Z_A^2 + r\right)^{1/3}$$

where p, q and r are constants for constant accelerating potential and C_{DL}. The author derived it by substituting into Ziebold's theoretical expression for C_{DL}(1) the known dependences of pure element intensity(3), signal-to-background ratio(4), and the Ziebold-Ogilvie empirical calibration constant(5) on excitation potential and mass absorption coefficients, on Z_A and Z_B. A more general representation of the results was thus achieved.

Although these results are strictly valid only for a Philips instrument operated under the stated conditions, they should be a useful practical guide since the conditions are those most commonly in use and the instrument has a takeoff angle (15.5°) comparable to most commercial instruments. Indeed, in the few instances where published work was performed under similar conditions(6,7), the results for C_{DL} shown here are in general agreement.

It should be emphasized that the general representation of these results as a contour map on a Z_A vs. Z_B graph may also be used for weight fraction detection limits for any set of conditions or for any instrument. In addition, it may

also be used for any variable which is a smooth function of Z_A and Z_B in finite regions. For example, the Ziebold-Ogilvie empirical calibration constant may be treated in this way by deriving an extrapolation function for it. The approach presented here thus has widespread applicability.

---

1. T. O. Ziebold, Anal. Chem., 39, 858 (1967).

2. R. Theisen, Quantitative Electron Microprobe Analysis (Springer-Verlag, New York, 1965).

3. R. Castaing, "Electron Probe Microanalysis," in Advances in Electronic and Electron Physics (Academic Press, New York. 1960), Vol. 13, pp. 317-386.

4. L. S. Birks, R. E. Seebold, B. K. Grant and J. S. Grosso, J. Appl. Phys., 36, 699 (1965).

5. T. O. Ziebold and R. E. Ogilvie, Anal. Chem., 36, 322 (1964).

6. A. Belk and B. Clayton, "The Practical Performance of Electron Probe Microanalyzers," in Optique des Rayons X et Microanalyse (Hermann, Pairs, 1966), pp. 409-417.

7. C. A. Andersen, Brit. J. Appl. Phys., 18, 1033 (1967).

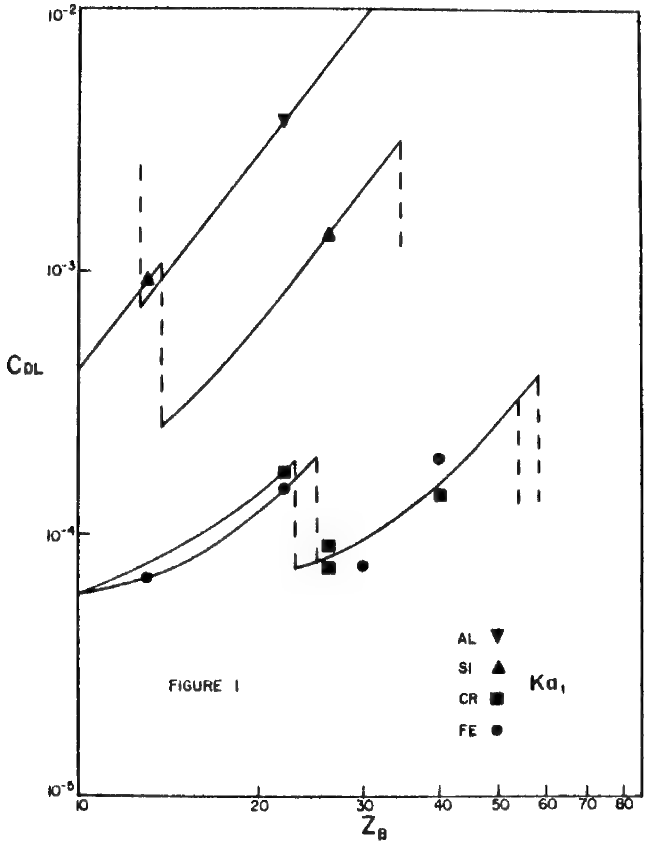

FIGURE 1

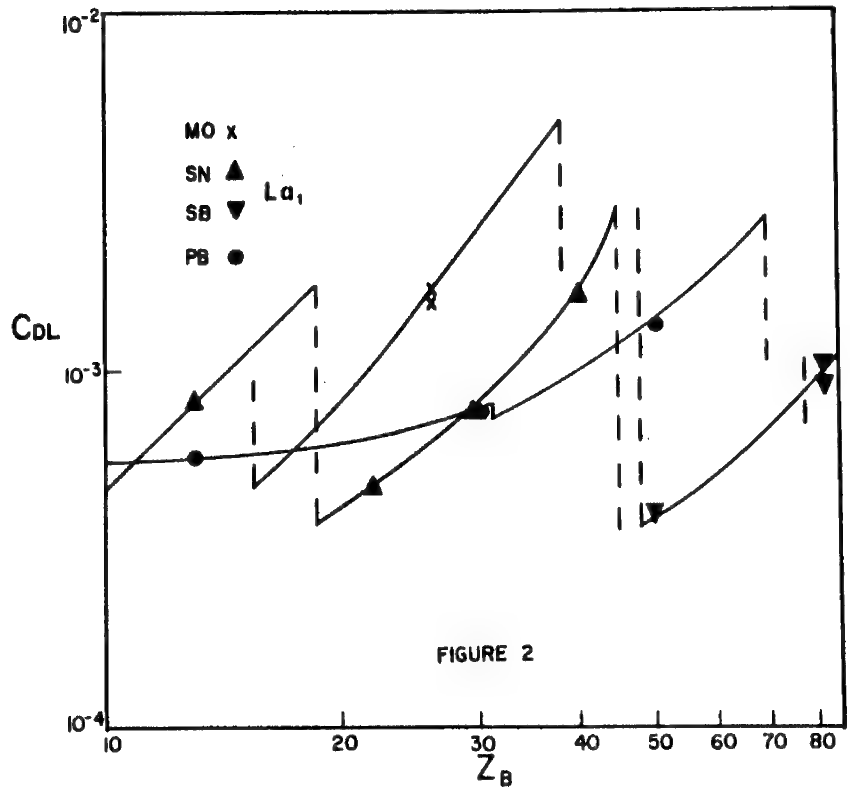

FIGURE 2

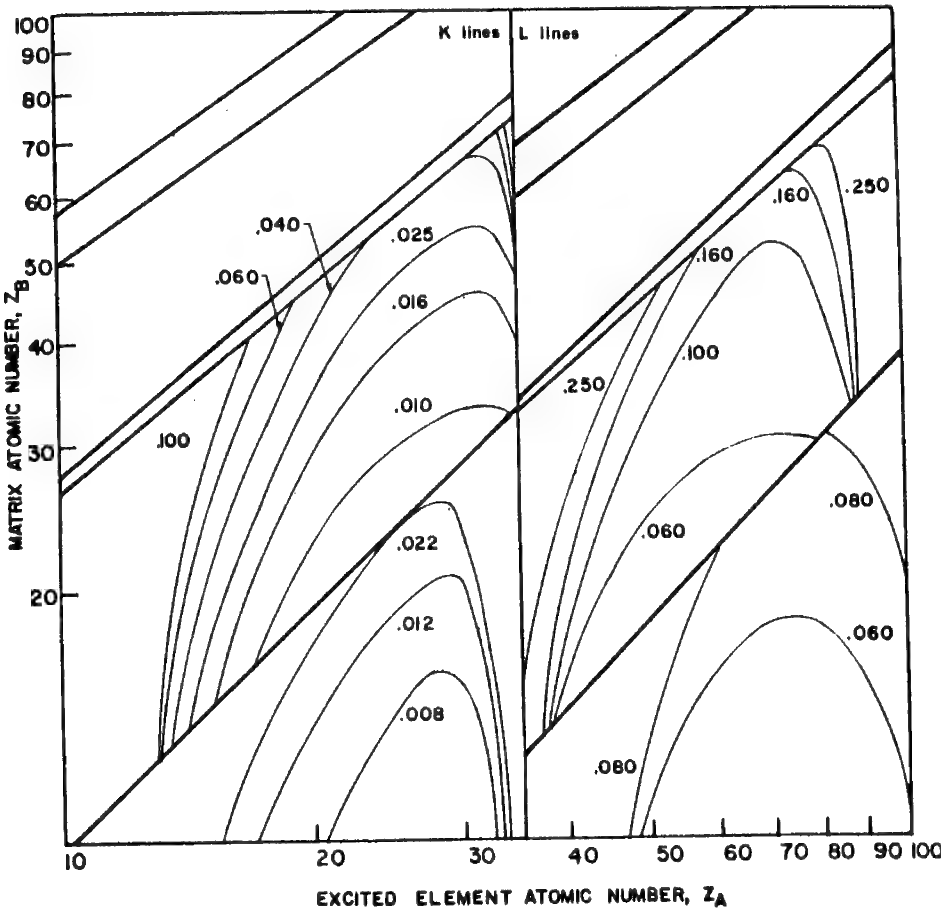

FIGURE 3

CONTOURS OF CONSTANT C_{DL} (%)

ABSORPTION CORRECTION IN QUANTITATIVE MICROANALYSIS OF REFRACTORY METAL CARBIDES

L. J. Gray

The development of large d-spacing stearate pseudocrystals and thin window proportional counters has made possible the application of electron probe x-ray microanalysis to metallurgical systems containing carbon, nitrogen and oxygen. In principle, when an analyzed phase is at or very near to a stoichiometric composition, microanalysis of carbide phases can be performed. The sample x-ray intensities would be directly compared to intensities from stoichiometric compound standards. However, accurate quantitative microanalysis of the many carbon-deficient refractory metal carbides has been hindered by a lack of available standards, that is, standards of composition less than stoichiometric, and homogeneous on a micron scale.

In an attempt to find carbon-deficient refractory metal carbides that could be used as standards, we analyzed single crystal samples of TiC_x ($x<1$) cleaved from boules grown by the Verneuil technique. In most cases, we found that the samples contained randomly distributed graphite inclusions, approximately 5 to 20 microns in diameter. It was concluded that in any given analysis, using such samples as compound standards, we could not guarantee that the electron beam excited volume did not contain at least part of a sub-surface inclusion, even though a graphite inclusion was not visible optically. Further, we were unable to find any samples of stoichiometric TiC_1. We thus discarded this attempt to do analysis by comparison to carbide compound standards.

Theoretically based correction procedures provide a second apprach to the characterization of the defect carbides. However, in the absorption correction, an obvious lack of fundamental data appeared; the mass absorption coefficients of the refractory metals for long wave lengths had not been measured. Two reasonably complete sets of tables for mass absorption coefficients by Heinrich(1) and Frazer(2) filled in gaps in experimental data by fitting data that had been obtained to a relation of the form:

$$(\mu/\rho)_z = C_z \lambda^{n_z}$$

after Leroux(3). Experimentally unavailable data was interpolated. Since both sets of tables terminate at wave lengths less than 20 Å, the question of a valid extrapolation to 45 Å arose.

Frazer gives mathematical relations for C and n as a function of atomic number while Heinrich provides a tabulation of his values. Both sets of values for the various wave length regions were plotted and graphically

extrapolated to the regions of interest. The test for applicability of the extrapolated values was the consistency of calculated absorption jump ratios, proximity of calculated mass absorption coefficients to the meager experimental data available at these long wave lengths, and correlation of the calculated absorption jump ratios and mass absorption coefficients for light elements with experimentally supported values as given by Henke et al.(4), Ogier et al.(5), and Cooke and Stewardson(6). The values for mass absorption coefficients and absorption jump ratios were tested in the analysis of the niobium sub-carbide, and tantalum oxide and sub-oxides. Several of the mass absorption coefficients obtained are listed in Table I.

It is concluded that extrapolation of mass absorption data as given by Heinrich provides reasonable values for mass absorption coefficients of the refractory metals for the long wave lengths of carbon, nitrogen and oxygen.

---

1. Heinrich, K. F. J., "X-ray Absorption Uncertainty," in The Electron Microprobe, T. D. McKinley, K. F. J. Heinrich and D. B. Wittry, eds., John Wiley and Sons, Inc., N.Y., 1966, pp. 296-377.
2. Frazer, J. Z., "A Computer Fit to Mass Absorption Coefficient Data," University of California, La Jolla, California, Report Number SIO 67-29.
3. Leroux, J., "Method of Finding Mass Absorption Coefficients by Empirical Equations and Graphs," Advances in X-ray Analysis, Vol. V, Plenum Press, New York, 1961, pp. 153-160.
4. Henke, B. L., R. L. Elgin, R. E. Lent and R. B. Ledingham, "X-ray Absorption in the 2 to 200 A Region," Air Force Office of Scientific Research Report AFOSR 67-1254, Contract AFOSR 689-64, June, 1967.
5. Ogier, W. T., G. J. Lucas and R. J. Park, "Ultra-soft X-ray Absorption Coefficients of Al, Be, O, C and F," Appl. Phys. Letters, 5, #7, pp. 146-147, 1 October 1964.
6. Cooke, B. A. and F. A. Stewardson, "The Absorption of X-rays in the Range 7 - 17 A by Be, Mg, Al, Cu and Ag," Brit. J. Appl. Phys., 15, pp. 1315-1319, 1964.

TABLE I

	Emission Wave Length		
Absorber	23.57 Å	31.68 Å	44.6 Å
Al	7800	15900	33000
Ti	10000	3900	6300
Ta	19600	20400	20440

TABLE I

SAMPLE DATA OF SILVER POWDER
EXPERIMENTAL AND CALCULATION SETS

Radius (Arbitrary Units)	Voltage kV	Characteristic Radiation Measured	Distance of Particle Center From Beam Center	I_e	I_{eN}	I_{pn}
11.7	50	$L_{\alpha}{}^{2}{}_{1}$	0.0	84	1.00	1.00
			9.5	72	.85	.84
			19.0	41	.48	.51
			24.0	27	.32	.33
			38.2	7	.08	.06

I_e - Experimental Intensity cps.

I_{eN} - Normalized Experimental Intensity

I_{pN} - Normalized Predicted Intensity

THE EFFECT OF MICROSTRUCTURE AND INTENSITY CORRECTION FACTORS ON THE USE OF MULTIPHASE ALLOYS AS CALIBRATION STANDARDS

G. W. Bruno and S. H. Moll

Previous experimental work(1) has shown that under certain conditions multiphase or inhomogeneous alloys may be used as calibration standards for electron microprobe analyses. This work proposed a beam traversing technique for analyzing the average chemistry of multiphase or inhomogeneous alloys. The diameter of the incident electron beam was increased to as much as a few hundred microns by defocusing the final lens only. Two-phase or inhomogeneous alloys were systematically translated beneath the electron beam during a suitable point counting interval. The beam size and traverse path were chosen such that consecutive traverses reproduce the measured x-ray intensity within the statistical deviation of the total number of counts collected. No attempt was made to rationalize the validity of the method on a theoretical basis. It was demonstrated, simply, that the technique would yield satisfactory results experimentally.

This method was utilized to study both single and two-phase alloys of known chemistry in several binary systems. Calibration curves plotting intensity ratios as a function of concentration were constructed for each system using the single phase values only. The best curve fit to the single phase values was obtained by use of the Ziebold-Ogilvie technique(2).

A comparison (Table I) was made of the deviations of the measured intensity ratios from the smoothly fitted calibration curve of the two-phase alloys to those of the single phase alloys. This comparison clearly indicated that the two-phase alloys yielded intensity ratios which were just as precise as those obtained from the single phase alloys since no systematic deviation was observed for the two-phase values. It was concluded, therefore, that two-phase alloys could be used for calibration standards if the technique described was employed.

However, more recent data suggests that under certain conditions this technique may yield inaccurate results. These conditions are present if; 1) the calibration curve shows a very large deviation from linearity, 2) there is a very large difference in the composition of the two phases in the alloy, and 3) the alloy exhibits an extremely coarse microstructure.

These conditions are present, for example, when the microprobe is used to determine Sn concentrations in the Pb-Sn system. The SnL_{α} calibration curve (Fig. 1) shows a large negative deviation from linearity. The two phases present are primary Pb and primary Sn, and the microstructure may be quite coarse depending upon the thermal history.

A COMPUTER PROGRAM FOR ELECTRON PROBE MICROANALYSIS IN THE FIELDS OF METALLURGY AND GEOLOGY

J. I. Goldstein

A comprehensive computer program has been written which should prove useful to investigators in both the fields of metallurgy and geology. The program is flexible in both input and output and is relatively easy for an inexperienced person to use. It is written in the Fortran language and can be used in the time sharing mode which is now available in many laboratories. The program is built up of a large number of subroutines which can be easily changed as the user sees fit or as new correction schemes become available. At present the following corrections are incorporated; the absorption correction of Philibert-Duncumb(1,2) recently modified by Heinrich(3), and atomic number correction of Duncumb and Reed(4) and the fluorescence correction of Reed(5). Both K and L x-radiation are considered and the program will operate in either of two modes; conversion of raw intensity data to composition using an iterative procedure or conversion of compositional data to expected x-ray intensities. For problems in geology involving oxides, calculations are made with oxygen considered as a matrix element. Specimens and complex standards each containing up to nine elements can be treated and several standards can be used for each element measured to check the consistency of the answer. Also characteristic lines of elements in a sample measured at different probe accelerating potentials can be handled.

The program is rather unique with respect to the method of data handling and ease of operation. All the critical data for a given element, such as x-ray wave lengths, fluorescent yields, atomic weights, absorption edge jump ratios and the necessary factors for the calculation of absorption coefficients from Heinrich(6) for that element are stored on cards. These data are then used as needed for the elements under consideration in each problem. The compositional data for each of the standards available to the probe user are also placed on cards to be used when needed. The input data which specifies the problem of interest then requires a minimum of information, for example the take-off angle, deadtime for each spectrometer, operating voltage, calculation mode and the elements which are measured on each spectrometer. Even this input data can be supplied in a non-rigid format.

The program determines internally whether a fluorescence correction is necessary and calculates the initial intensity ratios. An exhaustive print out of the various correction factors can be obtained if desired along with approximate error limits for each of the calculated data points.

---

1. Philibert, J., Third International Conference on X-ray Optics and Microanalysis (Stanford, 1962), Academic Press, N.Y., 1964, p. 379.

2. Duncumb, P. and Shields,P. K., The Electron Microprobe, McKinley et al. (eds.), Wiley and Sons, N.Y., 1966.

3. Heinrich, K. F. J., "The Absorption Correction Model for Microprobe Analysis," presented at the Second National Conference on Electron Microprobe Analysis, Boston, 1967.

4. Duncumb, P. and Reed, S. J. B., presented at the Symposium on Quantitative Electron Probe Microanalysis, National Bureau of Standards, Washington, D. C., 1967.

5. Reed, S. J. B., Brit. J. Appl. Phys. 16, 1965, p. 913.

6. Heinrich, K. F. J., "X-ray Absorption Uncertainty" in The Electron Microprobe.

A COMPUTER PROGRAM WITH SIMPLIFIED INPUT TO CONVERT MICROPROBE RELATIVE INTENSITY TO ALLOY COMPOSITION

L. R. Woodyatt and R. J. Henry

A computer program with a simplified input procedure has been written in Fortran IV to convert the microprobe relative x-ray intensities to actual chemical compositions. The data may be corrected as desired for detector deadtime, electron backscatter and ionization (atomic number effects), x-ray absorption and secondary fluorescence as outlined below. The computer program was written in a general fashion so that it can be used with data from any microprobe and with any computer. A significant innovation in the program is that all the correction constants are read in only once at the beginning of the program run and are recalled whenever needed. This is particularly important when a program run consists of data from more than one specimen. In this case, the constants are entered once rather than for each specimen--a considerable saving of time. Also, these initial input cards always remain the same, hence they need to be punched only once and are retained for all future runs. With this program the only necessary input data for each analysis are the actual microprobe intensity measurements. Input data from more than one alloy can be analyzed in a single computer run.

The computer program corrections are based on accepted theoretical and empirical relationships. The specific corrections to be applied are selected by an input control card. The first step in the program is an intensity dependent detector deadtime correction which is applied to all experimental measurements. Next, if desired, the data is corrected for electron backscatter by Ziebold's method. Then, optionally, the data is corrected for x-ray absorption by Philibert's relationship as reported by Brown. Secondary fluorescence corrections are performed by choosing and applying the relationships of either Castaing, Wittry, or Birks. In addition, modifications of these basic methods, such as the Green and Cosslett over voltage correction to the Castaing relationship, have been evaluated. These secondary fluorescence relationships are developed for binary alloys and are applied to complex alloys by assuming that 1) secondary fluorescence of each element is produced by all other elements present, 2) the effects of the elements are additive, and 3) there are not tertiary or higher order interactions. The program uses an iterative procedure to refine the predictions.

The effectiveness of the correction procedures were evaluated by measurements made on 55 fifty-gram arc-melted binary and complex button alloys containing iron, chromium, tungsten, molybdenum, vanadium, and cobalt at levels approximating tool steel matrix compositions. The alloys were homogenized by hot upset forging and soaking at 2200 to 2400°F for 24 hours. All intensity measurements were obtained from one-fourth-inch diameter, metallographically prepared specimens

using a Cambridge Mark II microprobe with an operating potential of 25 kV and a counting time of 100 seconds. The specimens were mounted in mounts that were identical to those containing the standards to minimize vertical alignment distortions. For each element measurements were obtained from three areas of the alloy. Measurements were obtained on the standards before and after examining the alloy to account for electronic drift which was assumed to be linear over the short time period. The results showed that the secondary fluorescence corrections by Castaing and Wittry were the most accurate and were equally effective. The various modifications to these equations did not improve their accuracy. Significantly, the correction procedures are as accurate for complex alloys with four or five elements as they are for binary alloys as can be seen in Table I which contains the results obtained for a number of representative alloys.

TABLE 1. REPRESENTATIVE ALLOYS SHOWING COMPARISON OF CHEMICAL WITH CORRECTED COMPOSITIONS*

	Chemical Composition	Measured I/I_o	Corrected Composition	Absorption Factor	Fluorescence Ratio
V	2.03	2.89	2.10	0.697	1.018
Fe	97.97	95.80	97.90	0.997	1.002
Cr	0.92	1.43	0.96	0.655	1.015
Fe	99.18	97.50	99.04	0.999	1.001
W	4.90	3.03	5.29	0.853	2.065
Fe	95.10	96.35	94.71	0.992	1.000
Co	9.11	9.41	9.41	0.982	1.032
Fe	90.89	93.30	90.59	1.002	1.003
V	1.01	1.19	0.89	0.711	1.011
Cr	5.21	7.32	5.21	0.672	1.017
Fe	93.78	90.15	93.89	0.995	1.005
W	2.00	1.13	2.01	0.848	1.964
Co	1.91	2.03	2.17	0.976	1.033
Cr	1.80	2.34	1.67	0.661	1.016
Fe	94.29	88.73	94.15	0.996	1.002
W	4.97	3.70	5.10	0.769	1.643
Mo	4.47	3.10	5.18	1.430	1.070
Cr	4.90	6.39	4.79	0.677	1.013
V	4.66	4.89	3.88	0.717	1.014
Fe	79.2	81.82	81.05	1.430	1.009

* Using modified Philibert and Castaing corrections.

THE USE OF THE ELECTRON PROBE IN CORROSION RESEARCH

A. P. von Rosenstiel and P. J. Berg

Introduction. There is a growing tendency towards the application of modern experimental techniques in the study of corrosion processes.

Conventional exposure tests are too time consuming, and in some cases even are slower in the testing of systems than the development of new systems. Sometimes the system of material and environment is so complex that an overall description is too broad, for example, in the case of exhaust gases.

A detailed analysis of local phenomena often gives evidence of the corrosion products formed, which may lead to identification of the components engaged in the chemical reactions.

The microprobe in this connection is a powerful tool, because minimum quantities of product can be detected, because the analysis is non destructive and can be continued in the electron microscope for example, and because minimal preparation gives optimum security that the product is not influenced by preparation. A few case histories illustrate these views.

Catalytic cracking installation. A catalytic cracking installation in a petrochemical industry encountered a failure that was ascribed to thermal fatigue. X-ray microanalysis of the type 304 stainless steel, however, showed on both sides of the crack broad zones of enriched Cr content with a marked decrease of Ni and Fe concentrations. In the cracks, islands of high Ni, Fe and S content were found. Probably the sulfur in the crude oil and the high temperature during operation caused Ni - Fe sulfides to form. The matrix was locally embrittled by Cr-rich zones.

Supporting plate in an oil fired ship vessel. A 25-20 Cr-Ni supporting plate of an oil fired ship vessel failed after about 7,000 service hours. Inspection showed catastrophic corrosion. From the surface into the matrix the following corrosion zones were found: 1)very high Cr and S concentrations together with V but no Fe or Ni, 2)high Si and S, and low Fe concentration, 3)Ni + S (NiS), 4)broad zones of $Cr_{23}C_6$ in the grain boundaries of the matrix. The failure was due to improper choice of the material for the specific conditions.

Razorblades. On 13% Cr steel razorblades in the as delivered condition a gray-brown surface layer was observed, which could not be identified, neither by x-ray diffraction nor by corrosion tests. X-ray microanalysis at low acceleration voltage showed a remarkable concentration of oxygen together with a slight decrease in iron content. The chromium level did not show any distinct variation. Subsequent electron diffraction on extraction replicas showed the presence of δ-FeOOH. The layer was due to traces of material left on the surface after grinding.

Digital switch. A digital switch failed after a short inactive period. Careful optical inspection yielded the impression of an extremely thin and diffuse gray surface layer on the rigid gold contact, whereas on the slider surface, no defects could be observed. X-ray microanalysis of the gold contact at low acceleration voltage showed a fixed Ag/S relationship corresponding with Ag_2S. Microanalysis of the Neyoro slider confirmed that initially silver sulfide was formed on the slider, which was transferred to the gold surface.

Antifouling paint layer. The paint consists of 80% Cu_2O in solution in vinyl resin and colophonium, and is fixed on red-lead. The antifouling properties are based on the poisonous effect of copper on organisms in sea water. After using this paint on ship skins, the copper goes into solution and is consumed by the organisms. After some time the layer has lost all copper and a thin gold-brown layer has formed on the surface.

The investigation showed: 1) the interpenetration of the Cu_2O paint in the red-lead, 2) between the Cu_2O-layer and the outer surface a high concentration of Cl and S, 3) the surface layer, which also has antifouling properties, consists for a great part of Fe, Cl and Ca.

Scanning indicated the surface consists of isolated areas of iron-oxide with Ca and Cl. Between these areas, where the spot has a greater penetration into the pure vinyl-resin, the underlaying copper rich layer was detected.

Precipitation and oxidation of Kunifer 10. The iron-modified Kunifer 10 in annealed condition has good resistance against impingement attack in sea water circuits. Hot-bending or welding may influence this resistance in the following ways. 1) Precipitation. The iron-content in the matrix is reduced by formation of iron rich precipitates. The analysis of this precipitate showed an iron-content of about 17%, 2) Oxidation. The oxide consists of three layers: an outer scale of pure CuO and two inner scales which consist of internal oxides of Ni and Fe. The brittle outer scale chips off. The surface in contact with sea water consists then of oxides of Fe and Ni and a strongly reduced Cu-concentration.

ELECTRON PROBE MICROANALYSIS OF INHOMOGENEITIES IN SOME ALUMINUM ALLOYS

W. A. Sipes

This electron probe investigation was part of an effort to evaluate causes for the deterioration and failure of aircraft components. In aluminum alloys, especially the high strength Al-Zn-Mg types, the mechanical properties (anisotropic behavior, etc.) relate to the degree of their homogeneity. This in turn is a function of differences, not only in their copper and iron content, but also in regard to the relative amounts of solute present.(1) Results of this study demonstrate that electron probe microanalysis can reinforce, if not replace, the often inadequate techniques of the classical metallographic approach. Even the cursory qualitative results of this study contributed to the solution of some recurrent puzzles in the failure analysis of these alloys.

Two materials were studied. The first was from an extruded 7075-T6 alloy which had been severely compromised by an atypical "interior" exfoliation corrosion. The second was obtained from a failed 2014 alloy forging, the exact causes of its fracture undetermined. In both cases, previous extensive metallographic examination had established the special areas of interest, after which the chosen specimens were exactingly repolished without etching for the electron probe microanalysis. The experimental approach made use of guidelines available from similar studies of steels.

Low target currents (0.010 to 0.015 micro-amps) were used so as to obviate deadtime corrections. Initial surveys and some data collection were done at the 25-30 kV accelerating voltages, but lower voltages closer to the critical excitation requirement for the element of interest were generally used in order to reduce fluorescence effects. For statistical evaluation purposes, after initial surveying runs, a preset counting mode (10,000 cts) was used for quantitative data collection. Background was checked by both methods, off-line spectrometer settings and counts from an element one or two atomic numbers lower while on the Kα peak of interest. Several sampling points for inhomogeneity were used (5 to 10 for homogeneous types, 20 to 60 for heterogeneous second phases). Intensity data for each x-ray line of interest, established during the initial survey, were collected seriatum. At least ten members of each identifiable species were investigated, ranging in size from those barely visible at 100X to the largest available, $\sim$ 30 x 200 microns. Intensity vs. distance scans were made across inhomogeneities to check their dimensions and, incidently, attempting to use the information as a guide to the integrity of the minimum probe diameter. The determination of the stoichiometric compositions depended on checking the collected data for a constant ratio between elemental constituents, assuming Castaing's First Approximation. Later, a theoretically derived calibration curve was used to check Al-Cu ratios. These numerous and time consuming precautions were somewhat relaxed in connection with the microanalysis of the 2014 forging alloy. There, emphasis was placed on contending with the problems of collecting data on the lower atomic number elements.

In the case of the extruded 7075-T6 alloy, in addition to the results given in Table 1, several surveys of the exfoliated cracks and their borders were made to ascertain the chemical composition of observed corrosion debris. Oxygen and carbon were detected along with silicon but the findings remain ambiguous since no determination has been made as to electron probe contamination effects. The heterogeneous second-phase particles containing copper (4 to 16%) and iron (12 to 26%), seemingly non-stoichiometric, provided serious difficulties for data collection. Trace elements seemed to collect in the rather regularly shaped boundaries of the iron-minor element conglomerates and heterogeneous second-phase types were entirely intergranular. This suggested that the exfoliation corrosion proceeded at the laminar grain boundaries which were thus highly anodic to the quite homogeneous alloy matrix. Electron backscatter and target current oscillograms indicated frequent small cracks at inhomogeneity boundaries.

Results from the study of the forged 2014 alloy specimens indicated, aside from the information given in Table 1, the presence of a massive magnesium-aluminum spinel (AB_2O_4). This exogenous inclusion was responsible for initiating the fatigue failure of an inner cylinder wall by its notch effect. Other specimens were studied in order to characterize the metallographic evidence for the misnamed "high temperature oxidation" effects lying in the observed crack path, centrally located in the forging. What appeared to metallographic examination as grain boundary micro-holes, yet having inner structure as observed by replication techniques of electron microscopy, were confirmed as minute holes by the obverse images of electron backscatter and target current oscillograms. Additionally, oxygen, carbon and silicon were detected. The carbon signal being so relatively strong as to suggest the possible presence of another type of exogenous inclusion. And, unlike the extruded 7075-T6 alloy, the forged 2014 alloy yeilded evidence of the $CuAl_2$ second phase.

In addition to the experimental collection and quantitative reduction of the data, the problems of which have been indicated above, there is a more subtle, final difficulty of identifying, or relating, the inhomogeneities to the aluminum alloy equilibrium diagrams.(2) For instance, although 7075-T6 is commonly classified as an Al-Mg-Zn alloy, the inhomogeneities, due to the minor elements impurities, perhaps could be better understood by judicious reference to Al-Cu-Fe and Al-Mg-Si ternary phase diagrams. The results of this investigation suggest that control of Fe and Si impurities in this alloy composition should have great effect in improving its mechanical properties and corrosion resistance.

---

1. H. W. Antes, S. Lipson, and H. Rosenthal, Trans AIME, 239, 10, Oct. 1967, pp. 1634-1642.

2. Equilibrium Diagrams of Aluminum Alloy System, The Aluminum Development Association, Information Bulletin No. 25, 1960.

TABLE 1 - INHOMOGENEITIES IN ALUMINUM ALLOYS

Alloy	Particle Type*	Color	Size X-Y Microns	Shape	Composition**
7075-T6 extrusion	1. Fe	blue-gray	6-9 to 20-56	dented ellipsoid	Major - Fe(20) Minor - Cr, Mn, Cu, Si Bal. - Al
	2. Fe-Cu	coppery	6-8 to 26-58	grainy irregular	Major - Fe(14), Cu(27) Bal. - Al
	3. Mg_2Si	black	1-20 2-34	needles in matrix	Mg(25) Si(24)
2014 forging	1. $CuAl_2$	gold	5-10	spheroidal	Cu(55), Al(24)
	2. Spinel	invisible	0.01-0.08 cm.	discus	$MgO-Al_2O_3$
	3. HTO***	black	5-10 dia.	circular	O_2(37), C(4), Si(16)
	4. Fe-Cu	coppery	10-20	irregular	Major - Fe(10), Cu(8) Bal. - Al

*Tentative assignment.

**Numbers in parentheses give percent according to Castaing's First Approximation. Theoretical binary calibration curves (G.E.) and a multicomponent curve for Al-Cu were also used. (Not reported above)

***High Temperature Oxidation.

MICROPROBE INVESTIGATION OF TIN PLATE SURFACE DEFECTS

H. Nikkel and J. W. Lodge

Surface imperfections or defects are a source of considerable expense to primary producers of flat rolled steel products. This is particularly true if the defect escapes early detection by quality control, and costly plating and coating operations are performed on reject material.

Considerable work has been done in classifying defects(1) and often they can be recognized and eliminated or controlled by simple straight forward steps. However, many times periodic problems come and go and never are resolved.

Our investigation of tin plate slivers and scab type surface defects was aimed at lowering the incidence of these problems through a better understanding of their origin. The general characteristics of these defects are illustrated and evidence presented that points to two major causes for their occurance.

The findings were obtained from tin plate samples that contained "typical" slivers and other more subtle defects. A relatively large defect, usually appearing as a black streak, was examined on pickle band. Pickle band is a term used for the hot rolled and pickled steel that is subsequently cold reduced and eventually becomes tin plate. In addition to the defective specimens mentioned above, other material like scabs from slabs, ingot scum and scarfing flash was also examined to help correlate possible defect causes.

The preparation of metallographic specimens of tin plate for this study involved a new technique for removing small increments of surface layers. A one-inch diameter disc was punched from the tin plate to include a portion of the sliver. The edge of the disc was cupped to a 45° angle to facilitate gripping in a special holder for polishing. The central three-quarter inch diameter flat area was polished on a one micron grit diamond wheel. An alumina final finishing wheel was used on the specimen for photomicrographs, but not used for the microprobe analytical work to avoid contaimination of the specimen with aluminum.

Fig. 1 shows the cupping die and press along with two polishing holders, one empty and disassembled and the other assembled with a specimen ready for polishing. In addition, the photograph shows a one-inch diameter disc cut from tin plate, a flat cupped disc ready for polishing and a polished specimen where a defect is visible on the mirror-like surface. The rectangular part is a spanner wrench used in tightening the polishing holder around the cupped specimen.

As successive layers are removed in polishing the sample, it is examined frequently under a light microscope to insure that no important features are overlooked or lost before their nature can be determined.

Our findings on these samples indicated that the defects can be classified in two categories. These are shown schematically in Figs. 2 and 3.

One type is a foreign body of iron carrying a high concentration of nonmetal inclusions that has been roll bonded to the surface of the strip. These inclusions are essentially iron-manganese oxides and sometimes contain trace quantities of other elements. It is believed that this type of defect may be a small portion of a scab that was not completely removed by scarfing.

The other type of defect is an alignment of surface tears caused by subsurface non-metallic inclusions. These inclusions are iron-manganese-aluminum oxides of the type normally found randomly distributed in the grade of steel used for tin plate. They cause the narrow streak type defect when they occur in clusters that have been elongated by rolling. The inclusions are believed to be the products of deoxidation and may reflect the manner in which aluminum is added to the steel.

The black streak surface defect in the pickle band samples fits the first category but it was a much more severe condition.

Scarfing flash was purposely used to produce slivers and they had a similar appearance to those encountered in regular production. However, microprobe data revealed that the non-metallic inclusions present in this case differed from those present in the original specimens. In this case, the non-metallic inclusions were essentially iron oxide and lacked the high Mn concentrations characteristic of the inclusions present in the defect metal which is roll bonded to the strip surface.

This investigation has added to our understanding of the detailed nature of slivers and provides evidence as to the origin of a considerable percentage of tin plate surface defects.

---

1. Steel Products Manual, Carbon Steel Sheets Section, p. 19-30, American Iron and Steel Institute, February 1964.

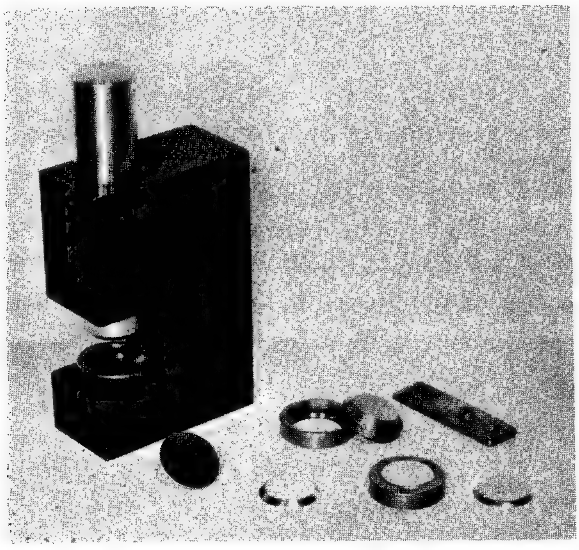

Fig. 1. Cupping die and press assembly; polishing holders and specimens in various stages of preparation.

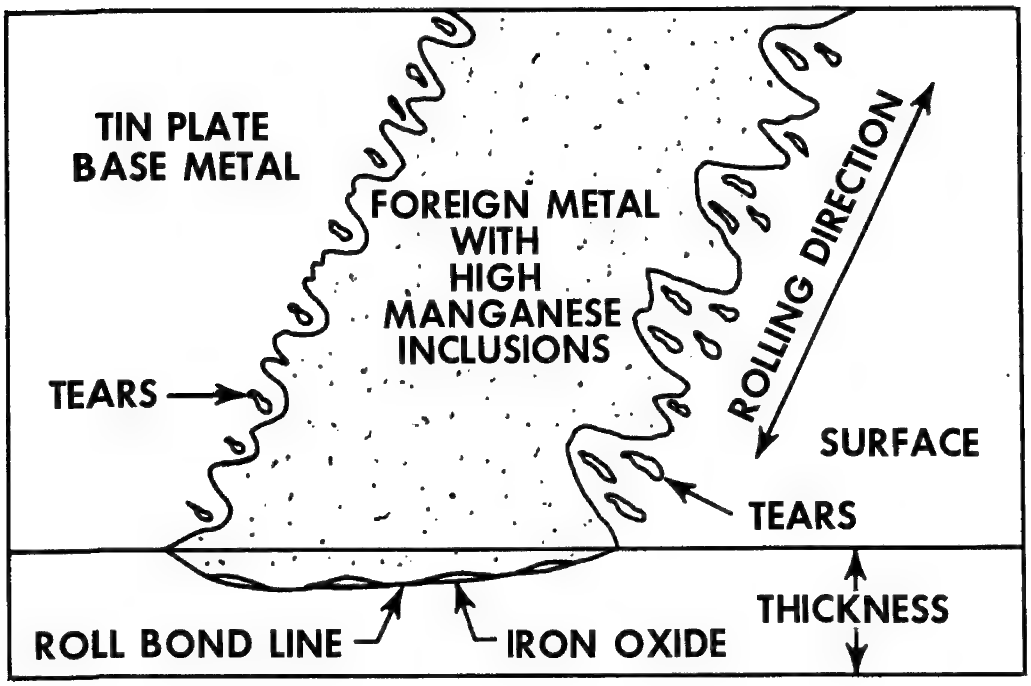

Fig. 2. Schematic of sliver condition caused by foreign metal roll bonded to surface.

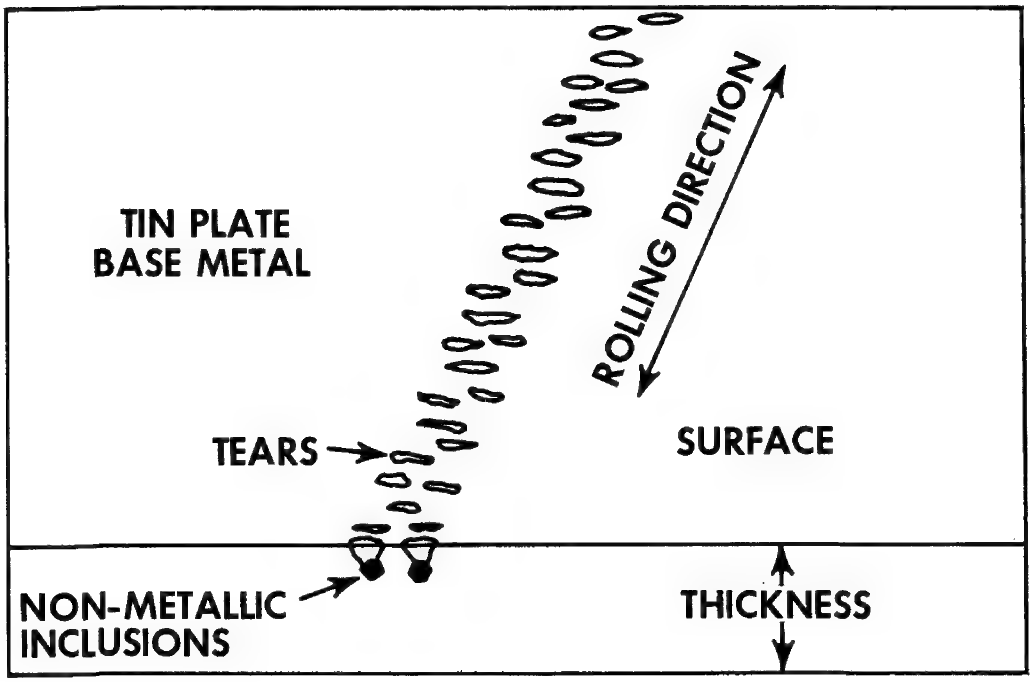

Fig. 3. Schematic of sliver condition caused by surface tears into subsurface non-metallic inclusions.

II

DIFFUSION OF COPPER IN BETA TITANIUM

O. Caloni, A. Ferrari and P. M. Strocchi

Recently, considerable interest has developed in the diffusion behavior of b.c.c. metals.(1) This is due largely to a combination of the growing technological importance of the refractory metals and to a natural extension of fundamental interest in these systems.

In some b.c.c. metals, such as β Ti, β Zr and γ U, there is a significant departure from the "normal" diffusion behavior(2); in fact, it is impossible to represent the diffusion process in terms of a single activation energy value.

As far as titanium is concerned, for temperatures in which the β phase is stable, an interpretation of the temperature dependence of the diffusion coefficient is possible in terms of two competing mechanisms represented by the Arrhenius relationship with different activation energies, one for temperatures below 1250°C, the other above 1300°C.

Considering the diffusion of group B elements of the IV period in β titanium, experimental data are not available for copper and zinc. This study covers the diffusion of copper over the temperature range 900°C to 1500°C and, at present, only data from 900°C to 1300°C are given.

Iodide-grade titanium sheets were vacuum annealed at 1300°C for 1 h to produce β grains of considerable size to avoid grain boundary diffusion. Afterwards a thin copper layer (∿1μ) was vacuum deposited.

Thermal diffusion annealing was carried out in vacuum at temperatures ranging between 900°C and 1300°C for times varying from 30 minutes to 5 hours. The temperature was controlled to ± 2°C and less than 5 minutes were required to heat or cool the samples.

With an electron microprobe, the distribution of copper down to 0.04% was measured in the diffusion direction at intervals of 10μ.

The solution to Fick's second law, which applies to the "thin-film", is given by:

$$C = \alpha/2\ (\pi Dt)^{1/2} \exp\ (-\ x^2/4\ Dt)$$

The diffusion coefficients can be calculated from the slopes of ln C vs. x^2 plots.

X-ray microanalysis gives only probe ratios of Cu Kα intensity, but in this case (dilute solutions) one may calculate the diffusion coefficients from the slopes of $\ln I/I_o = f(x^2)$, (Fig. 1).

The temperature dependance of diffusivity of copper in titanium is given in Fig. 2 and the straight line obtained can be represented by the relationship:

$$D = 2.1 \times 10^{-3} \exp(-29{,}260/RT) \text{ cm}^2/\text{sec}$$

The activation energy calculated in this investigation is much lower than that given by the empirical melting temperature rule but it is consistent with the values obtained by others(1) for impurity diffusion in β titanium. Also, the frequency factor, D_o, is too small to satisfy Zener's theory.

This anomalous diffusion behavior of copper in β titanium will be discussed on the basis of the recent models proposed.(3,4,5)

---

1. G. B. Gibbs et al.: Phil Mag., 8, 9, 1269, 1963.
2. R. G. Peart et al.: Acta Met., 10, 123, 1962.
3. A. D. Le Claire: Diffusion in b.c.c. Metals, ASM, 1965.
4. G. V. Kidson: Diffusion in b.c.c. Metals, ASM, 1965.
5. H. I. Aaronson et al.: Acta Met., 15, 385, 1967.

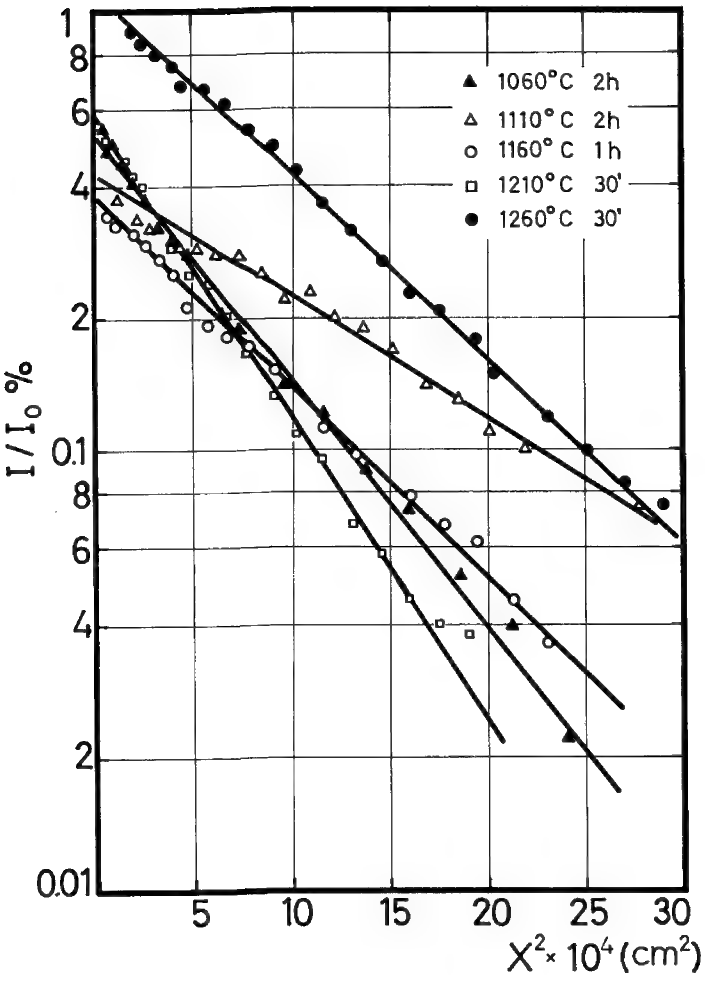

Fig. 1. Penetration profiles for diffusion of Cu in Ti at 1060, 1110, 1160, 1210 and 1260°C

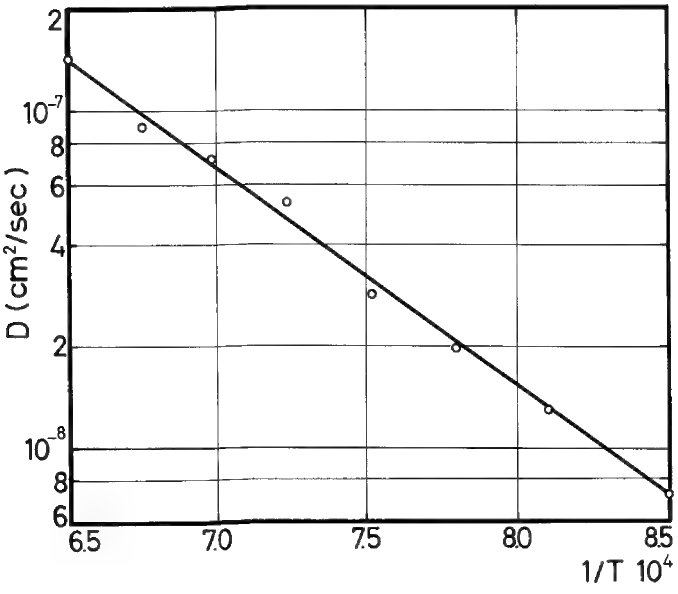

Fig. 2. Temperature dependence of the diffusion of Cu in Ti

ELECTRON MICROPROBE ANALYSIS OF NICKEL-IRON-COBALT THIN FILM WIRE MEMORY ELEMENTS

A. A. Chodos

Thin films on flat substrates are readily analyzed by either x-ray fluorescence spectrometry or the electron microprobe, but the analysis of thin films on a cylindrical substrate presents a more difficult problem. The substrate in our case is copper plated beryllium-copper wire approximately five mils in diameter with a maximum film thickness of nickel-iron-colbalt alloy of one micron.

The problem presented by the geometry of the sample was solved by copper plating the sample, mounting it in epoxy at a shallow angle to the surface, and lapping. The shallow lapping angle increases the cross-section of thin film presented to the electron beam while the copper plate prevents the beam from coming in contact with the epoxy during analysis.

As the exposed ternary alloy film cross-section is sometimes smaller than the beam diameter it is impossible to relocate the exact area analyzed. Sequential analysis for the three elements is therefore not possible and they must be determined simultaneously. The spectrometer arrangement of our microprobe is such that it is necessary to use the L alpha line for nickel on the light element channel. Unfortunately, the mass absorption coefficients for Ni L alpha radiation in iron and cobalt are not well known(1) and extrapolation from known values gave analyses that were in error by 20%. Therefore the empirical method of Ziebold and Ogilvie(2) was used.

Binary alloys of nickel-iron, iron-cobalt and nickel-cobalt were prepared using an induction furnace. These were compared to the pure elements to determine the a factors. These factors were tested by analyzing three bulk samples of ternary alloy and one sample of thin film, all of which had been chemically analyzed. These analyses are shown in Table I.

Each film was analyzed at the two locations where the shallow lapping angle increases the cross-section of the film the most. An acceleration potential of 15 kV was used with a specimen current of 0.04μA. The beam was kept centered on the film by use of an audio monitor on the iron channel. At least ten 10-second integrations were taken at each location. Each reading was corrected for background and calculated as an individual analysis. The reiterative calculation was of the type detailed by Lachance and Traill(3) or Bence and Albee(4). After convergence, normalization gives the composition of the film.

The effect of fluorescence of iron by the copper in the plate and substrate, if serious, would invalidate the results. Therefore this effect was evaluated by copper plating a bulk sample of nickel-iron and taking readings at 2-5μ intervals across the interface. These results, shown in Table II, indicate that analyses are valid for films giving 50% or more of the intensity of the bulk

sample. Even when the intensity had been reduced to 30% of that of the bulk sample, the results were in error by only 6% of the amount present, giving 20.2% Fe instead of 19.1%.

The precision of measurement and accuracy compared to chemical analysis is excellent. The standard deviation of ten measurement on typical bulk samples and films is 0.3% for nickel at the 78% level and iron at the 19% level and is 0.7% for cobalt at the 2% level. The method provides a rapid technique for the determination of the composition of ternary films and could be extended to the analysis of any three component micron or sub-micron sized sample.

Acknowledgements

The author is grateful to F. B. Humphrey and T. Suzuki of Caltech for the preparation of the standards, to R. M. Shoho and P. Husman of the Autonetics Division of North American Rockwell for the reference samples and chemical analyses, and to A. E. Bence of Caltech for discussions of the correction procedures.

---

1. K. F. J. Heinrich, "X-ray Absorption Uncertainty," in The Electron Microprobe, T. D. McKinley, ed., John Wiley and Sons, New York, 1966.

2. T. O. Ziebold and R. E. Ogilvie, Anal. Chem. 36, 322 (1964).

3. G. R. Lachance and R. J. Traill, Canad. Spect. 11, No. 2-3 (1966).

4. A. E. Bence and A. L. Albee, J. Geol., July 1968, in press.

Sample	Iron			Cobalt			Nickel		
	Chem.	Probe[a]	Std.dev.	Chem.	Probe	Std.dev.	Chem.	Probe	Std.dev.
1	18.53	19.44	0.35	2.53	2.11	0.07	78.94	78.45	0.27
2	18.80	18.48	0.32	5.58	5.36	0.07	75.61	76.16	0.34
3	17.56	17.97	0.30	9.74	9.87	0.22	72.70	72.15	0.21
4A[b]	18.27	18.40	0.73	3.50	3.86	0.07	78.24	77.74	0.79
4B[b]		18.01	0.35		3.71	0.13		78.28	0.41

Table I. Microprobe analyses of chemically analyzed alloys and thin film. a) Ten points on each sample. Fourth significant figures on all microprobe analyses are for statistical purposes only. b) Analysis of two different areas on same thin film.

	cts Fe	cts Ni	% Fe	% Ni
Pure Fe	74440			
Pure Ni		11910		
Body of alloy	17670	8134	19.30	80.69
Interface	17146	8123	18.91	81.09
	17202	7975	19.21	80.79
	15556	7324	18.99	81.01
	13396	6253	19.11	80.89
	12153	5665	19.13	80.87
	10725	5015	19.09	80.91
	7974	3448	20.19	79.81
	6055	2620	20.18	79.82

Table II. Analysis of the interface between the copper plate and binary alloy.

ENHANCED DIFFUSION DURING LOW TEMPERATURE FATIGUE

W. L. Bradley and M. A. Wilkov

It has recently been shown by Johnson and Johnson(1) that a large number of vacancies are generated during cyclic stressing of a copper specimen. The interaction of these non-equilibrium vacancies with the dynamic dislocations is not completely understood. The fact that the vacancies are annihilated by the moving dislocations has been shown by the reduction of resistivity displayed when a quenched, unaged specimen is immediately deformed at low temperature. This implies that the moving dislocations are either absorbing the vacancies or are sweeping them up and moving them to more efficient sinks such as the grain boundaries or surfaces. Recent experiments in strain aging by Aaron and Birnbaum(2) suggest that vacancies are attracted to static dislocations, forming a bound complex with them, rather than being annihilated at the dislocation cores. If a similar interaction between vacancies and dynamic dislocations exists, then it would seem reasonable that the dislocations should move the vacancies through the lattice either athermally or with a greatly reduced activation energy. Such a defect migration process would be detectable by enhanced diffusion at low temperatures during fatigue.

A series of experiments have been conducted to see if enhanced diffusion could be detected in a specimen fatigued at a low temperature where normal lattice diffusion is insignificant. Specimens of single-crystalline copper were prepared by nickel plating and then annealing in vacuum at 600°C for five days to give a diffuse interface. After fatiguing the specimen for five days at 197°K, they were sectioned and planed on a Servomet Spark Machine, along with an unstressed standard. The planning was done at an angle of 15° with respect to the surface, which resulted in five microns of distance along the planed surface being equivalent to one micron of penetration of the nickel perpendicular to the surface.

The specimen and standard were then examined in a Phillips Microprobe Analyzer. The nickel penetration profile was determined at increments of .64 microns over a distance of about 15 microns. Measurements were made with the beam stationary, counting over a time interval of 10 to 100 seconds. Five profiles were determined for each standard and specimen. The concentration at each distance of penetration was determined as an average of five data points and then a tenth order least squares polynomial was fitted to the data points. The results are shown graphically in Fig. 1.

The strain enhanced diffusion measured would be equivalent to the lattice diffusion obtained by heating the specimen to 500°C for a period of time equal to the duration of the fatigue test.

---

1. Johnson, E. W. and Johnson, H. H., Trans. AIME., 1965, 233, 1333.

2. Aaron, H. B. and Birnbaum, H. K., Acta Met., 1965, Vol. 13, 205.

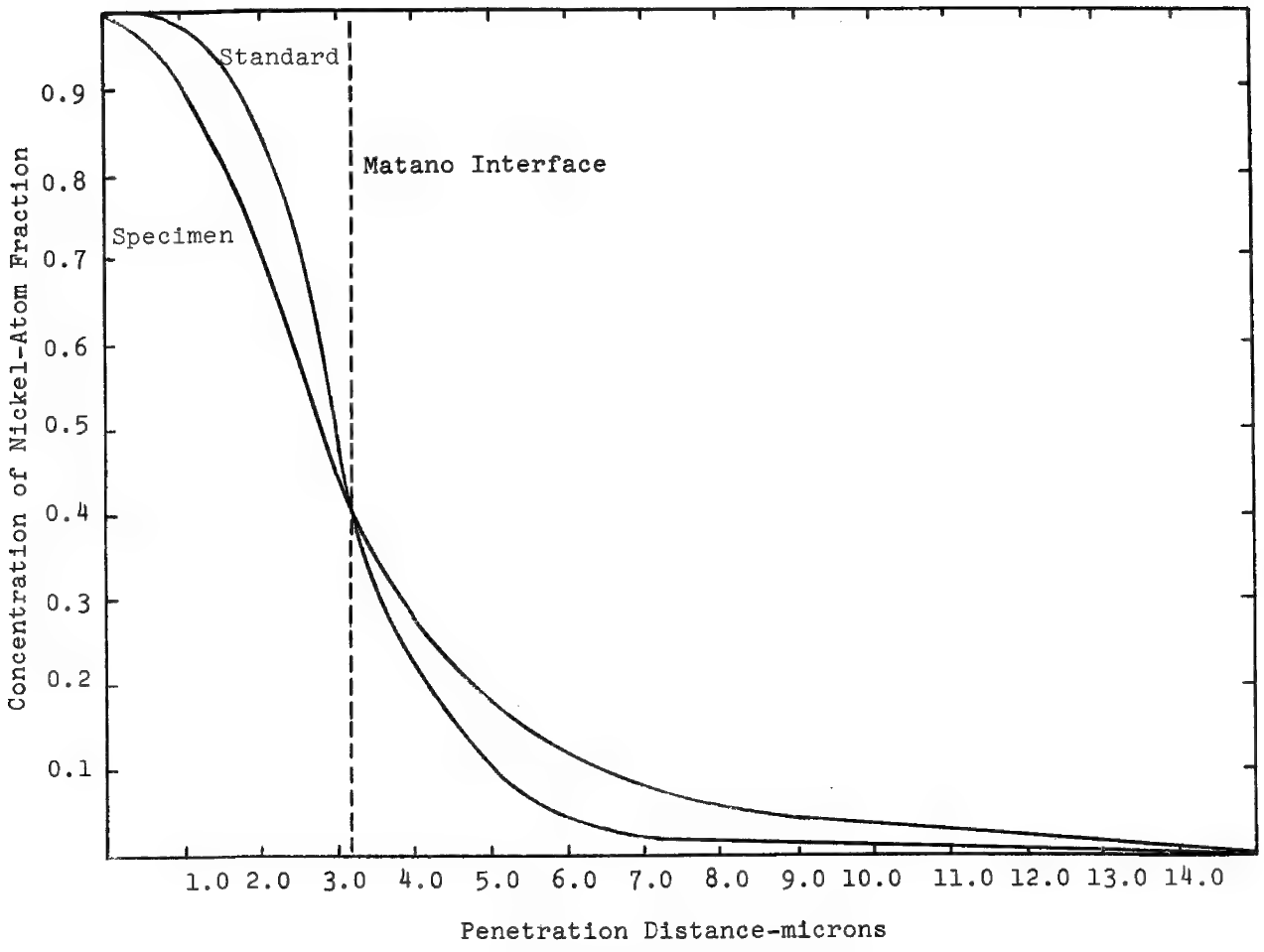

Fig. 1. Enhanced Diffusion Due To Fatigue at -77°C

DETERMINATION OF THE SOLID SOLUBILITY OF MERCURY IN ALUMINUM

D. R. Beaman

The solubility of Hg in solid Al at room temperature has been determined using the electron probe microanalyzer in conjunction with neutron activation analysis. Interest in the Al-Hg system was generated by a desire to understand the behavior of this material when used as an anode in cathodic protection.

Alloys containing from 0.003 to 1.4 wt.% Hg were produced in an enclosed furnace arrangement which allowed liquid Hg at 357°C to be added to molten high purity Al at 700°C. The furnace was continuously rocked and the alloys were slowly cooled (25°C/hour). All cast alloys were analyzed with the electron probe, by wet chemical means, and using neutron activation techniques. Three alloys were heat treated at 320°C for twenty-four hours in argon, followed by furnace or air cooling; however, no attempts were made to determine the temperature dependence of the solubility.

Point analyses and electron beam scanning photographs were obtained with the electron probe using LiF, quartz $(10\bar{1}1)$ and quartz $(11\bar{2}0)$ crystals. The figure is a plot of the measured Hg x-ray intensity vs. the chemical composition determined by neutron activation analyses. The x-ray intensity is seen to remain constant above 0.14 wt.% Hg. The Hg x-ray scans show an increasing density of circular regions of high Hg ("hot spots" henceforth) as the Hg content increases beyond 0.14 wt.% Hg while the matrix x-ray intensity remains constant. The observation of a second phase as the solubility limit is exceeded is normally a simple metallographic procedure; however, we were unable to detect the hot spots metallographically and x-ray images were essential. Heat treatment did not provide any significant changes in the observed Hg x-ray intensities.

The solubility limit could not be accurately determined because the alloys containing over 0.3 wt.% Hg were quite inhomogeneous and each such point is the average of a large number of measurements. However, the solubility is less than 0.14 wt.% Hg (0.144 wt.% alloy contains hot spots) and greater than 0.10 wt.% Hg (accuracy in the determination of the location of the horizontal line).

A crude estimate of the Hg in solid solution was made in the following manner. Several random x-ray and specimen current scans were obtained for the alloys containing hot spots to determine the distribution and size of the Hg concentrations. Using electron penetration data to estimate the number of particles per unit volume, it was possible to calculate the volume of Hg associated with the hot spots. Using a hot spot radius

of 1.3μ, the measured distributions gave values of 0.09 wt.% Hg in solid solution in both the 0.144 and 0.226 wt.% Hg alloys.

Since Hg wets Al there was a possibility that the observed Hg might simply have been a thin film on the Al surface that would form as internal hot spots were opened during polishing. We assumed that a film was present and attempted to prove its existence. The Hg intensity was monitored while the sample was heated and cooled in vacuum. Pure Al was abraded under Hg, then polished and examined in the probe. An electron probe characterized surface was subjected to ion bombardment etching and re-examined. The Al probe ratio was determined for various accelerating potentials between 2.5 and 33 kV. The results indicated the absence of a Hg film. Hg probe ratios were measured using a Hg-Ag alloy as a standard. The maximum film thicknesses that would account for the observed ratios were estimated from the work of Hutchins(1), and Cockett and Davis(2) to be between 20 and 60 Å. If all the Hg reported to be in solid solution existed as a film, the thickness would be considerably greater. The evidence, when considered as a whole, negates the film theory.

The reported solid solubility of 0.10 to 0.14 wt.% Hg in Al at room temperature does not agree with the values reported in Hansen(3): R. Müller--<0.027 wt.% (1929); I. Fogh--nil (1921); A. Dadieu--nil (1926); A. Smits and H. Gerding--5.5 wt.% (1925); and C. de Gruyter--39.3 wt.% (1925).

---

1. G. A. Hutchins, in The Electron Microprobe, T. McKinley, K. F. J. Heinrich, and D. B. Wittry, Eds., John Wiley and Sons, New York, 1966, p. 390.

2. G. H. Cockett and C. D. Davis, Brit. J. Appl. Phys., 14, 813, 1963.

3. M. Hansen, Constitution of Binary Alloys, McGraw Hill Book Company, Inc., New York, 1958, p. 99.

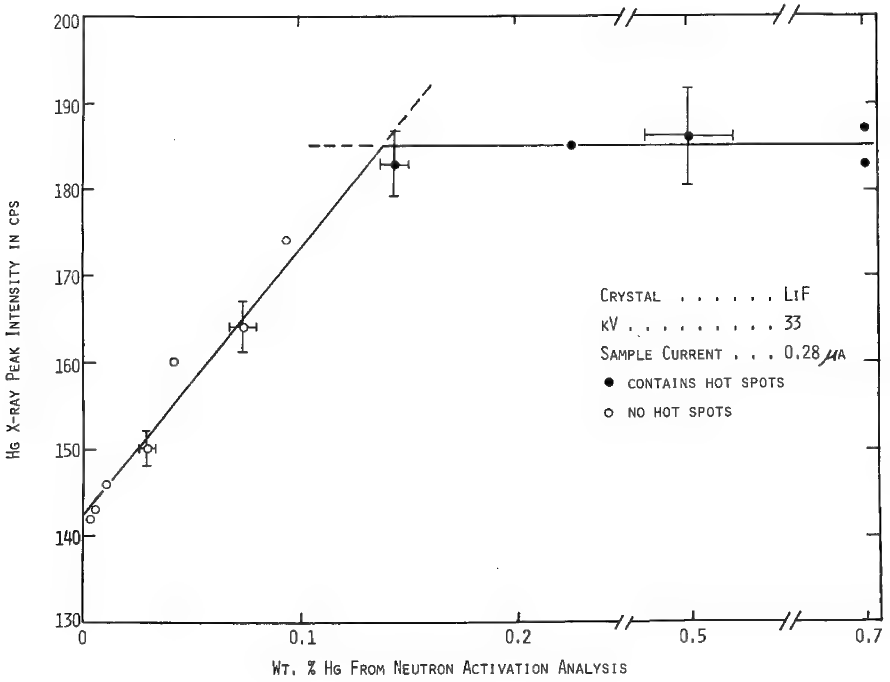

ELECTRON PROBE MULTICOLOR SCANNING IMAGES

James F. Ficca, Jr.

Color presentation of electron probe scanning data has been described by several authors(1,2,3). These techniques are based on the use of color filters and sequential imaging, thus making the process time consuming and lacking in definition, i.e., misregistration of the superimposed images. We have incorporated a color display computer oscilloscope* as an auxiliary readout display for the electron probe which has, in effect, added a new dimension to the readout system. The color readout display allows the simultaneous imaging of any three signals wherein each signal is identified by one of the primary colors (red, green or blue). Intermixing of the signals results in a color that is the additive of the contributing primary colors.

A standard oscilloscope camera and polaroid color film are used to photograph the faceplate of the color display to provide permanent color pictures.

The color display computer oscilloscope is basically a 19" rectangular, shadow mask, tricolor cathode ray tube with magnetic deflection and solid state circuitry. The unit was designed and built by I.T.T. Corporation for specific use in computer generated alpha-numeric or vector displays. We have made two minor circuit modifications to the basic unit: 1) the video amplifiers were modified to provide a linear intensity response instead of the normal on-off response, and 2) the convergence circuitry was modified to provide a white line anywhere within the 8 cm x 8 cm displayed area.

The block diagram (Fig. 1) of the signal selection capabilities of the multicolor display system demonstrates the flexibility of the readout system. Any three of the available signals may be simultaneously displayed to form composite color images. The patch panel position (#7) is provided to allow easy selection of those signals not indicated in the diagram, e.g., concentration mapping, topographical mapping, etc.

The color display has been used to advantage in all of the following modes of scanning analysis:

1. Multicolor Specimen Current Images

In this mode of analysis the specimen current may be used to modulate the intensity of the red, green or blue electron guns, or any combination thereof, to produce specimen current images depicting the variations in surface topography and/or average atomic number (whichever is predominant) as variations in hue and

* Model KM-906 I.T.T. Corp.

saturation of the primary colors. Further enhancement of the specimen current images have been obtained utilizing a three level D.C. discriminator* in conjunction with the color display. In this manner it is possible to form 3 color topographical maps containing large, intermediate and small signal excursions which are difficult if not impossible to record on a single black and white image.

2. Multicolor X-ray Scanning Images

In this mode of anlaysis the distribution of three elements may be simultaneously displayed wherein each element is identified by one of the primary colors. Variations in the mass concentration of an element are depicted as variations in the intensity (saturation) of the primary color assigned to the element. Spatial coincidence of the elemental constituents result in a color that is a function of both the saturation and hue of the primary colors assigned to the spatially coincident elements.

3. Multicolor X-ray Concentration Mapping

The technique of mapping selected ranges of concentration of an element has been described by Heinrich(4) and referred to as concentration mapping. The multicolor display is an ideal readout system for this mode of analysis. Three levels of concentration may be mapped in the three primary colors. The resulting image has a three dimensional appearance and makes the three concentration levels project with exceptional clarity.

4. Tricolor X-ray Intensity Profiles

In the line profiles mode of analysis a three trace preamp is used in conjunction with the color display to produce x-ray intensity profiles of three elements wherein each profile (element) is identified by one of the primary colors.

Examples of data obtained in all of the previously mentioned modes of scanning analysis will be presented.

---

* This is the same unit utilized in the concentration mapping mode of analysis.

---

1. K. F. J. Heinrich, Advances in X-ray Analysis, 7, University of Denver, Plenum Press, New York (1964), pp. 382-394.

2. M. P. Jones, J. Gavrilovic and C. H. J. Beaven, Trans. Instn. Min. Metall., (Sect. B: Appl. Earth Sci.) 75, (1966), B274-B277.

3. Metaalinstituut TNO Communications 1, ed. J. A. Jochems, Metal Research Institute TNO (Feb. 1966).

4. K. F. J. Heinrich, Rev. Sci. Instr., 33, 884 (1962).

BLOCK DIAGRAM OF SIGNAL SELECTION FOR COLOR DISPLAY

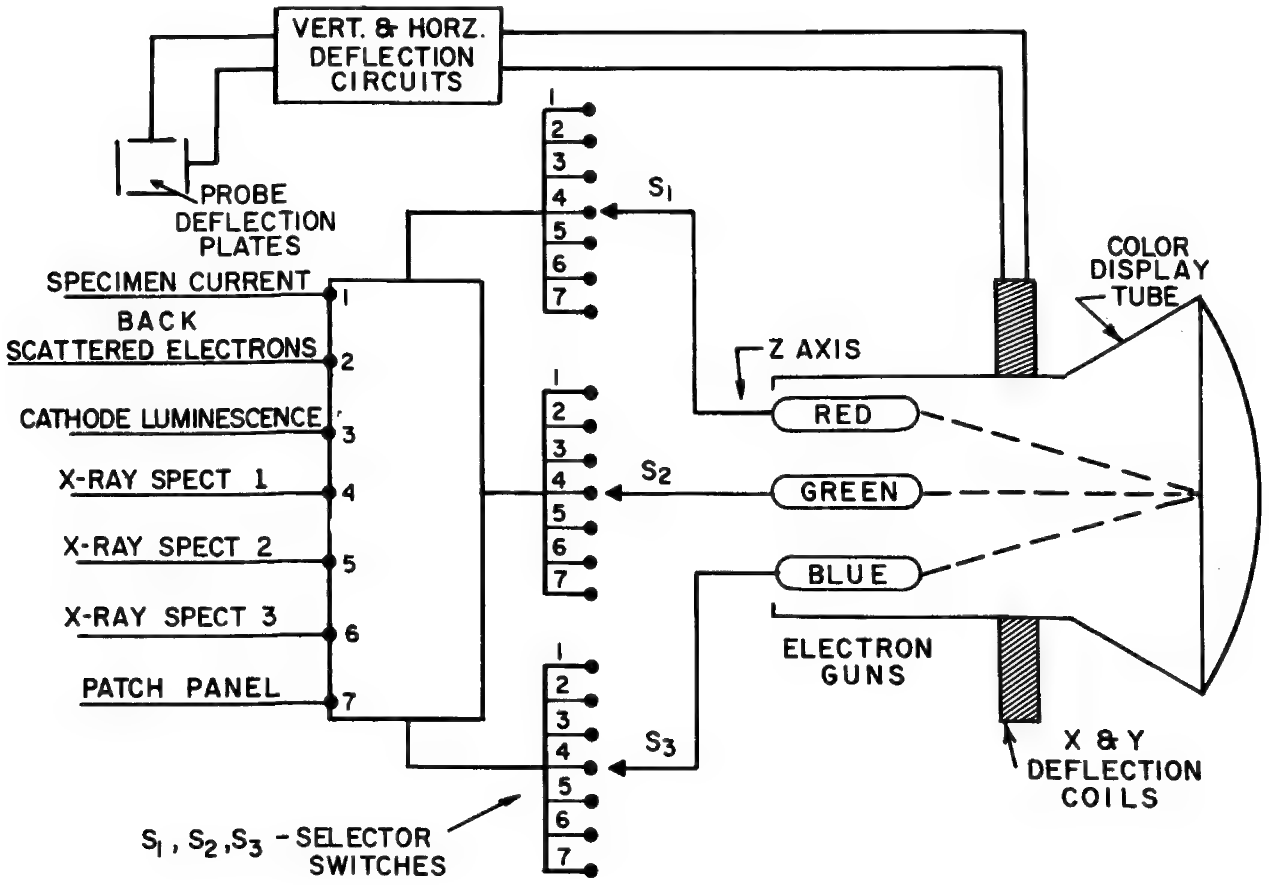

COMPOSITE MICROPROBE SCANNING IMAGES IN COLOR

H. Yakowitz, K. F. J. Heinrich and D. L. Vieth

A standard technique for the preparation of color composite photographs utilizing scanning x-ray and/or electron images from the microprobe has been developed. The technique provides composites which can be interpreted in terms of composition and which clearly show the microstructure.

The scanning electron probe microanalyzer(1) can produce images of microscopic areas as a function of the emission of x-rays or of electrons. The electron images provide mainly topographic information, while the x-ray images show the spatial distribution of the elements present in the specimen. Thus, the scanning electron probe is a microscope as well as an x-ray spectrometer.(2)

Black-and-white photographs showing the topographic distribution of a single signal are widely used. It is very difficult, however, to show the correlation of signals from two or more x-ray lines, or of x-ray signals with the topography provided by the electron images, without the use of color. Therefore, several investigators have used color photography for this purpose.(3,4,5,) Color micrographs of x-ray area scans can be obtained in three ways:

1. By the use of a three-gun color tube or oscilloscope and color photography of the three signals generated simultaneously.(6)

2. By using a single-gun oscilloscope, with color filters interposed between the oscilloscope screen and the color film in the oscilloscope camera. In this case, a phosphor of broad spectral distribution is used; and the three individual signals are registered serially, changing filters between exposures.(5)

3. By preparing conventional black-and-white scanning images, and obtaining the color composite photographically with the aid of color film and filters. (3,4)

The first method (which has not been used by us) is the only one permitting visual observation of the signals in their respective colors. As many as three signals can be registered simultaneously. This method requires, however, the addition of fairly expensive as well as massive equipment.

The second method requires only minor modifications if the conventional equipment for area scans is available. In this method, the various signals must be registered serially. Since the color composite is not visually displayed, this method is extremely tedious unless rapid-development film (Polaroid) is used. However, the low sensitivity of such films, combined with the low

brightness and limited spectral range of oscilloscope tube phosphors, presents difficulties in the registration of x-ray signals. Furthermore, if one of the three exposures is incorrect, the entire procedure must be repeated.

The third method also requires that the signals be registered serially (unless several oscilloscopes are provided with cameras). However, the exposures can be made by the usual techniques for black-and-white scanning photographs. As shown in this communication, color composites having good color quality can be produced routinely, with the aid of a copy camera equipped with rapid-development film. In addition, no large expenditures for equipment are necessary.

This copy camera technique can be easily used on a routine basis, by unskilled personnel, with a minimum of training. Another important advantage is the possibility of deciding upon the best color combination after the individual black-and-white images have been taken. The yield is 15 to 20 color composites of uniform quality per hour. In view of the advantages of this technique, most of the work presented in this communication has been performed by the copy camera technique.

The success of this technique depends upon the quality of: (1) the black-and-white images, (2) the characteristics of film and color filters, (3) the exposure times, and (4) the proper choice of color for each partial image. Care must also be exercised to avoid the relative displacement of the black-and-white images during the color exposure.

Regardless of the method of registration, the characteristics of the registration and perception of mixed colors must be taken into account. Failure to recognize the presence of primary colors in mixtures limits the number of possible primary components to three.

The effect of input subject quality, color filters used, film response, additive color mixtures, light sources, exposure time, development time and choice of color for a given x-ray scan have been investigated. Each of these factors will be discussed. Finally, examples drawn from several areas such as archeology, metallurgy, biology and mineralogy will be presented and evaluated.

---

1. P. Duncumb and V. E. Cosslett in x-ray Microscopy and Microradiography (V. E. Cosslett, A. Engström and H. H. Pattee, Jr. eds.) Academic Press, New York, 1957, p. 374.

2. K. F. J. Heinrich, ASTM Spec. Tech. Publ. 430, 1968.

3. P. Duncumb, Op. Cit. p. 617.

4. R. Theisen, Mem. Sci. Rev. Met. 60, 189, 1963.

5. K. F. J. Heinrich, Adv. X-ray Anal. 7, 382, 1963.

6. J. Ficca, Private Communication, 1967.

STABILIZATION OF GAIN SHIFT IN PROPORTIONAL COUNTERS

W. T. Kane

The use of pulse height analysis (PHA) in conjunction with proportional counters and dispersive x-ray optics is desirable for a number of reasons. PHA can eliminate higher-order reflections which overlay the wavelength of interest, exclude secondary fluorescence from the diffracting crystal itself, and reduce the normal radiation background.

Several authors(1,2) have pointed out that counting-rate-dependent shifts of the pulse height distribution act to limit severely the applicability of pulse height analysis in electron microanalysis. These shifts are decidedly nonlinear and, in some cases, have been observed to be time dependent(3). Thus, computational correction procedures must be both complex and inaccurate. The problem becomes particularly difficult when a pure element is used as a standard for a sample containing a low concentration. Suitably low count rates on the standard to preclude significant shifts will necessarily lead to very low sample count rates with decreased signal-to-noise ratios and increased instrumental drift effects. In many cases the advantages obtained by pulse height analysis are largely negated by these effects.

We have attempted to compensate for this effect by the use of the Hammer NC-20 spectrum stabilizer. This instrument, designed to provide long-term stabilization for gamma ray spectroscopy, is essentially a pulse height analyzer with a closed feedback loop which adjusts the detector potential through a range of approximately ±50 volts so as to lock the pulse distribution peak at the center of the selected window. Thus, as the count rate increases, the detector voltage is automatically increased to keep the pulse distribution centered in the window. Since the maximum voltage shift is only 100 volts, the possibility of operating the detector outside the proportional region is quite small. A null meter is provided to facilitate the centering of the peak and to indicate the relative magnitude and direction of the correction applied. The system will also compensate for drift in detector high voltage, amplifier or preamplifier gain, and detector gas gain. In Fig. 1 the count rate of a Si Kα peak is observed to drop off at high beam current due to shift of the energy distribution below the baseline setting of the analyzer. When stabilization is used, the peak remains centered, and no count roll-off is observed. In Fig. 2 the drift of the peak position of an ARL sealed neon proportional counter is seen to decrease in voltage in an approximately linear manner with increasing count rate. With the use of the spectrum stabilizer, it was possible to fix the peak

position in this case in the range from 10 to 18 thousand counts/second. It was noted, however, that with increasing detector voltage there was a distinct increase in the width of the pulse height distribution. This necessitated the determination of the base line and window settings at the high end of the count rate range selected to prevent the loss of the high and low tails. It was also found that the dynamic range of the stabilizer was insufficient to retain automatically the pulse lock condition when the count rate was varied from 10 to 80 thousand counts per second. Manual adjustment of the detector voltage was then used to recenter the distribution by centering the null meter, re-establishing the lock in condition. No change due to the use of stabilization was noted in the 2.25μ sec. deadtime of our system nor has any change in system noise level been detected.

Our results thus far suggest that the use of this closed-loop servosystem provides a practical solution to the problems inherent with the use of pulse height analysis in quantitative microprobe analysis.

---

1. Bender, S. L. and Rapperport, E. J., 1966, Non-Proportional Behavior of the Flow Proportional Detector in the Electron Microprobe, McKinley et al. Ed., John Wiley and Sons, New York.

2. Spielberg, N., Rev. Sci. Instr. 37 1268 (1966).

3. Spielberg, N., Mechanism of Gain Shift in Proportional Counters Second National Conference on Electron Microprobe Analysis, 1967.

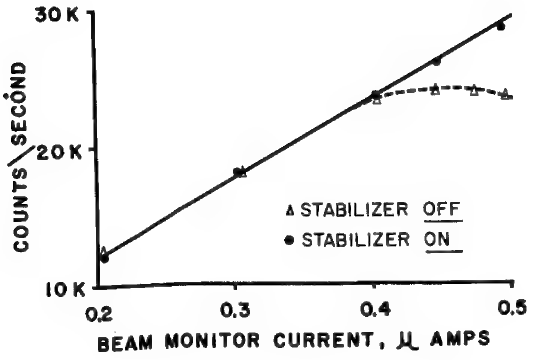

Fig. 1. Effect of stabilization upon observed count rate roll-off.

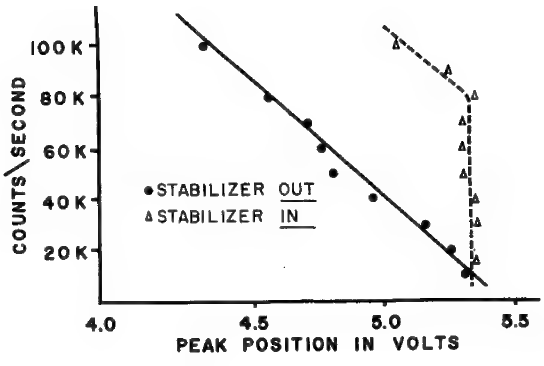

Fig. 2. Effect of stabilization upon voltage distribution peak position.

A COMBINED SCANNING ELECTRON MICROSCOPE-MICROPROBE ANALYZER

V. G. Macres, O. Preston, N. C. Yew, R. Buchanan

The instrument described here is a development of the Materials Analysis Company Model 400 x-ray microprobe analyzer. It incorporates all the x-ray microanalysis capabilities of the earlier instrument, and in addition allows scanned electron images to be formed with up to 1000 Å resolution.

A cutaway drawing of the instrument is shown in Fig. 1. The column comprises a triode electron gun, electromagnetic double condenser lens, and objective lens. The electron gun uses a conventional hairpin filament, autobiased Wehnelt cylinder and anode. An externally controlled filament-Wehnelt cylinder height adjustment is provided for optimizing gun performance at all operating potentials. The double condenser lens is unitized and has two lens regions and a common energizing coil. The estimated minimum focal length of each lens is about 0.33", which provides a maximum total demagnification of about 100X. The final demagnifying lens has a minimum focal length of about 1" and this, in conjunction with the double condenser lens system, can produce an electron probe with a diameter of less than 0.15μ containing up to 0.2 nanoamp of electron current on a routine basis. The back bore of the objective lens houses the electromagnetic beam scanning coils, an electrostatic stigmator, and an additional set of electromagnetic coils which are used for fine positioning of the probe on the specimen surface.

The objective lens also houses a purely refracting light microscope, which views the specimen surface at normal incidence through the objective lens bore. The magnification range of the microscope is variable up to 640X and it has a resolution of 0.5μ.

Up to three fully focusing Johansson-type crystal spectrometers can be used on the instrument. The crystals, which view the specimen at a constant effective x-ray take-off angle of 38.5°, cover a 2θ angular range of 20° to 145°. With the crystals available, namely LiF, PET, ADP, KAP, LOD, this allows the analysis of all elements in the periodic table down to boron. The mechanical design of the spectrometers is particularly simple, and this has been achieved at no sacrifice in performance, e.g., the linearity is at least 0.02° at $2\theta = 20^{\circ}$ and 0.1° at $2\theta = 145^{\circ}$, while the reproducibility is better than 0.004° at $2\theta = 20^{\circ}$ and 0.02° at $2\theta = 145^{\circ}$.

A transistorized electron beam scanning system has recently been developed which provides a simple switch control for changing from one display mode to another, thus eliminating the need for patch plug connections. In addition to a wide range of scan speed controls, a small area high speed (15 frames/

second) scan control is provided for fine adjustment of the instrument. Also, a calibrated magnification control is provided which has automatic compensation to allow switching the accelerating potential without changing the magnification of the display. By designing and building the raster control circuitry, rather than using that in the oscilloscope as was done previously, it has been possible to completely eliminate hum from the scanned image display.

Scanned images may be formed using selected monochromatic x-radiation, backscattered electrons, secondary electrons (including voltage contrast images), specimen current, electron beam induced conductivity and cathodoluminescnece. The images may be shown in either intensity modulation or deflection modulation. A Si surface barrier P-N junction is used to detect the backscattered electrons. Due to the high collection efficiency and sensitivity of this system, it is possible to obtain high resolution images of uncoated insulating specimens at probe energies above 10kV. Examples of such images are shown in Figs. 2 a) and b) , intensity modulation and deflection modulation respectively. The sensitivity of the system is such that images can be formed in about 20 seconds with detected backscattered electron currents as low as 20 picoamps. The secondary electron detector is of the conventional scintillator/electron multiplier type. The use of separate electron detection systems for backscattered and secondary electrons allows the detectors to be optimally located for their separate functions.

Fig. 1. Electron Microprobe Analyzer

1. Electron Gun Assembly
2. Upper Shield
3. Auxiliary Lens Assembly
4. Intermediate Shield
5. Intermediate Chamber Assembly
6. Turret Microscope Assembly
7. Objective Lens Assembly
8. Suspender Unit
9. Spectrometer
10. Static Beam Shield
11. Specimen Stage Assembly
12. Table Top
13. Aperture Control

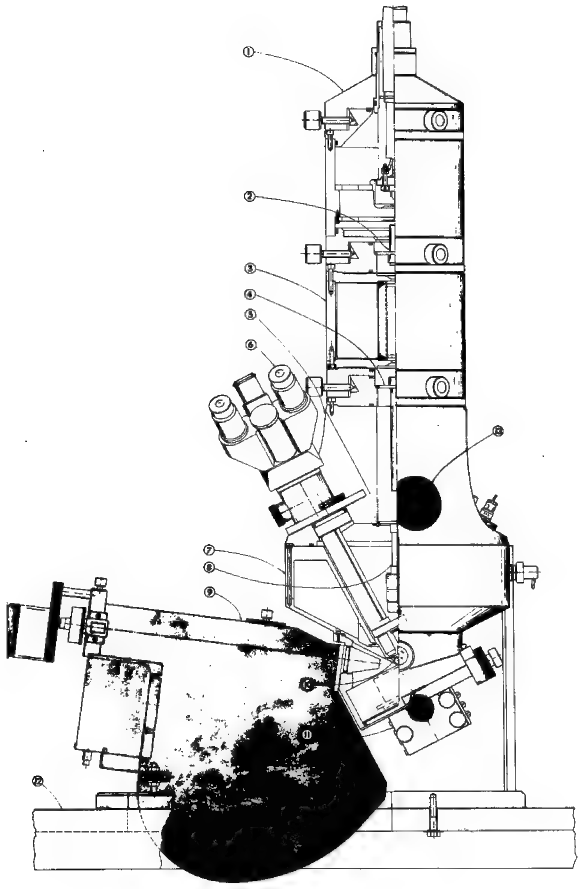

Fig. 2. Uncoated Conodont (fossilized teeth)

a) Intensity Modulated Display

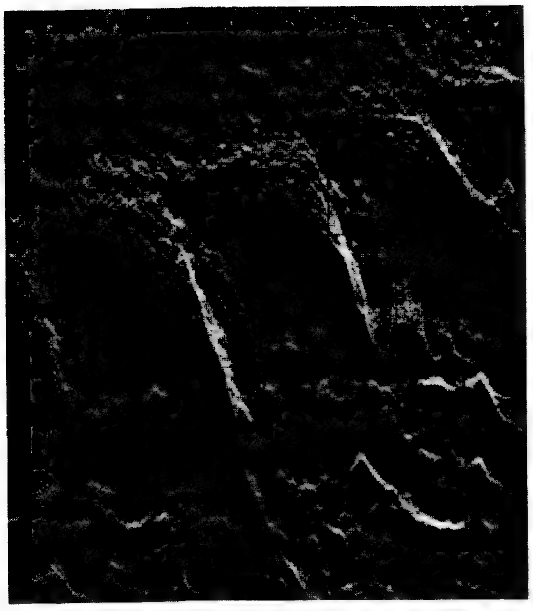

b) Deflection Modulated Display

REDUCTION OF CONTAMINATION EFFECTS IN ELECTRON MICROPROBE ANALYSIS

Hermann Neuhaus

During the process of sample analysis in an electron microprobe, some form of contamination on the sample surface can be expected. The contaminants are usually in the form of a carbonaceous deposit. The accumulation of contaminants and their influence on the analytical results depend on the sample structure, the sample temperature, the vacuum pollutant and on the surface temperatures of the enclosure around the sample.

During experiments to be described, it was concluded that the main source of contaminants originates within the sample chamber, often from the sample itself. It is recognized that the proximity of cold surfaces around the sample tend to trap the contaminants before they can reach the sample. Cold plates have been put to efficient use in electron microscopes for some years. However, in electron microbprobes, where most instrumental design functions take place above the sample surface, a cold plate may be an interfering object.

Large surface areas above the sample in the form of the electromagnetic objective lens are usually in existence, as an integral part of the electron microprobe structure. A commercial instrument, on which the experiments were performed, features a magnetic objective lens of low mass and built-in water cooling. With minor modifications, this lens was adapted for cold temperature operation. A reduction of contamination deposit by a factor of twenty or more could be obtained with moderate objective lens temperatures in the -30^{o} to $-70^{o}C$ range. Fig. 1 shows the contamination effect on iron by changing the temperature of the objective lens structure. Cooling of the lens is by means of liquid nitrogen, or with a closed-loop refrigeration system. Either cooling system can be automatically controlled to maintain the lens temperature within $1^{o}C$ for stable instrument operation. Fig. 2 is a diagram of the cooling system in the closed-loop refrigeration mode. In this case the refrigerant is pumped through a needle valve into the spectrometer tank toward the objective lens. A solenoid valve, actuated by a temperature and control unit, regulates the flow of coolant through the objective lens. The remaining coolant energy is then utilized for cooling the diffusion pump baffle before being pumped back into the refrigeration condenser. To assure continuous refrigerant circulation, a coolant bypass coil is provided inside the spectrometer tank.

If both liquid nitrogen and refrigeration cooling systems are installed, as shown by the diagram in Fig. 2, the conversion from one to the other can be made in a few minutes by opening or closing the appropriate valves.

To establish a reference for measuring the contaminants, the instrument functions and measuring methods must be standardized. For this purpose the carbon x-ray

output from the accumulating deposit is compared to the carbon x-ray output from pure graphite. The carbon content of the contaminating deposit was found to be constant for such units as time and static conditions of the sample environment. The variable analytical conditions for which a change in the carbon contamination rate can be expected are the electron beam voltage, the sample area bombarded by the electron beam, the electron beam current and the electron beam spot size. Fig. 3 shows the effect of the electron beam spot size, or the electron bombarded area, in respect to the carbon contamination rate of the sample surface.

Experimental evaluation has established that low temperature operation of the electromagnetic objective lens above the sample surface is one of the most efficient methods to reduce the formation of carbonaceous contaminants on the sample surface.

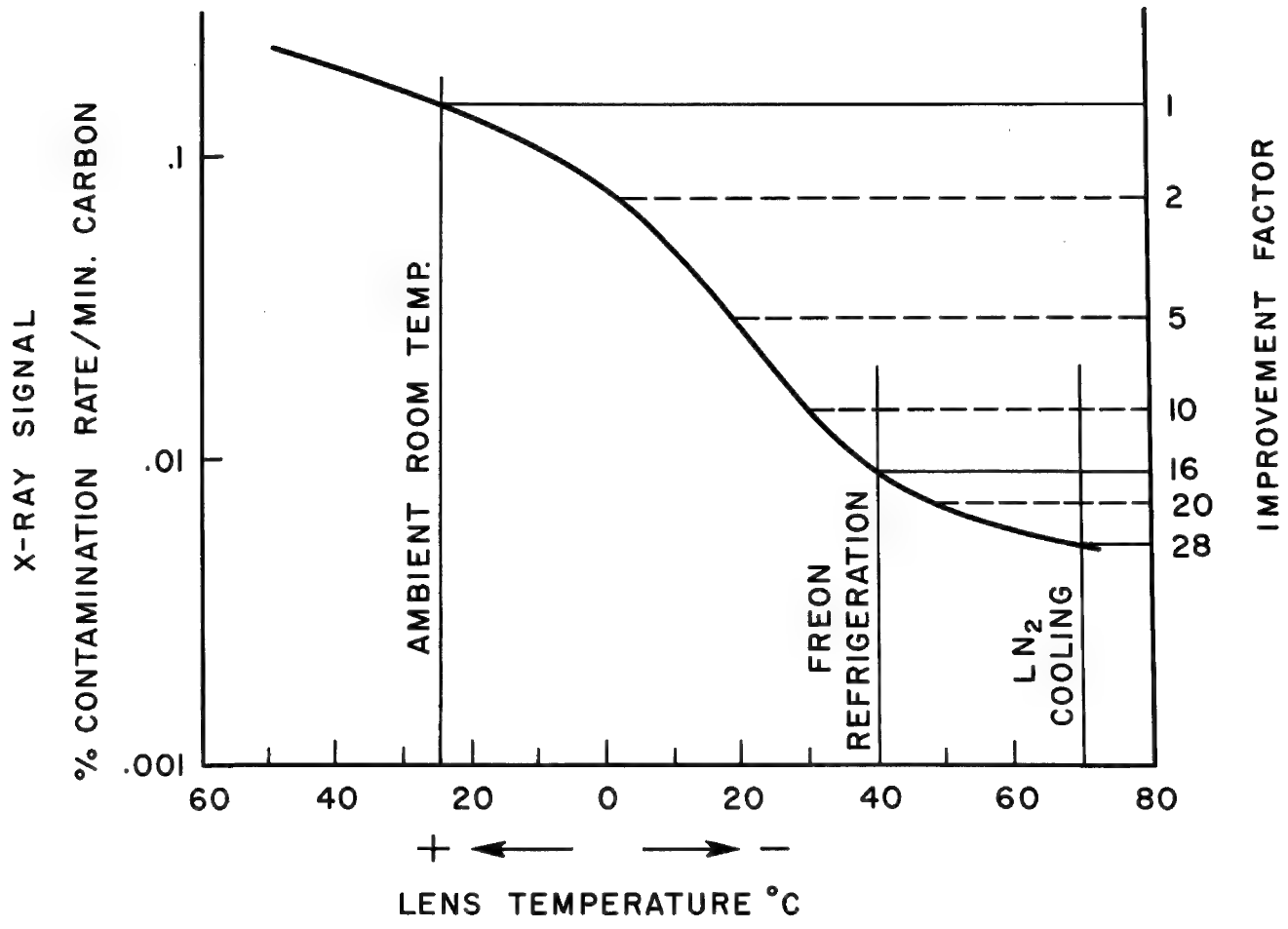

Fig. 1. Contamination Rate %C/Min./Lens Temperature ^{o}C
10 kV; 0.1μA on Fe; 8000μ^2; 5 x 10^{-5} Torr.

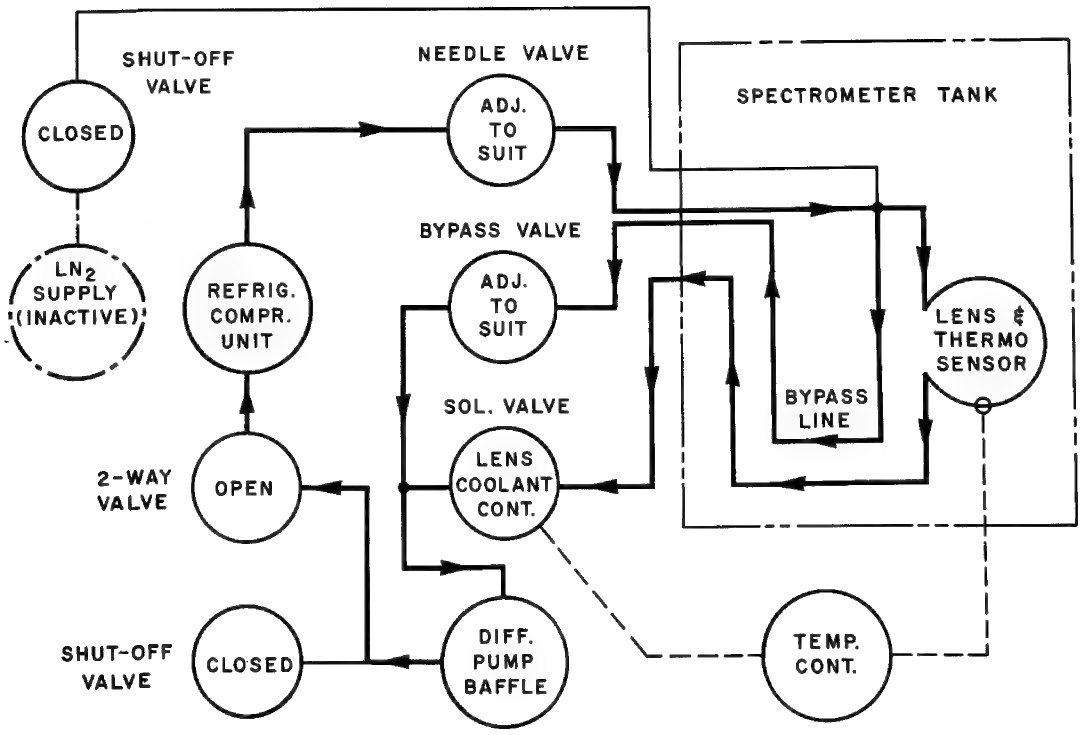

Fig. 2. Objective Lens Cooling System. Closed Loop Refrigeration.

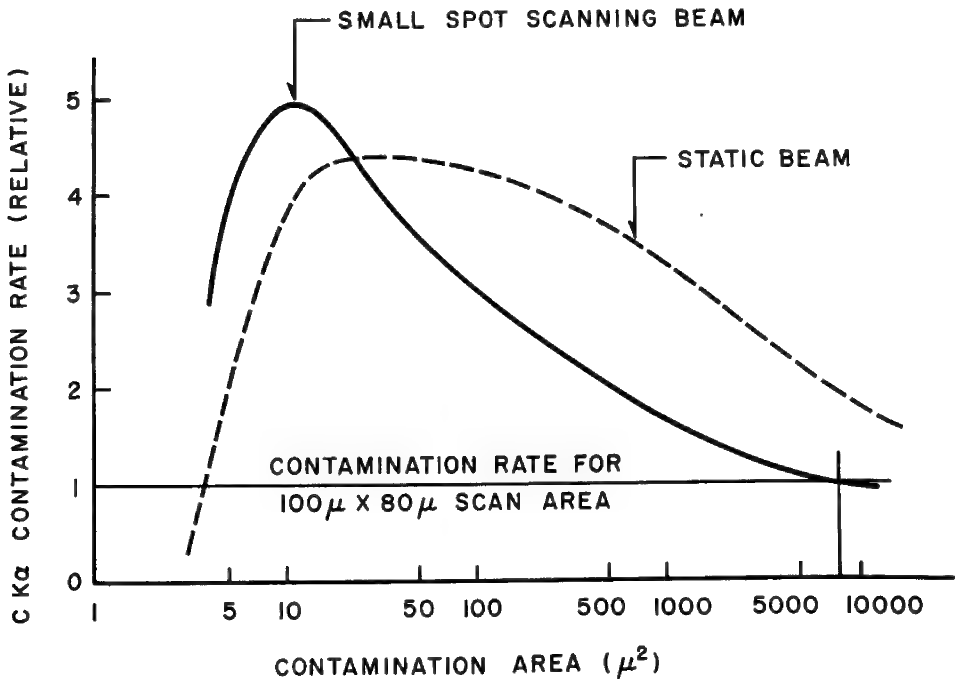

Fig. 3. Contamination Rate/Area
10 kV; 0.1μA on Fe; Lens = 20°C; 10^{-4} Torr.

THE "ELMISONDE" A UNIVERSAL COMBINATION OF ELECTRON PROBE, SCANNING ELECTRON MICROSCOPE AND HIGH RESOLUTION TRANSMISSION ELECTRON MICROSCOPE

K. Toegel and J. Hellgardt

The "ELMISONDE" is a microscope, which can be converted into a high resolution electron microscope, type Elmiskop IA, or vice versa the microscope can be changed quickly into a microprobe. Even the existing electron microscopes, Elmiskop I or IA, can be converted after minor adaptions.

This concept of combination of sub-units does not at all impair the performance of the individual instrumentation. On the contrary, the individual instrument benefits from the features common to all of them.

For the generation of a beam spot of 0.1 to 0.2μ, a two lens system consisting of condenser two of the Elmiskop and the fine beam lens is sufficient. For a scanning electron microscope with a beam diameter of 100 to 200 Å, a third lens, the objective lens of the Elmiskop, is required.

For electron probe microanalysis the parts of the Elmiskop column from the airlock to the projector tube are exchanged for a compact unit consisting of an intermediate tube with fine beam lens, sample changer, optical microscope and two x-ray spectrometers with a take-off angle of 30°.

Light Microscopy. In order to use all modern techniques in optical microscopy to their full advantage a design with separate "electron optical" and "optical" axes was chosen. By means of a motor mechanism the sample is moved quickly under the microscope or the electron beam. A reproducibility of a few microns is guaranteed.

Specimen Stage. The exchangeable specimen stage accepts three samples of 8 mm width up to 25 mm diameter besides eighteen standards and an alignment field.

Sample scanning with a range of 20 mm in x and y for screening the sample is possible manually and automatically. Ten different speeds of 1μ/min. to 10 mm/min. in x and y are selectable by a switch. By combining different motor speeds, a mechanical line scan in any direction can be achieved so that a sample rotation is not required.

Electronics. In the fully transistorized compact electronic panel the modules which are operated most often, are conveniently located in the center. In the lower part of the two panels the following modules can be inserted: up to four pulse channels for the dispersive and non-dispersive x-ray analysis; the DC channels for the electron and sample current pictures; the quadruple pulse gate for concentration mapping and a switch module. In the center part there

are: the scanning generators; up to five oscilloscopes to be connected to any of the measuring channels; the sample current instrument with electronic integrator for measurements at constant sample current; integral and digital read-out; the pulse scope for display of the non-dispersive x-ray spectrum and the setting of the discriminator; and finally, the electronic timer scaler which takes counts of up to seven channels simultaneously. A printer can be connected to the timer scaler. The spectra and line profiles are recorded by Kompensograph recorders. All combinations of channels and recording methods can be chosen simply by switching positions.

For convenience the electronic magnifications are maintained during HT changes and correspond to the light optical magnifications. The numberous fixed magnifications between 100X and 6400X together with scanning speeds from three pictures/sec. through one line per 100 min. with free choice of line speed and line number assure sufficient versatility for various problems. Additional techniques, for example, transmission scanning microscopy by means of a Faraday cage, the use of luminescence detectors and SE detectors provide ways to adapt the instrument to special problems. The different modes of operation of the electron microprobe are shown in the figure.

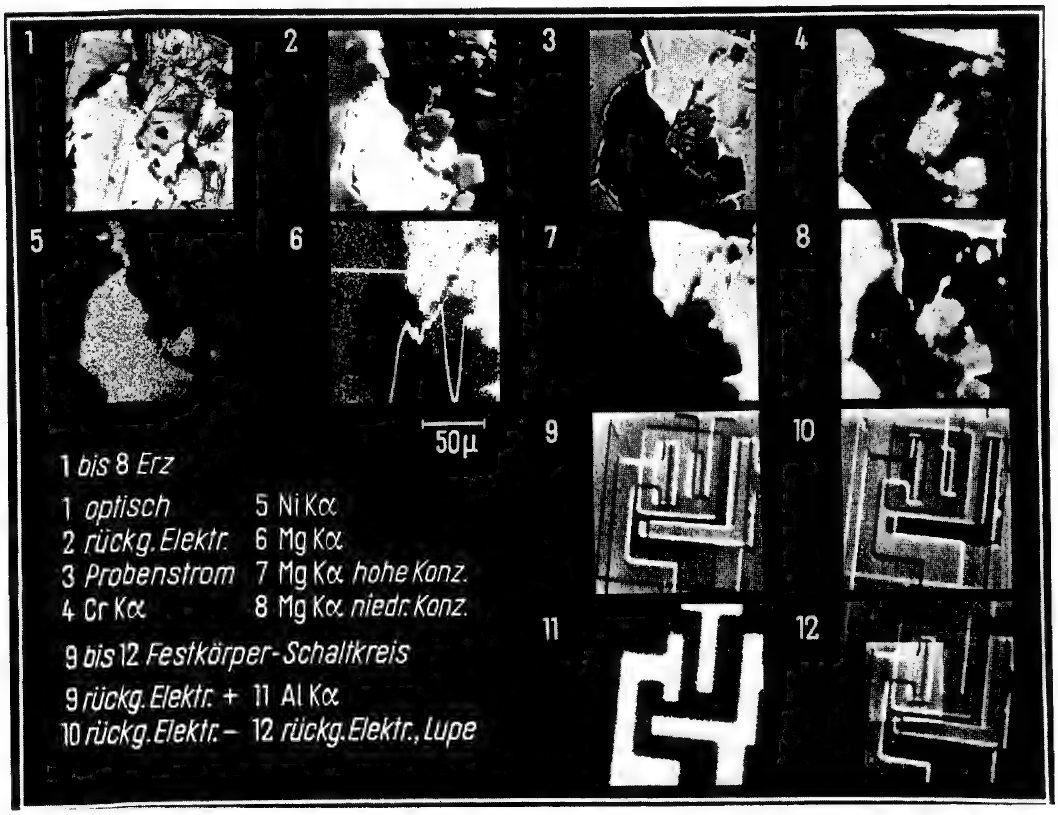

Fig. Various applications of the Elmisonde

A NEW QUANTITATIVE PHASE ANALYZER

M. Tong, C. Conty and R. Lewis

A new quantitative metallographic analyzer has been designed as an accessory to the CEC/CAMECA electron probe microanalyzer. This accessory allows the volume concentration of a well defined phase to be determined. In addition, such characteristics as mean diameter and number per unit volume may be obtained when the phase is in the form of precipitates.

The advantages of using a "flying spot" device to determine the number of precipitates present, their type, size distribution and the area fraction occupied by each, have been dealt with in considerable detail(1,2). By utilizing the highly specific analytical information provided by the electron probe microanalyzer, the application and usefulness of these spot scanning techniques can be expanded considerably. Theisen(3) has discussed the types of problems that can be examined and Melford has described an instrument of this type(4). The accessory described here makes maximum use of the capability of the CEC/CAMECA electron probe microanalyzer for performing quantitative phase analysis.

With the electron probe set to explore the specimen in its beam scanning mode of operation, a specific phase is selected by processing the analytical data with a logic system. By setting up a number of preselected conditions, a particular phase can be selected unambiguously. The analytical data can be of two types: x-ray intensity signals from any of the four x-ray spectrometers or electron current (absorbed, backscattered or secondary).

The volume concentration is determined by making surface concentration measurements. These are obtained from the ratio of the time the electron probe traverses the specific phase to the total scanning time. To record the time measurements, the signal from a clock pulse generator is fed to a counter, U, and the signal gated on and off as the boundaries of the phase are traversed while another counter, T, records the total scanning time. To determine the mean diameter and distribution density of a precipitate, the length of a scan line, number of traverses across the specific phase and the total number of line scans are recorded.

In addition to the measurement of a well defined phase, it is also possible to make surface concentration measurements of a component whose element concentrations are within selected limits. An image of the latter may also be recorded on the CRT.

The analyzer system consists of three identical x-ray channels, one electron current channel, three coincident gate circuits and one oscilloscope modulation circuit. The electron current channel may be used to process additional x-ray information when the current signal is not being used.

Some typical types of analyses that may be performed are the following: 1) analysis of a phase characterized by the concentration of two elements — precipitate counting, 2) analysis of a phase characterized by the concentration of an element and absorbed current — precipitate counting, 3) analysis of a phase characterized by the concentration of an element into three size groups, 4) mapping the spatial distribution of an element at three different concentration levels and displaying the output on the CRT, 5) analysis of three different phases, each of them characterized by the concentration of one element, 6) analysis of two phases, each of them being characterized by two different concentrations of two elements.

For an oversimplified model which assumes precipitates made up of identical spheres whose volume distribution is random and isotropic, the following formulae can be derived.

Formulas	Probable deviations	
	$l_m/\Delta < 1$	$l_m/\Delta > 1$
$C_V = U/T$	$1/(N_U)^{\frac{1}{2}}$	l_m/Δ $1/(N_U)^{\frac{1}{2}}$
$l_m = C_V N_L/N_U$		
$d_o = 3/2\ l_m$		
$n_o = 6\ C_V/\pi d_o^3$	$2/(N_U)^{\frac{1}{2}}$	$(d_o/\Delta)^{\frac{1}{2}}$ $2/(N_U)^{\frac{1}{2}}$

Where:

L length of a line scan

N_L number of lines per frame

Δ average distance between two successive lines

U number of pulses totalled by the "U" counter during scanning

T number of pulses recorded by the "T" counter during same scanning

N_U number of traverses

d_o mean diameter of precipitates

l_m mean value of scan length across analyzed phase

C_{vi} volume concentration of analyzed phase i

n_o number of precipitates per unit volume

$C_i(E)$ mass concentration of element E in phase i

It is possible to calculate the total concentration of an element E from the measurement of C_v, providing the concentrations of the element E in all phases of the specimen and the density, ρ, of each phase are known. For example, in a two phase sample, the mass concentration is given by:

$$C_m(E) = \frac{\rho_1 C_{v1} C_1(E) + \rho_2 C_{v2} C_2(E)}{\rho_1 C_{v1} + \rho_2 C_{v2}}$$

A typical analysis of an Al_2O_3 phase appearing in the form of precipitates in pure iron will be given.

---

1. F. Roberts and J. Z. Young, Proc. Inst. Elec. Eng. 111 a 99, 747, 1952.

2. J. A. Belk, Iron Steel Inst. Spec. Rep. 77, 25, 1963.

3. R. Theisen, Euratom Report No. 386F, 1963.

4. D. A. Melford and K. R. Whittington, "IV International Conference on X-ray Optics and Microanalysis" Hermann, Paris, 1965.

HIGH RESOLUTION CATHODOLUMINESCENCE WITH THE SCANNING ELECTRON MICROSCOPE

L. H. Pruden, E. J. Korda, D. P. Smith and J. P. Williams

Cathodoluminescence mapping of materials with resolution greater than 1000 Å can be obtained by simple modification of a scanning electron microscope (SEM). This high resolution is possible because the electron beam spot size of a SEM is nearly two orders of magnitude less than the one to two micron spot size of an electron microprobe. Several other instrumental as well as phenomenological factors affect resolution, including beam current required to generate luminescence, electron gun accelerating potential, spectral response of photomultiplier tubes, persistence of luminescence in materials and light scattering.

Modifications made to obtain sequential secondary electron emission and cathodoluminescence photomicrographs with a Cambridge Instrument Company Stereoscan are shown schematically in Fig. 1. Ends of individual glass fiber optic light guides are arranged in a 320° arc around and just above the surface plane of the specimen. This array of fiber optic guides provides an efficient light-gathering assembly and subsequent light path to a photomultiplier tube. A slot is incorporated in the assembly to permit collection of secondary electron emission from the specimen by means of the regular scintillator-tipped light pipe and photomultiplier. A second photomultiplier tube housing was installed on the SEM at right angles to the original housing so that conversion from the secondary emission mode to the cathodoluminescence mode could be made without disturbing the specimen in the vacuum chamber. With this arrangement, identical areas of the specimen can be examined by either mode of operation. Surface charge buildup from the electron beam is especially critical in cathodoluminescence work. The entire fiber optic assembly is coated with silver, and the specimen surfaces are coated with vacuum evaporated aluminum. Optimum aluminum film thickness on the specimen is around 150 Å.

A P-16 phosphor is an ideal material to demonstrate cathodoluminescence, because maximum light output at 3850 Å matches the peak spectral response of the photomultiplier tube provided with the SEM. Secondary electron emission and cathodoluminescence micrographs of the same field of view of a P-16 phosphor powder sample are pictured in Fig. 2. A comparison of the two micrographs indicates various degrees of fluorescence among the individual phosphor particles. The high resolution possible with the cathodoluminescence mode is illustrated in Fig. 3 which shows a contact point of two phosphor grains at 21,000X. Resolution on this micrograph is approximately 750 Å. The cathodoluminescence image of a complex mineral specimen is illustrated in Fig. 4. Various degrees of fluorescence are demonstrated including a very long-persistence phase as indicated by the bright horizontal streaks. A very slow scan rate is necessary to produce satisfactory micrographs of materials containing long-persistence fluorescence.

High resolution cathodoluminescence mapping which is readily obtained with a SEM can provide valuable information concerning materials. While only one photomultiplier tube was available for this study, a wide spectrum of light emission can be observed by employing photomultiplier tubes having different spectral response peaks. Color pictures of cathodoluminescence can also be produced by standard color separation techniques.

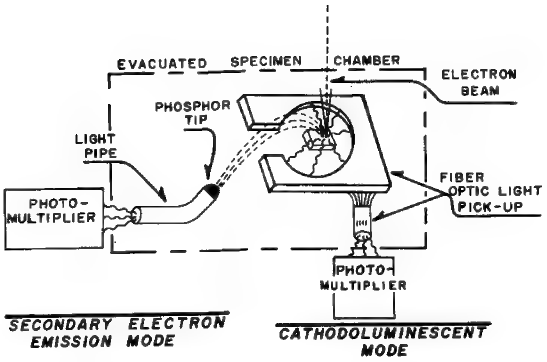

Fig. 1. Diagram of cathodoluminescence pickup device, scintillator light pipe, and photomultiplier tubes.

(a) (b)

Fig. 2. Comparison of secondary electron emission (a) and cathodoluminescence (b) images of P-16 phosphor. Accelerating potential 20 kV.

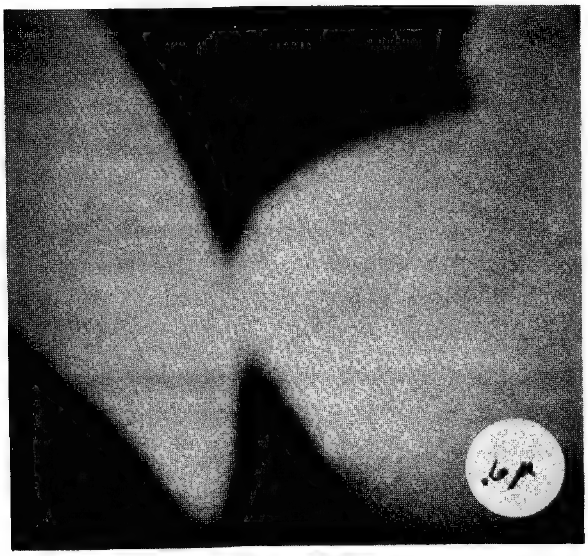

Fig. 3. High resolution cathodoluminescence image of P-16 phosphor. Accelerating potential 5 kV.

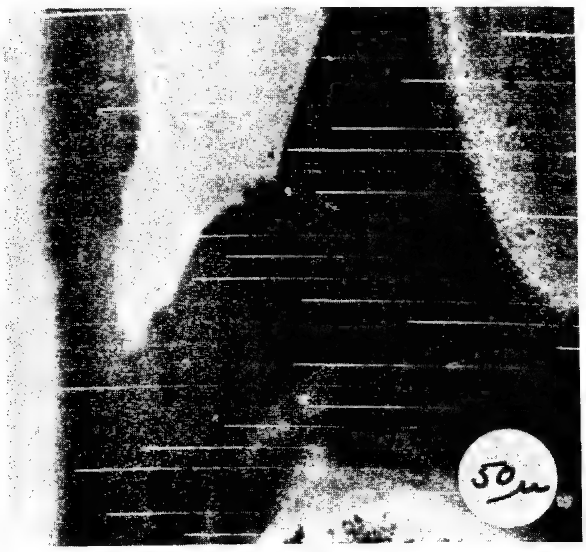

Fig. 4. Cathodoluminescence map of mineral with willemite, calcite, and unknown phase. Accelerating potential 20 kV.

DETECTION OF SECONDARY ELECTRONS WITH A CHANNEL ELECTRON MULTIPLIER

P. S. Ong

A channel electron multiplier has successfully been used by Hughes, Sulway, Wayte and Thornton (Communication in Journal Applied Physics, p. 4922, 1967) in a scanning electron microscope. Although the sensitivity is very good, the bandwidth is limited to 10 Kc.

Our experiments with the channel electron multiplier (Mullard B410BL) are concerned with their use as a particle counter for measuring extremely low currents (10^{-14}) as well as a mean current level detector with currents of 10^{-11} ampere and up.

The signal is picked up from both the "ground" side with a limited bandwidth but with a good low frequency response as well as at the "high voltage" side through a blocking condenser, as is illustrated in Fig. 1.

The signal at the "ground" side behaves rather peculiarly. The frequency response depends on the intensity of the input signal and shows a maximum for a certain input current level. At extremely low values of input current, the output is a pulse modulated signal and becomes more amplitude modulated as the separate pulses start to overlap. There is a range of input currents by which a maximum bandwidth with usable noise level is obtained. Further increasing the input signal causes the high frequency components to drop.

The "high voltage" side of the multiplier gives a signal which is usable in a wide range of input currents. Electron counting mode of operation (below 10^5 pulses/sec) goes gradually over into a mean level detection system similar to the "ground level" signal but high frequency components become more pronounced as the statistical noise level started to drop by increasing the input current.

In our present setup we use a blocking capacitor to isolate the high voltage. Electronic circuitry will be necessary to restore the very low frequencies. A low pass filter will also be useful to cut down excessive high frequency noise.

So far, good signal levels have been obtained using incident sample current of 10^{-11} to 10^{-6} ampere and 90 volt bias. The electron counting mode of operation could basically detect some 70% of every electron with an energy of greater than 200 volts (according to a report by the manufacturer).

Fig. 2 shows the relative counting rates of detected electron pulses vs. bias voltage, using an incident electron energy on the sample of 17 kV. This graph was obtained using our standard Norelco light element x-ray detection circuitry. It proves that this detector, when properly biased, is predominently a low energy electron detector.

The pulse counting mode, although theoretically more sensitive, proves to be rather disappointing for image formation. This is mainly caused by the fact that contrast enhancement cannot easily be done.

Several methods of coupling the output (which is at 2 to 4 kV above ground) to the amplifier (which is at ground potential) are now being evaluated for the open as well as for the closed end tubes.

Two important parameters now under investigation are the effect of lesser than good vacuum and the effect it has on the life expectancy of the multiplier.

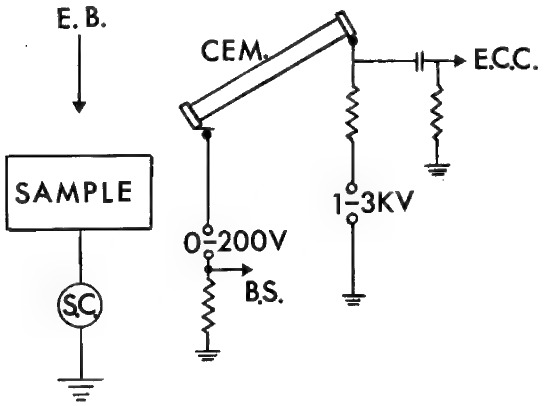

Fig. 1. Schematic diagram of the electrical circuit.

E.B.	Electron Beam
CEM	Channel Electron Detector
S.C.	Sample Current
B.S.	Beam Scanner
E.C.C.	Electronic Counting Circuit

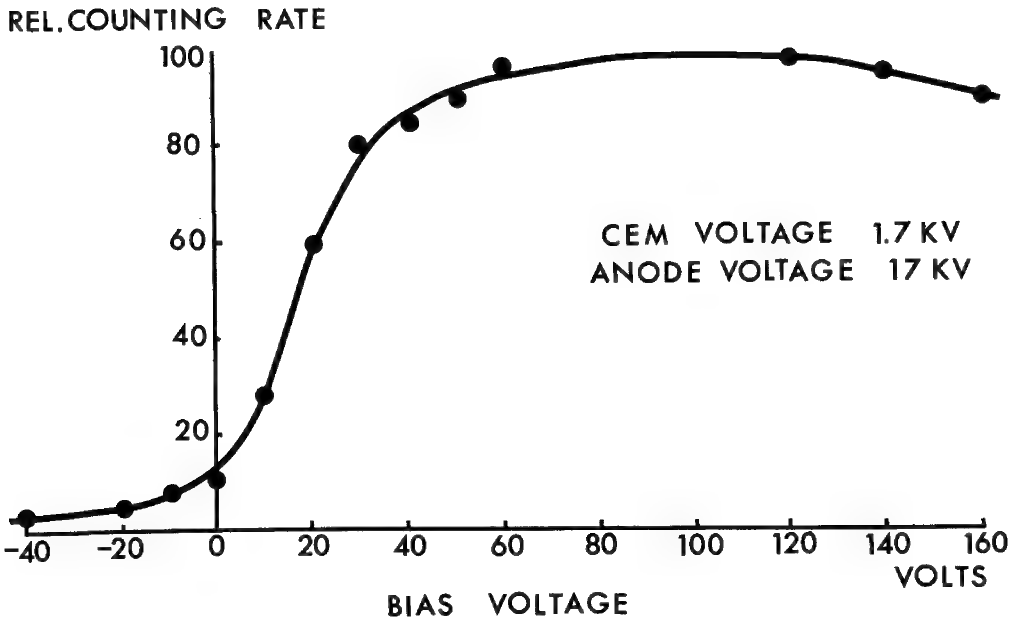

Fig. 2. Relative counting rate of detected electrons vs. bias voltage obtained with the circuit shown in Fig. 1. Pulses were measured at the point denoted by E.C.C.

PROGRESS IN ANALYTIC METHODS FOR THE ION MICROPROBE MASS ANALYZER

C. A. Andersen

The ion microprobe mass analyzer(1) permits the chemical analysis of a microvolume of the surface of a solid sample through the mass analysis of the constituent isotopes. This analysis is accomplished by bombarding the sample with a finely focused beam of high energy ions. The impinging primary ions lose energy through a series of atomic interactions to the atoms of the sample. A fraction of the sputtered atoms leaves the surface as ions and these secondary ions are collected and analyzed in a mass spectrometer.

Practical application of the ion microprobe requires a stable secondary ion yield. The ion yield should be high, permitting sensitive analysis and should be related to the atomic concentration of the atom at that point in the sample. Previous investigators employing the sputtering mechanism for the mass analysis of solids have used a primary ion beam composed predominatly of an inert gas such as argon. Experiments performed in this laboratory have shown, however, that this approach is unsatisfactory for the practical analysis of metals as the secondary ion yield is not constant and falls exponentially with time. This occurs because the secondary ion yield is very sensitive to the chemical state of the surface. The surface chemistry is in turn related to chemisorbed gases. Much higher ion yields are observed in the presence of such gas layers. The fall of the secondary ion yield under inert gas bombardment can be correlated with the removal of the chemisorbed gas layers under the eroding action of the primary ion beam. This behavior is shown in Fig. 1a. The final value of the ion yield is determined by the equilibrium established between the sample, the bombarding primary ions and the arrival rate of reactive gases from the residual atmosphere in the instrument. It is important, therefore, to keep the composition of the surface layer constant under the action of the sputtering beam.

We have found that it is possible to control the composition of the sputtered layers by using a primary ion beam consisting of a reactive gas. In this way the arrival rate of the reactive gas and the rate of bombardment are equal and it is possible to establish and maintain a constant composition having high secondary ion yield. This result is illustrated in Fig. 1b. Once such a layer is formed its composition is independent of current density and secondary ions are produced in direct proportion to the primary beam current.

Relative ion yields for many different elements and compounds have been experimentally determined using a variety of reactive gases in the primary bombarding beam. The compounds studied have high ion yields. The yield of Al^{+}_{27} ions from Al_2O_3 can be seen in Fig. 1c. Both positive and negative mass spectra have been studied and it is observed that ions with high electron affinity are abundant in the negative spectrum while those with low affinity are abundant in the positive spectrum.

The instrument using the methods of analysis proposed here produces a highly sensitive isotopic analysis of the surface of the sample. Trace analyses performed to date indicated mass detection sensitivities on the order of a few parts per million to a few parts per billion. For example, using a 10kV monatomic oxygen beam, 0.01% Mg and 0.10% Fe in Al gave 80,000 and 52,000 c/sec respectively. These count levels are equivalent to detection limits of about 20 and 100 PPB for integration times of one second using a 3σ deviation of the background. The ability to analyze the uppermost surface layers of a material is of great importance in many areas of research such as catalysis chemistry and corrosion studies. For example, we have observed that the oxidized phase on the surface of 304 stainless steel is predominatly Cr. The instrument would appear to have great promise in areas where isotope analysis on a micron scale is important. Such areas include geochemical and biochemical problems, radio-acitve age dating and self-diffusion studies.

---

1. C. F. Robinson, H. J. Liebl, C. A. Andersen, Third National Conference on Electron Microprobe Analysis, Chicago, 1968.

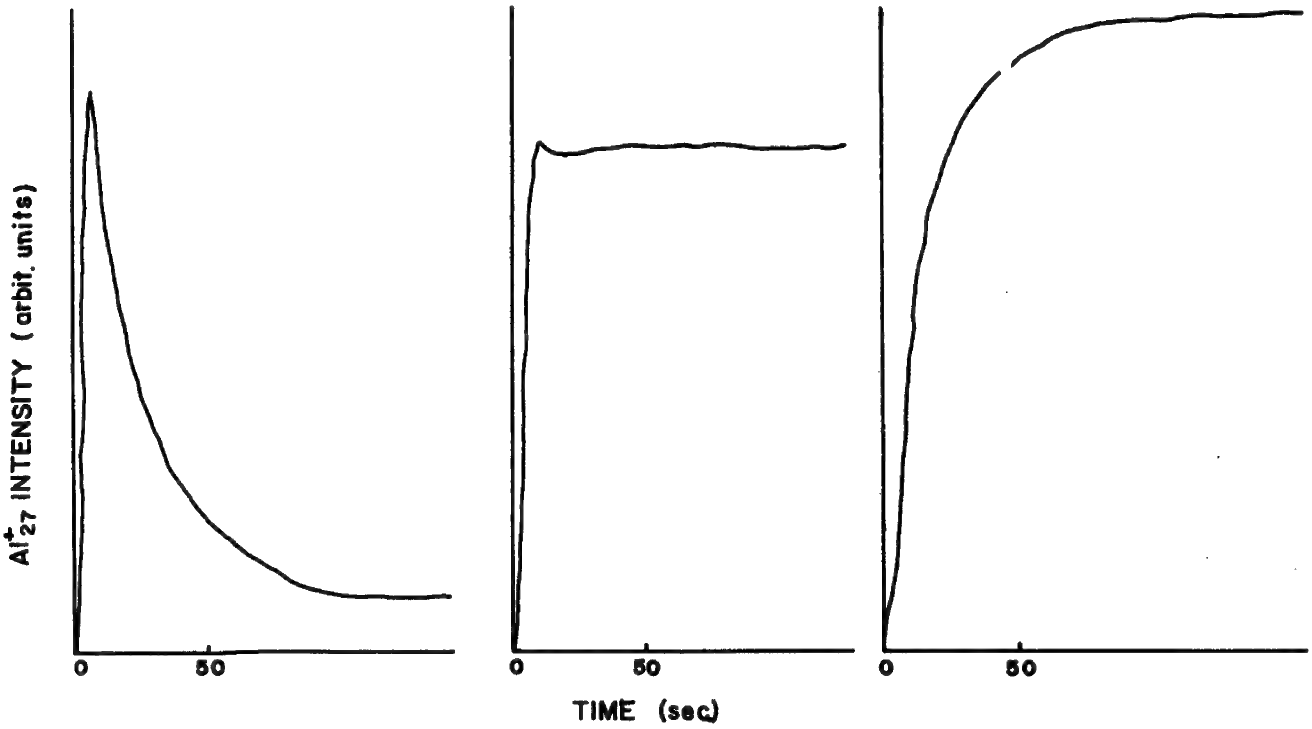

(a) 100% Al; Argon Primary Beam

(b) 100% Al; Oxygen Primary Beam

(c) Al_2O_3; Oxygen Primary Beam

Fig. 1. Al^{+}_{27} Intensity As A Function Of Time

A SECONDARY ION EMISSION MICROANALYZER

J. M. Rouberol, J. Guernet, P. Deschamps, J. P. Dagnot,
J. M. Guyon de la Berge and C. M. Judson

An improved version of the Secondary Ion Emission Microanalyzer of Castaing and Slodzian(1) has been designed. This version uses a double filtering system(2) with magnetic filtering of mass and electrostatic filtering of energy. It also has provision for observation of images of either positive or negative ions, and permits four alternative methods of observing images.

The basic ion optical system consists of a sputtered ion source, an ion accelerating lens, and a stigmatic mass spectrometer with energy filtering. A 10 kV primary beam of argon ions is generated in an RF source and condensed with an electrostatic lens to a 15μA beam on an area with a diameter of 0.3 mm. The secondary ions emitted are accelerated to an energy of 5 kV and simultaneously focussed by an electrostatic lens into a beam which carries an image of all of the types of ions extracted. This image is not allowed to form but is filtered in mass by a magnetic field and in energy by an electrostatic mirror. The mirror being convex and the magnetic filtering being made by two deflections in opposite directions, the angular dispersion is small and the chromatic aberrations are minimized. Because of the non-normal entry of the beam into the magnetic field, the fringing field has a transverse focussing action on the beam. By proper selection of the angle of incidence, the transverse and radial focal points can be made to coincide forming a stigmatic image.

After the second magnetic deflection, the ions enter the image converter which consists of a post-acceleration lens, a projection lens, and the image converter itself. This is an immersion lens whose cathode is bombarded by the ion beam and emits secondary electrons. The lens system projects the image on the cathode of the converter. The secondary electrons emitted are accelerated to 30 kV in the opposite direction and are focussed by the lens of the converter as an electron image which can be observed on a fluorescent screen.

The image converter can be used in four ways. 1) for visual observation, displaying the image on a fluorescent screen which is observed in transmission by a 5 power microscope, 2) for image recording, recording on film in a camera placed within the converter chamber, 3) for measuring current from a small area, replacing the fluorescent screen by an aperture corresponding to a sample diameter of several microns, and measuring the current with a scintillator coupled to a photomultiplier, and 4) for measuring current from a large area, using an aperture corresponding to a diameter of the order of 100 microns. The choice of these different modes of measurement is made by use of a moveable magnetic prism which can be rotated about the axis of the converter to deflect the electron beam to the camera or to the aperture holder, and the adjustment of the aperture holder which selects the use of a fluorescent screen or one of two apertures.

The performance of the instrument can be described by the mass and spatial resolution, the sensitivity, the time required to make a measurement and the resolution in depth. The mass resolution is 350 with 10% valleys between peaks. The spatial resolution is one micron at the center of the image. The magnification is of the order of 100 so that one micron is magnified to 0.1 mm on the film.

The sensitivity is determined by the collection efficiency, the transmission of the ion optical system and the sensitivity of the detector. The efficiency for collecting and transmitting ions is high. The limiting angle for collection of ions is 20 degrees for 1 volt ions and 9 degrees for 5 volt ions at the aperture settings used for maximum resolution. When used with a pulse height analyzer, the detector can detect a few ions per second; when used with a current amplifier, an ion current of 10^{-16} amperes can be detected.

The time required to record an image on film varies from a few milliseconds to a few tens of seconds. The amount of material sputtered during this time is of the order of one atomic layer. Because of penetration of the primary ions into the target, the resolution in depth is not equal to a single atomic layer but is of the order of 50 to 100 Å.

A variety of applications of the instrument have been studied. The most important advantage over the electron microanalyzer is probably the resolution in depth. The application to isotope analysis, which is not possible with the electron probe, has been demonstrated by a study of the diffusion of oxygen isotopes in uranium oxide. Application to the entire periodic table including the lightest elements can be demonstrated. In some cases at least, sensitivity exceeding that obtained in the electron probe can be obtained. Finally the image can be continuously observed while moving the sample without any limitation caused by the time required to scan a picture.

---

1. Castaing and Slodzian, Jour. de Microscopie, 1, 395, (1962).

2. Proceedings of the 4th International Congress on X-ray Optics and Microanalysis, p. 48, Hermann (publisher) Paris, 1966.

BERYLLIUM DETERMINATION IN MICROPROBE ANALYSIS

S. Kimoto, H. Hashimoto and H. Uchiyama

In the most recent microprobes, a stearate multilayer analyzer is used for the x-ray analysis of light elements heavier than boron. Other multilayer analyzers, having a larger 2d spacing than that of stearate, have been developed to expand the detectable wavelength region to include beryllium x-rays.

Lead lignocerate, cerotate and melissate analyzers, which have 2d spacings of approximately 130, 140 and 160Å respectively were deposited on a mica base by a method similar to that used for a lead stearate crystal. The radius of the focusing circle of the analyzer was 140 mm, and the take off angle of x-rays was 40 degrees. A gas flow proportional counter with a thin nitrocellulose film was used for detecting boron, carbon, etc. x-rays. The flow gas mixture was 90% argon and 10% methane.

In the case of the lead lignocerate analyzer, the peak intensity for pure beryllium was 1000 cps with an accelerating voltage of 10 kV and a probe current of 1.0μA. This intensity was equal to 1/18th of that for pure boron under the same conditions. The peak intensity to background ratio was 30, and the sensitivity was 0.16 wt% when measured for 100 seconds under the above conditions. The above sensitivity is defined as

$$s(wt\%) = \frac{2(2)^{\frac{1}{2}}\, w(B)^{\frac{1}{2}}}{(P-B)\,(t)^{\frac{1}{2}}}$$

where w represents the weight percentage of the measured element in a specimen, P the peak intensity in counts per unit time, B the background intensity per unit time and t the measuring time.

The melissate analyzer has not as yet performed as well as the lignocerate analyzer. The peak intensity is 30 cps and the background 4 cps for an incident beam of 10 kV and 1μA.

The lignocerate analyzer was applied to Be-35% Mo, Al-5 to 13% Be, Ni-1 to 5% Be and Cu-4% Be alloys. Fig. 1 shows the beryllium distribution in the Al-Be alloy. Beryllium is concentrated at the grain boundaries, and the concentration is nearly 100%. Fig. 2 shows the application to the Be-Mo alloy. The dark phase in the composition image contains 94% beryllium and the bright phase, 67% beryllium. The beam conditions in the above applications were 10 kV with 0.3 and 0.5μA respectively.

Practical sensitivity is indicated by the results of the Cu-4% Be analysis. The peak intensity of beryllium radiation was 964 counts for conditions of 10 kV, 0.35μA, and 100 seconds measuring time. The background intensity, which was measured using pure copper and setting the spectrometer at the same position as that for measuring above peak intensity, was 868 counts. This means that beryllium contained in such materials as copper is detectable even if the concentration is lower than 4%.

All above applications have been done with a beam voltage of 10 kV. As occurs in the case of other light elements, however, lower beam voltage givesbetter results for some specimens. Surface contamination generated by probe bombardment greatly reduces the intensity of beryllium radiation. A liquid nitrogen cooling finger was effectively used in this case.

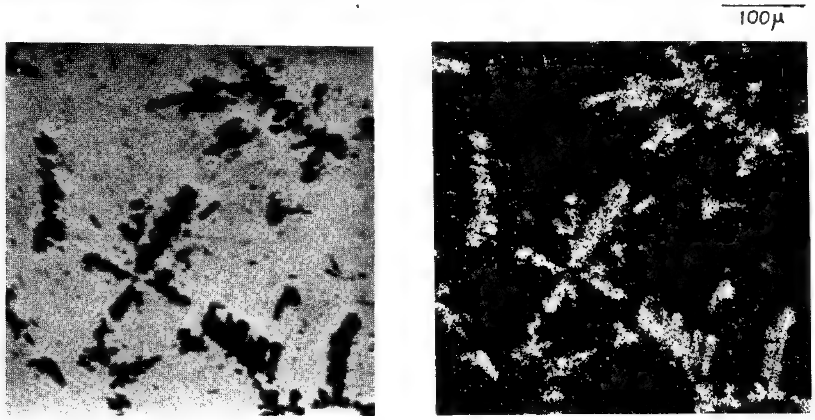

a. Composition b. Be Kα X-ray image

Fig. 1. Analysis of an aluminium-beryllium alloy

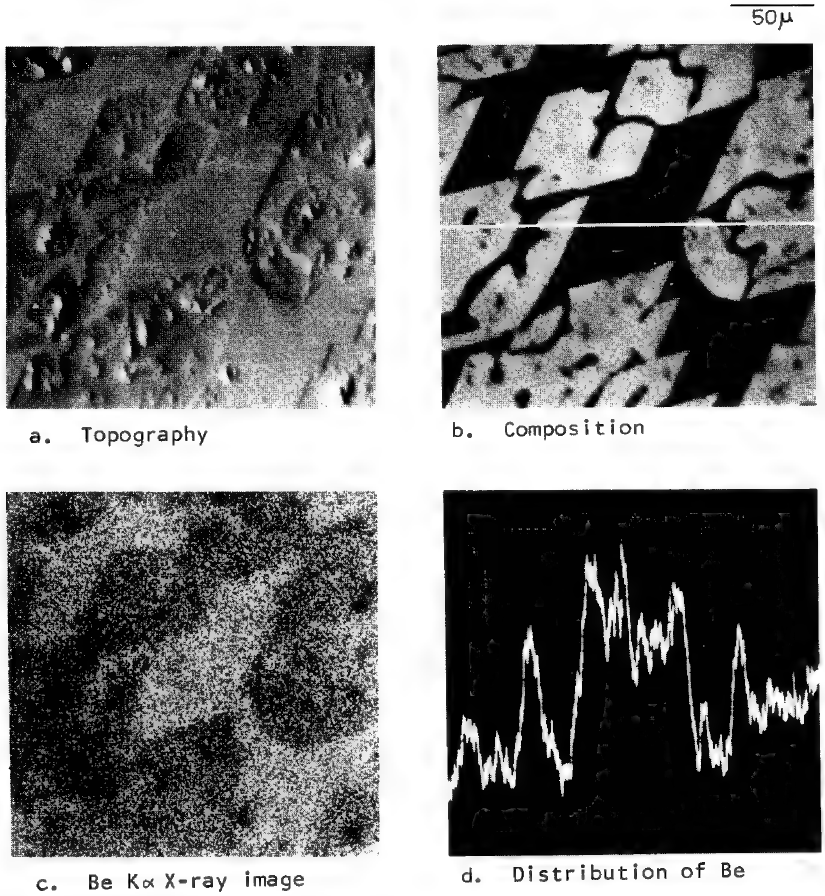

a. Topography b. Composition

c. Be Kα X-ray image d. Distribution of Be

Fig. 2. Analysis of a beryllium-molybdenum alloy

THE USE OF BLAZED GRATINGS IN THE ELECTRON MICROPROBE

James B. Nicholson

Several years ago, it became obvious that work in the ultrasoft x-ray region would be severly limited by the lack of proper diffraction crystals. At that time, this laboratory began a study of the requirements necessary for high grating efficiency in this region. This paper will outline the results of that study with illustrations of performance in the 20 - 170 A region and the analysis of carbon in steel with a limit of detectability of 100 ppm.

Blazed gratings, if properly used, can enhance a diffracted line, thus improving system sensitivity. Blazed gratings were originally developed to improve efficiency in the region of optical spectra. The ruling diamond is tilted to some angle with respect to the ruling surface so that as it rules, it deforms and inclines the surface instead of removing it. The magnitude of the deformation at the surface is a function of the angle of contact between the ruling diamond and the grating surface. Imperfections that occur near the outer edge of the groove are eliminated by replicating the ruled surface. The imperfections then appear at the bottom of the groove and the sharp edge ruled by the diamond point appears on top. Thus the original surface has been replaced with ruled areas consisting of a narrow land for each groove that is tilted at an angle β, termed the blaze angle, with respect to the original grating surface. These tilted plane rulings specularly reflect when the angle of incidence and reflection to the grating land are equal. Thus by an appropriate choice of blaze angle it can be arranged that the incoming radiation is specularly reflected to the position on the focal circle where the diffraction line appears.

In the soft x-ray region, metals may have indices of refraction slightly less than unity, so that total reflection can occur near grazing incidence. This suggests that blazed gratings used near grazing incidence should have much higher efficiency in x-ray diffraction than crystals. However, because of the relatively short wavelengths involved, reflectance is markedly impaired by grating imperfections such as surface roughness or surface corrosion that would be imperceptible at optical wavelengths.

The reflectance is very selective below 80 Å, that is, there is a unique imput angle where intensity can be maximized as a function of wavelength.(1) This characteristic not only provides the possibility of line enhancement but can also allow physical discrimination against second order short wavelength radiation, thus improving line-to-background ratios. A comparison of the grating system with a pseudo-crystal system indicated that on the basis of equal solid angles, the grating system was 22 times as efficient.(2)

Problems of efficiency dropoff due to contamination have been minimized to the point where no measurable effects have been noticed in 8 months of continuous operation.

The resolution of the grating spectrometer in the microprobe has proven to be as good as that obtained in conventional spectrometers that utilize a true primary slit instead of the electron spot. Fig. 1 is a wavelength trace of Si_L(135.5 Å) from pure silicon. The shape and wavelength position of this band compares favorably with that reported by Ershov and Lukirskii.(3)

---

1. J. B. Nicholson, C. F and G. L. Griffin, Adances in X-ray Analysis, Vol. 8, 309, 1965.

2. J. B. Nicholson and M. F. Hasler, Advances in X-ray Analysis, Vol. 9, 420, 1966.

3. O. Ershov and A. P. Lukirskii, Soviet Physics-Solid State, 8, #7, 1966, Jan., 1967.

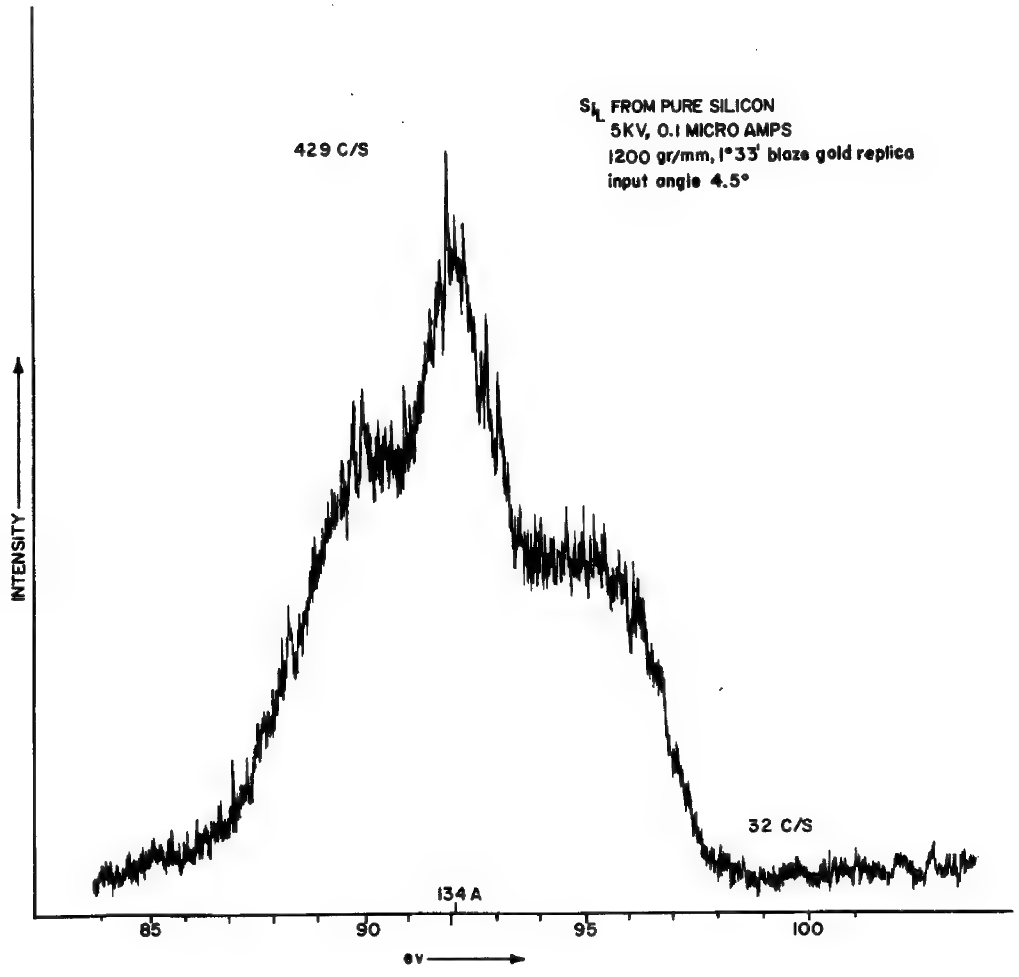

Fig. 1.

IMPROVEMENT OF THE "BUILT-UP ANALYZING CRYSTAL"

H. Okano, T. Tomura and K. Hara

Improvements in the energy dispersion characteristics of "built-up analyzing crystal" will be reported. A sharp spectral line results in good wavelength resolution, a high line-to-background ratio, and it gives information on the state of emission bands.

The measured width of a spectral line is affected by the components described below:

1. The natural width of the characteristic line.
2. The geometrical condition of the spectrometer.
3. The effective number of layers in the "built-up crystal" that contribute to diffraction.
4. The degree of misorientation in the "built-up crystal".

To obtain a good geometrical condition in soft x-ray spectroscopy, a Johansson type "built-up crystal" was developed. It is impossible to grind the surface of a "built-up crystal" as is done with ordinary crystals so the soap-films were built up on a specially designed base that had several curved steps on its surface. In the low atomic number region the characteristic x-ray peaks have considerable natural breadth. Therefore, the tolerance in the Bragg diffraction law is fairly large and a "pseudo-Johansson type" crystal gives satisfactory results. For example, a three-step, 40 mm long Johansson type "built-up Pb-stearate crystal" has a maximum $\Delta\theta$ of 2.2×10^{-3} rad. in the case of C-K line analysis, which is only 20% of that of the ordinary Johann case. This $\Delta\theta$ is nearly equal to the corresponding $\Delta\theta$ for the natural breadth of C-K line.

The width of the spectral line ($\Delta\lambda$) is related to the effective number of layers of the "built-up crystal" as follows,

$$\Delta\lambda = 1.28\, d^2 \mu_l$$

where d is the spacing of the crystal and μ_l is the linear absorption coefficient of the crystal for the x-rays to be analyzed. In accordance with this result, a reduction of the fraction of metal atoms in the "built-up crystal" was tried.

A small spacing also gives a good energy dispersion. Namely, from the Bragg diffraction law,

$$d\theta/d\lambda = \tan\theta/2d$$

is obtained. To realize this improvement, a built-up Pb-tridecanoate and Pb-laurate crystal were examined.

By the improvements mentioned above, a half width of 1.32 Å for the C-K spectral line from a graphite specimen was obtained and its profile fitted satisfactorily that obtained with the optical grating. The peak-to-background ratio of the C-K line was increased 3 to 5 times compared with the ordinary case and the "built-up Pb-laurate crystal" also gave good analyzing sensitivity in the analysis of fluorine.

CORRECTION FOR COINCIDENCE LOSSES AND DETERMINATION OF DEADTIME IN THE ELECTRON PROBE X-RAY MICROANALYZER

F. Borile, M. A. Short and J. Tabock

In quantitative electron probe microanalysis, pure elements are frequently used as standards which give rise to high x-ray intensities. It is necessary, therefore, to correct for coincidence losses occurring in the detectors and counting electronics. Two methods have been used in the present work to correct for coincidence losses: the ratio method described by M. A. Short(1) to determine the linear region of the counting system and the corrections above this region; and the deadtime determination method suggested by K. F. J. Heinrich, D. Vieth and H. Yakowitz,(2) the true counting rate being then calculated from the well-known formula $N = N_o/(1-\tau N_o)$.

In applying Short's method to the determination of coincidence loss corrections on our Applied Research Laboratories EMX electron probe microanalyzer, we have measured the intensities of the ZnKα and ZnKβ lines simultaneously on two spectrometers over a wide range of counting rates. Fig. 1 shows the ratio of the observed intensities plotted as a function of the observed ZnKα intensity. At low counting rates this ratio was found to be constant, implying that there were no detectable counting losses in this region; as the losses become appreciable, the ratio, of course, decreases. Because the two detection systems may have different deadtimes, measurements of the two lines were made on both spectrometers. The two Kβ/Kα ratios are shown in Fig. 1 from which it can be seen that the two systems do have different deadtimes. Correction factors were then obtained from this data using iterative procedures(1) and are shown in Fig. 2. Calculations were also made of the effective deadtimes of the two systems using the formula already quoted, assuming it is applicable to the system. The results are shown in Fig. 3 from which it can be seen that the effective deadtimes are functions of the counting rate. The particular advantages of the ratio method are that the accuracy of the correction factor depends basically on x-ray counting statistics, that there need be no mechanical movement of the spectrometers, and that there are no deleterious effects on the ratio due to drift in the beam current or to contamination.

The deadtimes of the two counting systems have also been determined using the method of Heinrich, et al. Fig. 4 shows linear and logarithmic plots of N_o/i vs. N_o for one spectrometer, where N_o is the observed counting rate and i is the sample current. From the linear plot, the deadtime for the system was calculated to be 1.44 microseconds. Using this value, correction factors have been calculated and are shown in Fig. 2.

It can be seen that there is a descrepancy in the correction factors given by the two methods. If the ratio method suggested by Short yields a

reproducible linear region of nondetectable coincidence losses, a plot of N_o/i vs. log N_o should give the same linear region assuming that the sample current can be measured with an accuracy of considerably better than 1% and that the sample biasing effect(2) can be corrected. If we consider that in our experiment the linear region was determined with sample current values from approximately 1 to 10 nanoamp, an accuracy of even 1% in the current measurement is not easily obtainable. Beam current measurements could not be used in our experiment since they were found not to be proportional to the sample current over the full range. The logarithimic plot in Fig. 4 indicates a possible linear region, and the dotted line in the same plot indicates the effect of applying a zero correction of .018 nanoamps to the measured values of sample current. On the linear plot, it is possible that, due to the compression of the abscissa, the constancy of the ratio at low counting rates could be overlooked, deriving therefore the deadtime from the measurement at high counting rates. The dotted portion of the plot is due to the extreme amount of pulse shrinkage above 45000 cps.

Both methods present instrumental difficulties. In the ratio method(1) the linear portion of the curve must be defined very accurately and since this region is obtained at low counting rates, which implies long integration time to obtain good statistics, particular attention must be paid to overall stability of the instrument (temperature, sample stage movement, etc.). In the linear method, the accuracy of the sample current measurement is the determining factor. Instability of the voltage to frequency converter or of the digital voltmeter, used in measuring the sample current, together with the drifting of the zero setting, which is affected by the overall noise of the system, seriously compromise the accuracy at low sample current values.

---

1. M. A. Short, Rev. Sci. Inst., 31, 618, 1960.

2. K. F. J. Heinrich, D. Vieth and H. Yakowitz, Advances in X-ray Analysis, Vol. 9, Plenum Press, New York, 1965, p. 208.

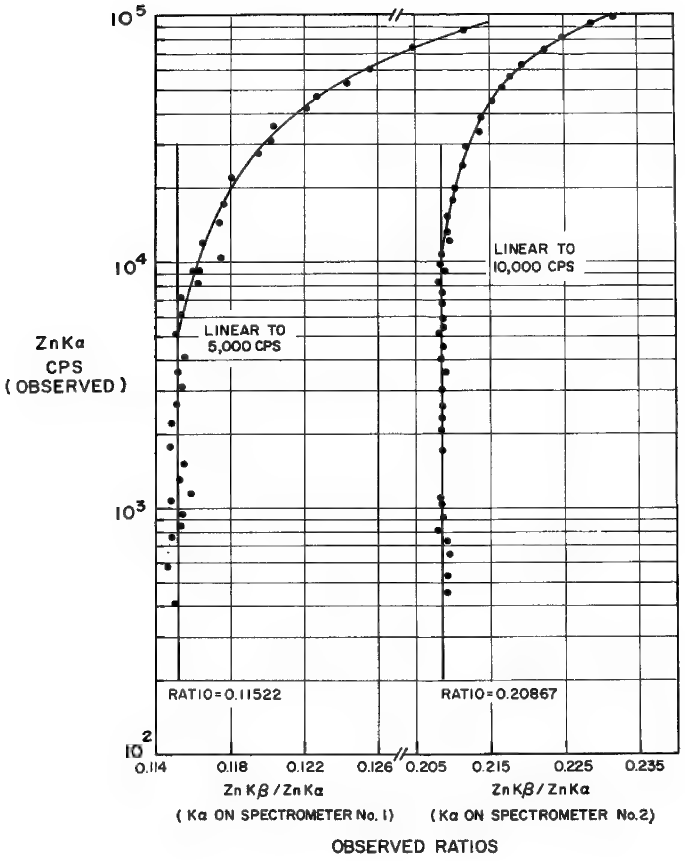
10^5
10^4
10^3
10^2
ZnKα
CPS
(OBSERVED)
LINEAR TO
5,000 CPS
LINEAR TO
10,000 CPS
RATIO=0.11522
RATIO=0.20867
0.114
0.118
0.122
0.126
0.205
0.215
0.225
0.235
ZnKβ/ZnKα
(Kα ON SPECTROMETER No. 1)
ZnKβ/ZnKα
(Kα ON SPECTROMETER No.2)
OBSERVED RATIOS

Fig. 1

Fig. 2

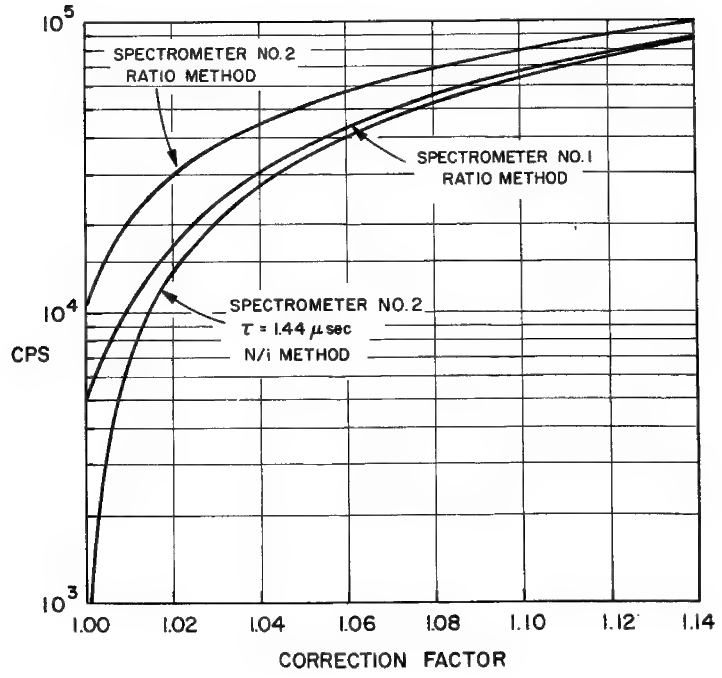
10^5
10^4
10^3
CPS
SPECTROMETER NO.2
RATIO METHOD
SPECTROMETER NO.1
RATIO METHOD
SPECTROMETER NO.2
τ = 1.44 μsec
N/i METHOD
1.00
1.02
1.04
1.06
1.08
1.10
1.12
1.14
CORRECTION FACTOR

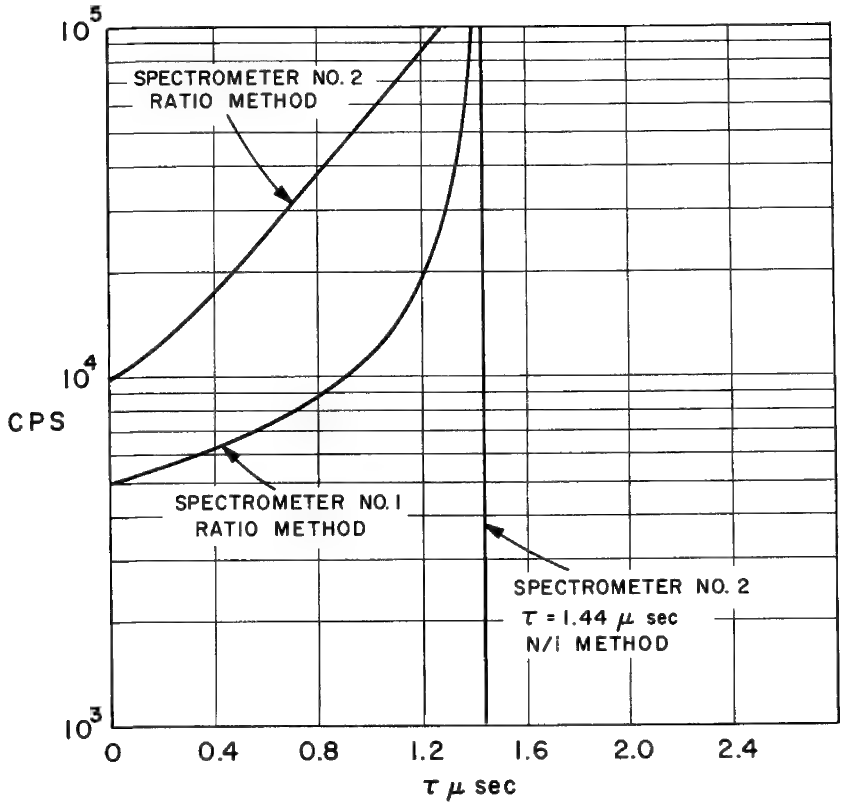

Fig. 3

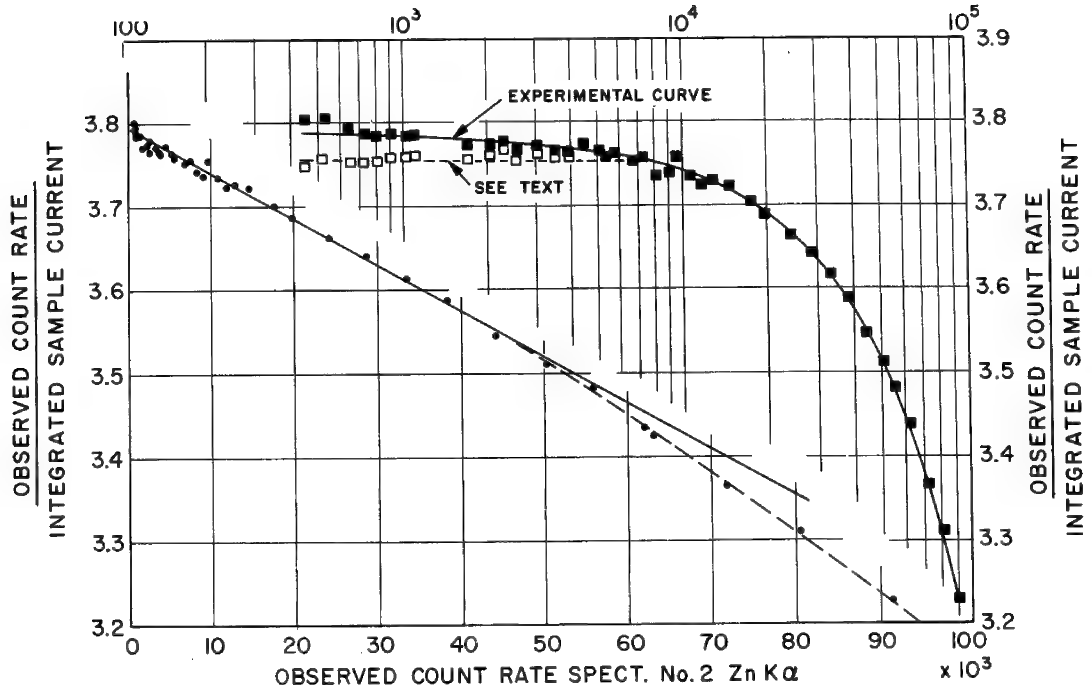

Fig. 4. Deadtime determination using sample current measurement.

A STATISTICAL EVALUATION OF THE X-RAY INTENSITY MEASUREMENTS FOR AN ELECTRON MICROPROBE ANALYZER

James P. Smith and John E. Pedigo

The use of normal Gaussian statistics to estimate the precision of an electron microprobe analysis has been criticized by many analysts as being too optimistic. Many analysts list a standard deviation three times larger than the square root of the count total. This practice admits some uncertainty as to the precision of the data and should be examined in more detail. Quantitative evaluations of the factors which determine the precision of an analysis under actual experimental conditions are reported here, made on the MAC model 400 electron microprobe analyzer. Different electron microprobes will yield different results, yet general trends as well as a demonstration of a need for such evaluations were elucidated.

The major cause of poor precision is the difficulty in reproducing the sample placement(1). The x-ray spectrometers and the optical microscope are focused to the same point, proper sample placement being effected by focusing the microscope. Thus, precision is a function of the relative depth of focus of the light and x-ray optics. The depth of focus of a refractory microscope depends on the numerical aperture (N.A.) of the objective lens. The depth of focus of the spectrometer is dependent on the design, geometry, diffracting crystal and the 2θ setting.

Several sets of 80 x-ray intensity measurements were made using high purity elemental samples (gold, tin, iron, titanium, and aluminum). Over 10,000 measurements were recorded on punched tape and computer processed. The effect on precision of the 2θ settings, the diffracting crystals, and microscope objectives were evaluated. Three microscope objectives were available with N.A. values of 0.13, 0.23 and 0.33; three pairs of diffracting crystals were used (LIF, ADP and KAP); x-ray lines at several 2θ settings for each crystal were used. The optical focusing was repeated between each measurement using each of the three objectives. The ratio of the count variance to the mean count was calculated as a measure of the precision. The chi square distribution predicts that this ratio would be in the range 0.7 to 1.3 if the distribution of counts was determined only by random photon emission.

The results are summarized in Figs. 1 and 2. No significant difference was observed in the variance to mean ratios for the ADP and LIF crystals. Fig. 1 shows that the precision of an analysis is determined solely by random counting when the 0.33 N.A. objective is used with an ADP or LIF crystal set at a 2θ value greater than 50^{o}. The majority of analyses are made in this wavelength range. The ratio of variance to mean obtained with the KAP crystals was quite large, quantitative work being impossible using the 0.13 N.A. objective. One

would expect the lower resolution crystals to produce the larger spectrometer depth of focus but this is also a function of the d spacing of the crystal. For the MAC spectrometers, a change in the sample placement, ΔZ (in microns), along the optical axis produces a change of

$$\Delta\lambda = 8 \times 10^{-6} \, d \, \cot\theta \, \Delta Z$$

in the measured wavelength. This equation explains qualitatively the curves in Fig. 1, but experimental evaluations are required to fully characterize the precision of a given analytical arrangement.

Interchanging crystals in spectrometers and defocusing the spectrometers slightly to one side of the peak did not significantly effect the variance to mean ratio. The background noise did not remain strictly random as one might expect but demonstrated trends similar to x-ray peak measurements.

The precision of an electron microprobe analysis can not be simply estimated. One should be conservative in these estimates but not too pessimistic. These experimental evaluations have shown that the precision of microprobe data appears to be clearly related to the experiment arrangement. Since good counting statistics can be achieved on homogeneous samples with proper focus, the poor precision that is often observed must be due to other factors (i.e. sample charging, sample homogeneity, surface contamination, surface roughness or unstable electronics).

---

1. T. O. Ziebold, Anal. Chem. 39, 858 (1967).

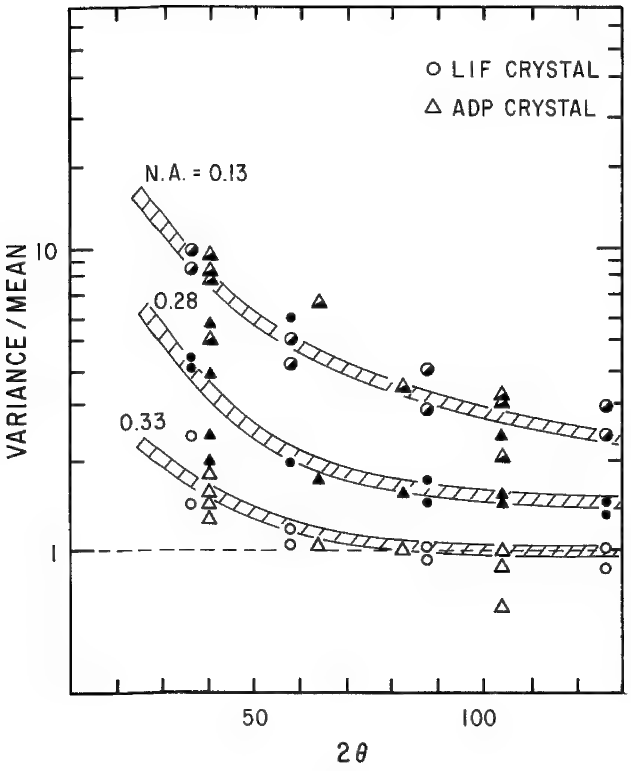

Fig. 1. The variance to mean ratio observed while using various objectives and wave length settings for the ADP and LIF crystals.

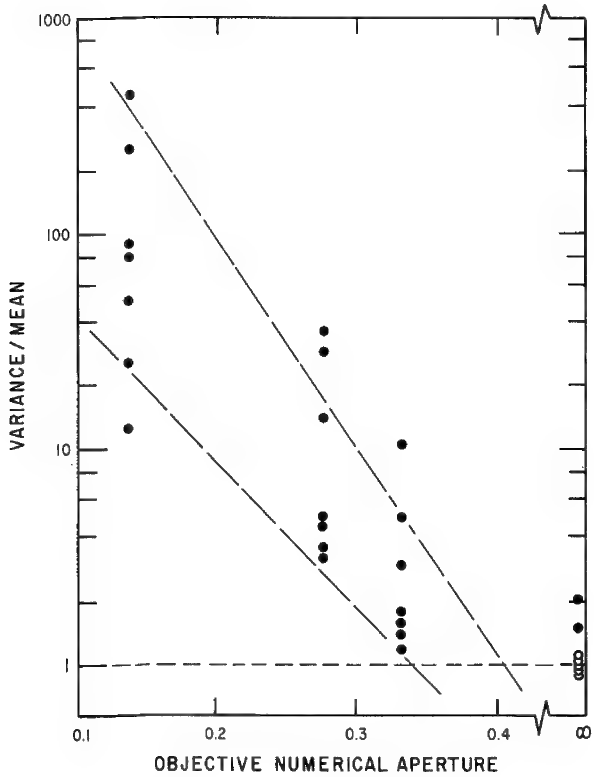

Fig. 2. The variance to mean ratio observed while using various light optical objectives for the KAP diffracting crystal.

FURTHER STUDIES ON MECHANISM OF GAIN SHIFT IN FLOW PROPORTIONAL COUNTERS

N. Spielberg

Evidence has previously been gathered to indicate that the counting rate dependent gain shift in flow proportional counters is related to the adsorption of gas, possibly debris from the quench component of the counter gas filling, on the anode wire(1). It was argued that the adsorbed gas was released from the surface of the wire under the average action of the counter avalanches, and this gas either captured electrons from the final stages of the individual avalanche or increased the amount of energy required to create ion pairs in the final stages of the avalanche. The rate of evolution of the adsorbed gas should be dependent upon the density per unit time, per unit area of anode wire, of the charge transported to the anode wire by the avalanches. This would account for the observed dependence of the shift on counting rate, gas gain, anode wire diameter and counter geometry. Subsequent further work carried out at this laboratory encountered considerable difficulty in reproducing earlier results; in fact, it became quite difficult to produce significant shifts in some of the wire materials which had earlier shown the effect.

It was finally observed that if a counter tube having a 50 micron stainless steel wire was conditioned by setting it into self-sustained discharge for a period of about two hours, then all the previously observed gain shift symptoms were obtained including various time constant effects. It was possible to recondition the counter tube to obtain "shiftless" operation by placing the tube in high vacuum and glowing the anode wire at a dull red color for about 30 minutes at a pressure of 10^{-6} torr. No other bakeout or processing of the counter tube envelope was necessary. This process of deteriorating the counter tube characteristics by setting it into discharge and then reconditioning it by high vacuum bakeout of the anode wire could be repeated several times.

Examination of the anode wire under the microscope showed it to be essentially clean and smooth prior to deterioration. After deterioration it was apparent that there was a thin film on the surface of the wire. This film was not uniform, but tended to be localized on certain portions of the wire. After the bakeout, this film was no longer visible.

It may be inferred from the above results that setting the counter tube into a self-sustained discharge is effectively a very rapid "aging" process, and is equivalent to a long term operation of the counter tube at high counting

rates. To check this equivalence, an experiment was performed in which the counter tube was operated at rates approximating 10^5 counts/second over a period of several days, and it was shown that the shift phenomenon could be observed after that time. This counting rate, at the level of gas gain used, results in an integrated signal current of 2 to 4 nanoamperes. The self-sustained discharge, on the other hand, was carried out at a level of about 1 microampere. Presumably, it should be possible to draw a correlation between the amount of electric charge passing through the counter and the amount of "debris" deposited on the anode wire, and thereby estimate a useful lifetime for a given counter before the onset of serious intensity-dependent gain shift effects. It might be expected that this lifetime would depend upon the gas gain, the energy of radiation absorbed in the counter gas, the anode wire diameter, the anode wire material and treatment, and the geometry in which the counter is used.

A useful way of studying some of these dependencies, in particular the role of the anode wire diameter and its material and treatment, is by means of rapid aging of the counter tube by the continuous discharge technique. Using this technique we do verify that the lifetime increases with increasing anode wire diameter, and is affected by the anode wire material and treatment. We are as yet unable, however, to specify a best material, although it is clear that glowing the wire in vacuum to clean it up is beneficial.

These experiments may be taken to be additional evidence pointing to the role of adsorbed gas from the anode wire in the counting-rate dependent gain shift phenomenon.

---

1. Spielberg, N., Rev. Sci. Instru., 37, 1268 (1966); 38, 291 (1967); Trans. Second National Conf. Electron Microprobe Analysis, Boston (1967), paper no. 55.

ADDITIONAL DIFFRACTING PLANES IN EDDT CRYSTALS

R. D. Wantman and G. A. Hutchins

Fairly strong additional diffraction peaks have been measured for x-ray lines in the wave length range from 1.2 to 2.8 Å with EDDT analyzing crystals. These extra peaks are important because they may be confused with emission lines from other elements diffracted from the (020) lattice spacing of 4.404 Å.

The relative intensity of the extra lines is greatest for hard radiation, indicating that the corresponding diffracting planes may be present only at some depth within the crystal. The additional peaks are broader than (020) diffraction lines and some show a tendency to double or split. Maximum intensity for the extra lines occurs at a slightly different spectrometer alignment than for the (020) lines. This indicates that the additional planes may be more pronounced in one portion of the crystal or that they are not exactly parallel to the (020) planes.

All additional K diffraction peaks occurring between $2\theta = 36^{\circ}$ and 140° are listed in the table. Additional L diffraction peaks are also observed. The extra peaks fall into three series labeled X, Y and Z. The X series has an average d spacing of 2.92 Å and could correspond to (300) or $(\bar{1}02)$ planes of EDDT. The Y and the much weaker Z series have d spacings of 1.75 and 1.25, respectively, and are unidentified.

The two crystals studied showed qualitative agreement, but it is expected that other crystals may show more, less or none of the extra reflections discussed.

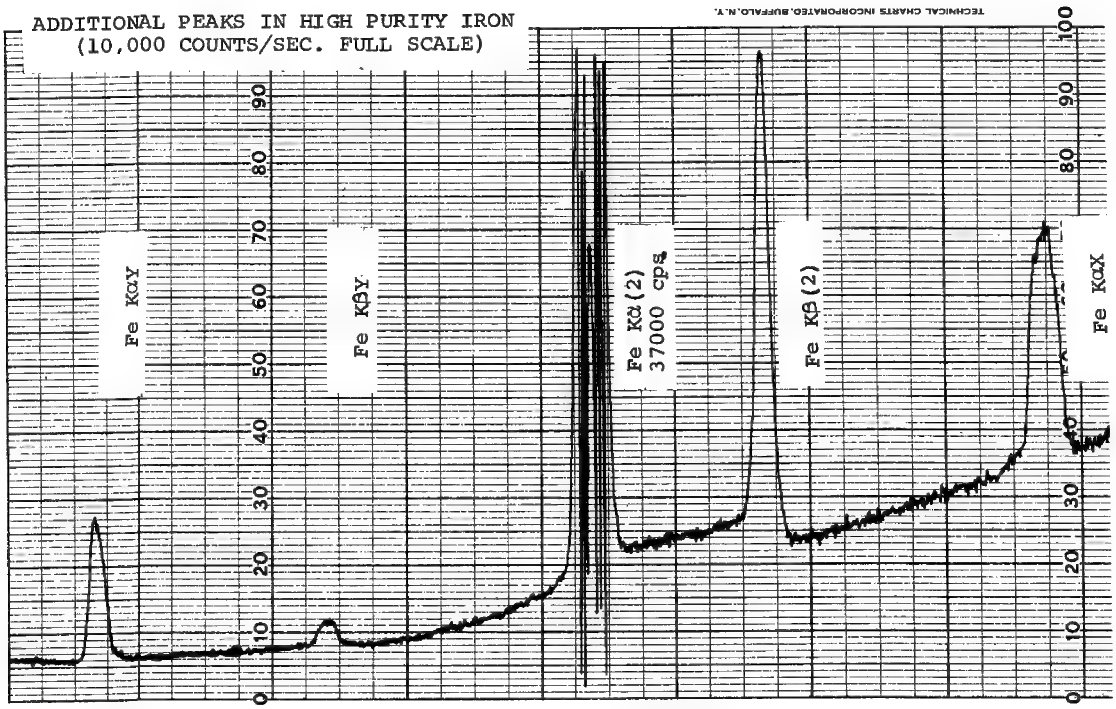

		X SERIES			Y SERIES			Z SERIES		
		2θ	d	R.I.[1]	2θ	d	R.I.[1]	2θ	d	R.I.[1]
Ti	Kα	56.8[2]	2.891	1.9	102.3[2]	1.765	0.1			
	Kβ	51.3[2]	2.903	1.0						
V	Kα	51.0	2.909	6.9	90.5[2]	1.763	0.2			
	Kβ	46.2	2.911	1.1						
Cr	Kα	46.2	2.920	8.1	81.1[2]	1.762	0.7	not detected for soft radiation		
	Kβ	41.8	2.922	1.5	73.4	1.744	0.5			
Mn	Kα	42.0	2.934	8.7	74.0[2]	1.747	2.3			
	Kβ	37.8	2.949	1.3	66.3	1.746	0.8			
Fe	Kα	38.6	2.931	8.7	67.4	1.746	5.3			
	Kβ				60.3	1.749	0.9			
Co	Kα				61.5	1.751	5.3	91.4	1.251	0.2
	Kβ				54.9	1.758	0.7			
Ni	Kα	not measured			56.5	1.752	7.2	83.0	1.252	0.3
	Kβ				50.3	1.765	0.9			
Cu	Kα	2θ less than 36°			52.0	1.758	8.4	75.8	1.255	0.6
	Kβ				46.8	1.753	1.6			
Zn	Kα				48.5	1.748	8.7	70.0	1.252	0.7
	Kβ				43.2	1.759	1.5			
Ge	Kα				42.0	1.753	30.0	60.0	1.255	2.0
As	Kα				39.1	1.759	30.0	55.7	1.259	3.0

[1] Intensity in percent relative to second order Kα except for Ge and As which are relative to third order Kα.

[2] Strongest line of a doublet or triplet.

Additional Diffraction Lines From EDDT Crystals

ELECTRON PROBE MICROANALYSIS OF PAPER AND PAINT FILMS

J. F. Ficca, Jr.

The purpose of this investigation was to demonstrate the feasibility and practicality of utilizing the electron microprobe as a tool for characterizing the cross-sectional distribution of opacifiers, fillers and extenders in paper and in dried paint films. The primary objective, successfully resolved, was the characterization of the distribution of titanium dioxide pigment. This has readily been extended to yield information on the distribution of inoragnic fillers and extenders such as clay, calcium sulfate, barium sulfate, calcium carbonate, talc, etc.

The sectioning of a flexible, fibrous, high-void material, such as paper, presents obvious difficulties. The operation must be carried out in a manner so that the paper is not distorted and the mineral contents are not redistributed by smearing or the final observations will be misleading. Several sectioning techniques were evaluated and the best results were obtained by the technique described below.

Both surfaces of the paper specimen are spray coated with 2 or 3 coats of varnish (allowing 8 hours to dry between coats). After final drying, the specimens are cross-sectioned with a conventional razor blade and the section surface examined optically at 200X magnification under polarized light. When smearing of the particulate matter in the paper onto the varnish occurs, it is clearly visible as highly reflecting surfaces. Fig. 1A and 1B show examples of good and poor quality cross sections. The poor section was intentionally produced by applying too little pressure to the razor blade during the sectioning of the sheet.

The cross-sectioned specimens are mounted (in groups of up to 10 specimens) in a spring-loaded miniature vise which holds the sections in an upright position. They are then coated with carbon by conventional means. The vise, with specimens in position, is then mounted in a standard A.R.L. sample holder and ready for examination in the microprobe.

The resolution of the electron microprobe is not sufficient to resolve individual particles of pigments or most fillers. This is of little moment for purposes of the examination since it is concerned with the degree of agglomeration and the general distribution. Qualitative information is best obtained by area scanning and display of characteristic x-rays. Figs. 2A and 2B show examples of data obtained on two commercial papers. Paper A shows a relatively uniform cross-sectional distribution of TiO_2 from felt to wire side of the sheet. Paper B shows heavy two-sidedness (higher concentration of TiO_2 near felt side of sheet). Fig. 2C is the same paper as Fig. 2B but was cross-sectioned with the opposite side (wire side) up and demonstrates that the sectioning technique does not alter the observed cross-sectional distribution of the TiO_2.

Another technique has been found superior for obtaining semi-quantitative data on cross-sectional distributions. The electron beam is deflected to yield a line of electrons about 270μ long x 1μ wide. The sectioned paper specimen is mechanically traversed in a direction perpendicular to the line and the intensity of characteristic x-rays are plotted on a strip chart recorder. The line beam averages out variations in concentration along the line while maintaining a resolution of a few microns in the cross-sectional traverse.

Figs. 3A and 3B show the effect of utilizing a line beam in contrast to a focused beam. The line beam gives a more representative plot of the average cross-sectional distribution. Figs. 4A and 4B show the average cross-sectional distribution of TiO_2 for the same two papers shown in Figs. 2A and 2B. Note that the TiO_2 concentration near the felt side of Paper B is 8 to 10 times higher than the TiO_2 concentration near the wire side of the sheet.

The majority of commercial paper specimens analyzed showed some degree of two-sidedness with the felt side of the sheet containing the highest concentration of TiO_2. A few showed higher concentrations of TiO_2 near the wire side of the sheet and only a few showed relatively uniform distribution. These observations are in agreement with data obtained by other workers utilizing the paper splitting technique which consists of splitting the paper into several sections and performing a chemical analysis of the ashed sections.

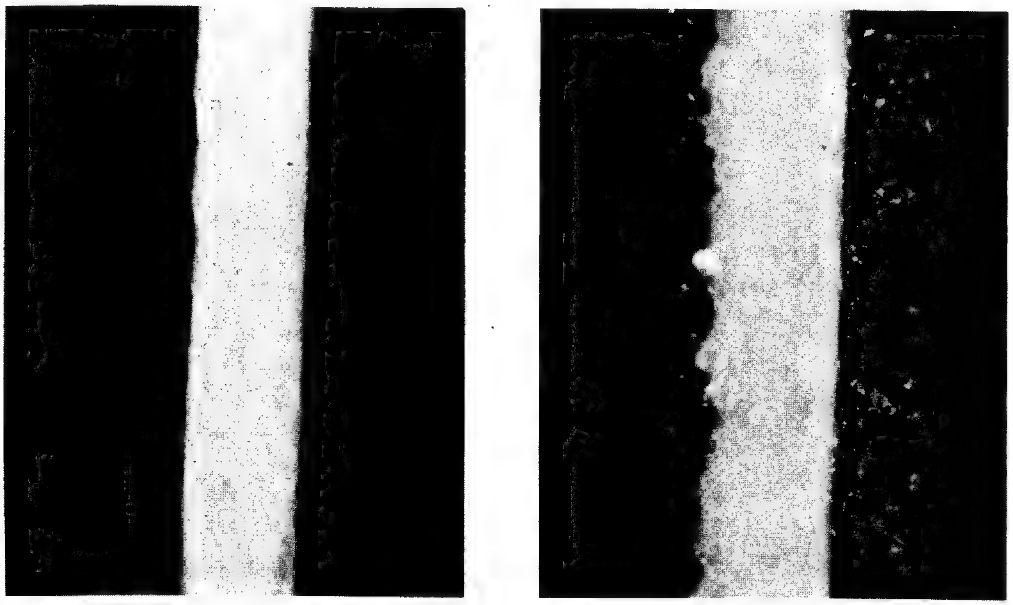

Fig. 1. Optical micrographs of good and poor cross sections of paper.

Paper A - Ti x-ray image. Cut felt side up.

Paper B - Ti x-ray image. Cut felt side up.

Paper B - Ti x-ray image. Cut felt side down.

Fig. 2. Qualitative cross-sectional distribution of TiO_2 in commercial paper.

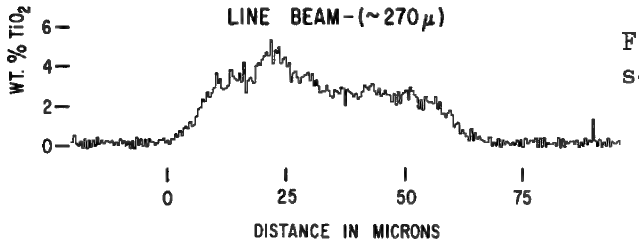

Fig. 3. Line beam vs. spot beam, Cross-sectional distribution of TiO_2 in paper.

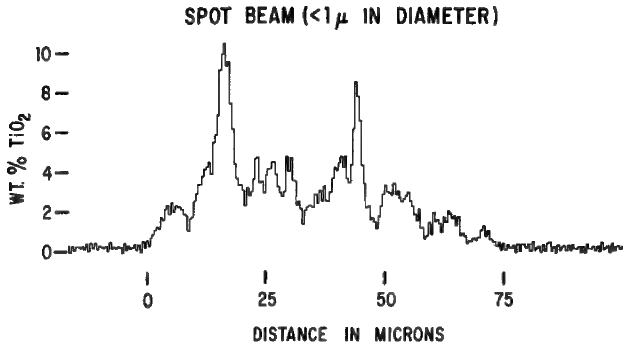

Fig. 4. Semi quantitative cross-sectional distribution of TiO_2 in two commercial papers. (Line Beam)

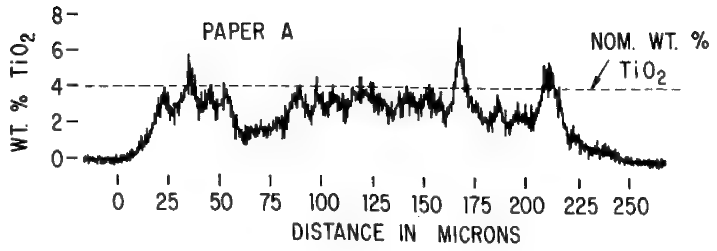

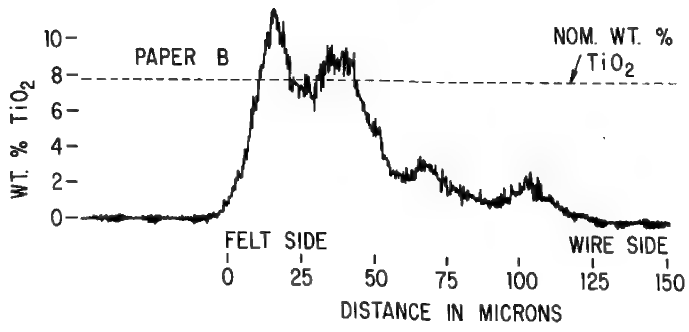

ELECTRON BEAM MICROPROBE TECHNIQUE TO MEASURE PHOSPHOSILICATE GLASS THICKNESS AND COMPOSITION

J. J. Gniewek and N. G. Koopman

Present silicon device technology utilizes the masking properties of SiO_2 films to control the geometry of diffused junctions. During phosphorus diffusion into the silicon, a thin phosphosilicate glass (PSG) layer is also formed atop the SiO_2 masking film. It has been established that the presence of this PSG is beneficial for stable device operation.(1) Characterization of the film requires measurements of both the thickness and the composition. The electron beam microanalyzer*, using variable beam accelerating voltages, has been used for this characterization.

The phosphosilicate glass layers normally range from 500 to 5000 Å thick containing 10 to 20 mol % P_2O_5 in SiO_2. In this thickness range, the small differences in silicon and oxygen content between the PSG layer and the underlying pure SiO_2 layer precludes the use of Si Kα or O Kα lines. One is left with two unknowns (thickness and composition) and only one analytical line to measure--P Kα. Therefore, a variable accelerating voltage technique, similar to that first described by Schumacher(2), was used.

Fig. 1 shows the curve obtained for the P Kα intensity vs. accelerating voltage** for a sample with a 1840 Å PSG layer. The intercept at 5.9 kV is a measure of the PSG thickness reflecting the transition from electron penetration less than the PSG thickness to penetration greater than the PSG thickness.

Using standard samples characterized by other techniques, a calibration curve of kV intercept vs. thickness can be obtained as shown in Fig. 2. In principle, the method of thickness measurement by variable electron beam energy should be absolute. However, at present, there are not sufficiently accurate means of correcting for the critical ionization potential nor is the range-energy relationship unambiguously established. With the calibration standards, however, the thickness can be measured to within approximately 150 Å in the range 700 to 4000 Å. This is in contrast to the recent work of Rehme(3) who sets a lower limit of 5000 Å on this determination.

Total phosphorus content, reported as a surface density, is then measured using a more conventional calibration curve of P Kα x-ray intensity measured at a fixed high (30 kV) accelerating voltage. This curve, P Kα intensity vs. total phosphorus content, is linear up to at least 30×10^{16} P atoms/cm^2 reflecting the compensating effects of x-ray absorption and electron excitation function. This measurement can be made to approximately $\pm 0.5 \times 10^{16}$ atoms/cm^2. The concentration of the PSG film, in mol % P_2O_5 is then calculated from the measured values of thickness and total phosphorus content.

In order to make these measurements, a highly accurate beam voltage supply and a faraday cage for monitoring beam current are essential.

---

* Applied Research Labs EMX.
** Measured at constant beam current.

---

1. IBM Journal Research & Development 8, 366-427, 1964.
2. B. W. Schumacher and S. S. Miltra, Proc. 1962 AIEE Electronic Components Conference, Washington, D. C., p. 152.
3. H. Rehme, Natur-wissenschaften 13, 329, 1966.

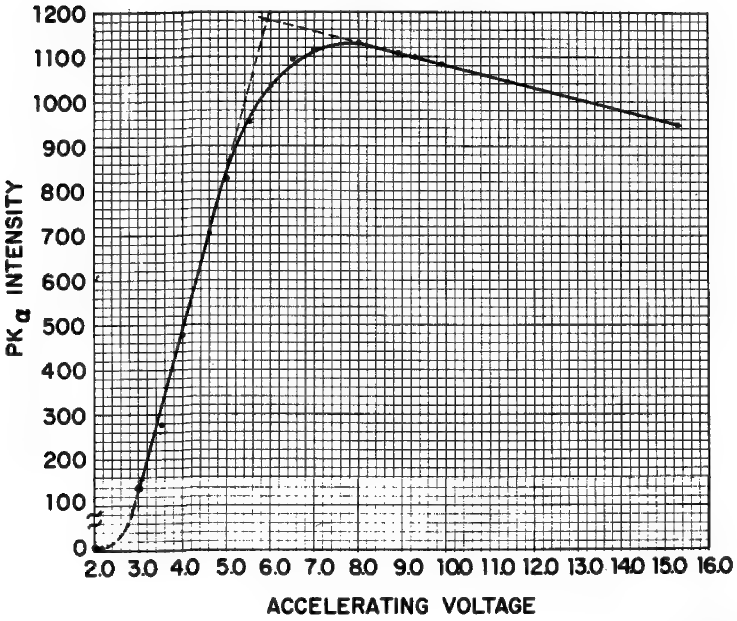

Fig. 1. Accelerating voltage vs. intensity.

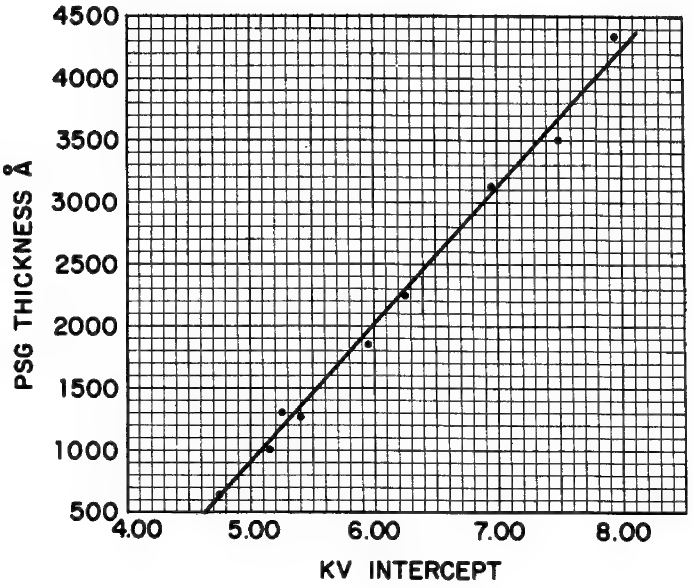

Fig. 2. Voltage intercept vs. thickness in Å.

CATHODOLUMINESCENCE AS A ROUTINE ANALYTICAL METHOD FOR THE SEMICONDUCTOR INDUSTRY

James P. Smith

Several specialized applications of cathodoluminescence (CL) measurements made with electron microprobe analyzers have been described in recent years(1-9). These applications have provided sufficient justification for the incorporation of such measurements into many electron microprobe analytical services. The information which can be derived from such measurements are summarized in Table 1. This information is particularly important for the characterization of semiconductor and ceramic materials. Although the required instrumentation is easily developed, the abstraction of much of the quantitative information from raw CL data requires further theoretical developments. However, the present state of the art is adequate for many qualitative and some quantitative applications.

The requirements of the instrumentation for a service CL attachment is in many ways more demanding than those for a research attachment. A service attachment should be very versatile and should not hinder normal microprobe operations. Table II outlines some general requirements for an adequate service CL attachment. These requirements have been derived through examination of the literature and from personal experience. The 90° take-off angle is quite important because of a small surface critical angle exhibited by some materials. The output of the monochromator should be adequate for scope intensity modulation. Our system has good response in the wavelength range 0.35 to 1.40 microns with a resolution better than 0.01 microns.

The composition of pseudo-binary compounds such as Ga(As,P), (Ga,Al)As and Zn(S,Se) have been determined from the spectral distribution of their CL radiation. In the range of interest, the peak wavelength of the excited radiation should be a linear function of composition but the absorption by the sample can result in an apparent shift in the peak. The use of a low accelerating voltage minimizes this effect. Simultaneous x-ray intensity measurements can be used to calibrate the wavelength of the peak radiation. The composition of thin films of these compounds have been measured by CL when the x-ray methods could not be applied due to the finite thickness. Also, samples which have been lapped at very small angles have been analyzed by peak wavelength determinations. The accuracy of this type of determination is dependent on the resolution of the monochromator. Results were estimated to be within a 7% error.

The identification of an unknown material strictly from its CL spectra is not practical since the ambient temperature spectra generally consists of very broad structureless peaks.(5) However, in many cases the unknown material can be identified as one of several possibilities when their spectra are available. We record the spectra of anything that exhibits CL during the course of an analysis; these are on file for future reference.

The relative composition of dopant or activator in some semiconductors and phosphors can be determined from the intensity of their CL radiation(2,4). The relative dopant concentration over the surface can be mapped by scope intensity modulation methods. In this way striations parallel to the direction of growth have been observed in cross sections of vapor grown Ga(As,P). These are attributed to variations in dopant concentration. This type of mapping has also been used extensively to examine the surface condition of II-VI crystals and to map dislocations and topological variations on GaAs surfaces.

The quality of bulk GaAs material can be monitored by CL intensity measurements(6,9). This intensity, given as a function of accelerating voltage yields diffusion length and surface recombination velocity and has been used to estimate the ultimate worth of the material for the construction of transistors and light emitting diodes.

Joining a ceramic material to a metal commonly involves the formation of metal rich glassy interface. Using combined CL and x-ray analysis, the metal which has interred a glassy phase can be differentiated from that which has not. Molybdenum-manganese metallization on alumina ceramic has been studied by this method.

Cathodoluminescence measurements have been shown to compliment the regular electron microprobe analysis of several types of samples. The projected importance of CL measurements is sufficient to warrent serious consideration of the construction of high vacuum units which will allow routine measurements on samples at low temperatures.

---

1. D. B. Wittry and D. F. Kyser, J. Appl. Phys., 35, 2439 (1964).

2. D. F. Kyser and D. B. Wittry, "The Electron Microprobe," p. 691, John Wiley and Sons, Inc., New York (1966).

3. H. C. Casey and R. H. Kaiser, J. Electrochem. Soc.: Solid State Science, 114, 149 (1967).

4. H. C. Casey, ibid, 1953 (1967).

5. J. R. Davey, "X-ray Optics and Microanalysis," p. 566, Hermann, Paris (1966).

6. D. B. Wittry and D. F. Kyser, J. Appl. Phys., 38, 375 (1967).

7. D. F. Kyser, J. McCoy, and D. B. Wittry, Second National Conference, Boston (1967).

8. R. T. Greer and E. W. White, ibid.

9. H. Stack and J. P. Smith, Electrochem. Soc. Meeting, Chicago (1967).

TABLE I. INFORMATION THAT CAN BE DERIVED FROM CATHODOLUMINESCENCE MEASUREMENTS

TYPE OF DATA	INFORMATION CONTAINED
Spectral Distribution of CL Radiation	Composition Band Structure Dopant-Activator Characterization Homogeneity — electrical, composition, chemical
Spacial Distribution of CL Radiation	Map of Original Reaction Interfaces Map of Dislocations Surface Condition Diffusion Profiles
Transient Phenomena of CL Radiation	Trapping Density Relaxation Time of Excess Carriers
Intensity of CL Radiation	Dopant Concentration Diffusion Length Surface Recombination Velocity Absorportion of Emitted Light
Excitation Dependence of CL Radiation	Trapping Density Temperature Effects Efficiency of Radiative Recombination

TABLE II. REQUIREMENTS FOR A CATHODOLUMINESCENCE ATTACHMENT FOR ROUTINE SERVICE WORK

1. Should not interfer with normal microprobe operation
2. Should be quickly and easily attached
3. Should allow simultaneous x-ray and cathodoluminescence operation
4. Should have a 90^{o} cathodoluminescent take-off angle
5. Should have a reliable 50 kV maximum accelerating voltage
6. Should be highly versatile
    a. selective wavelength by filters and monochromator
    b. record spectra at several scan speeds, slit widths and sensitivities
    c. allow two-dimensional intensity displays
    d. pulse modulation of electron beam
    e. varieity in intensity measurement channels
    f. two channel operations: (1) 2-D display (2) monochromator
7. Should be accurately calibrated
    a. wavelength
    b. intensity response
8. Monochromator wavelength resolution should be at least .01 micron
9. Adequate sensitivity in the wavelength range of interest
10. Simple to use and maintain.

DISTRIBUTION OF PLUTONIUM AND URANIUM IN A MIXED OXIDE FUEL IRRADIATED IN A FAST NEUTRON FLUX

N. R. Stalica and C. A. Seils

Segregation of plutonium and uranium during the in-pile lifetime of a mixed plutonium oxide (20 wt.%)-uranium oxide (80 wt.%) fast nuclear reactor fuel could have significant effects on the operational safety of the reactor. In particular, the segregation of uranium and plutonium oxides within the fuel may seriously decrease the effectiveness of Doppler broadening as a shutdown mechanism in a nuclear reactor, since more time will be required before heat generated within the plutonium oxide can be transferred to the uranium oxide.

A partially shielded ARL-EMX electron probe microanalyzer has been used to obtain complete radial distributions of uranium and plutonium on a micron scale for a complete transverse cross section obtained from the midlength of a fully enriched UO_2-20 wt.% PuO_2 fuel pin. The fuel pin was irradiated in Argonne National Laboratory's Second Experimental Breeder Reactor, a fast neutron breeder reactor, until three per cent of the uranium and plutonium atoms had fissioned.

The thickness of the specimen used for electron probe microanalysis was reduced to 1 to 3 mils by grinding and polishing in order to minimize the radioactivity emanating from the irradiated fuel. This was necessary for two reasons: 1) to minimize the biological hazard to the electron microprobe operator, and 2) to lower the background on the x-ray detectors to an acceptable level. The activity of the sample measured at 12 inches was 10^3 mR/hr γ and 10^4 mR/hr β-γ.

Biological shielding as well as detector shielding was also added to the instrument to further reduce the β-γ activity level.

Analyses were obtained for several different radial segments of the fuel cross section. The distribution and homogeneity of the uranium and plutonium oxides were found to be directly associated with the typical concentric microstructural regions that characterize a radial cross section of these fuels. A photomicrograph of one of these segments and a corresponding plot of the radial distribution for uranium and plutonium are shown in Fig. 1. The concentrations of both plutonium and uranium are combined in the plot as wt.% ($PuO_2/PuO_2 + UO_2$). Each of the points in the plot are average values for contiguous areas 90μ square and approximately one micron in depth along a radius near the center of the micrograph.

The innermost zone which was irradiated at the highest temperature contained long and short columnar grains. The concentration profiles of uranium and plutonium in the long columnar grains (A to B in Fig. 1) were similar for each columnar grain examined. The grains were grouped in clusters of three or four having identical uranium and plutonium concentration profiles (within 0.1 wt.% for any given radial position). However, a shift along the concentration axis occurred for adjacent clusters of grains. The maximum difference observed between groups of grains for identical radial positions was 2 wt.%. In the long columnar grain region, the uranium and plutonium oxides formed a solid solution that was homogeneous on a micron scale. Distribution curves obtained by analyzing areas of 1, 100 or $8100\mu^2$ were identical.

Homogeneity was almost complete in the band of short columnar grains (B to C in Fig. 1.) Throughout this region, plutonium or uranium analyses of one square micron area differed at most by 6 wt.%; analyses of areas 0.1 mm apart differed at most by 2 wt.%. The radial distribution curves in this region were not identical in shape; peaks and valleys occurred at different radial positions from curve to curve. The peaks in the distribution curves for plutonium or uranium were attributed to the presence of original particles of the respective oxides in the as-blended material.

Partial homogeneity and solid solution occurred in the transition zone (C to D in Fig. 1) which was irradiated at intermediate temperatures in which equiaxed grains have crystallized. The distribution curves varied markedly from one radial position to another; the peaks and valleys observed were much more extreme than in the region of short columnar grains. Many plutonium-free UO_2 particles exceeding 50μ in cross section and smaller uranium-free PuO_2 particles were observed in this region.

Little, if any, solid solution occurred in the outer zone of the fuel (D to E in Fig. 1) which was irradiated at the lowest temperature. The fuel in this region consisted of discrete particles of UO_2 and PuO_2. Particles of UO_2 as large as 200 to 300μ in cross section were observed. However, most particles of UO_2 were less than 50μ in cross section; particles of PuO_2 never exceeded that size.

These findings are most significant to the operational safety of a nuclear reactor. Since gross segregation of plutonium oxide has not occurred in a mixed uranium plutonium oxide fuel during irradiation, the Doppler shutdown mechanism would not be affected.

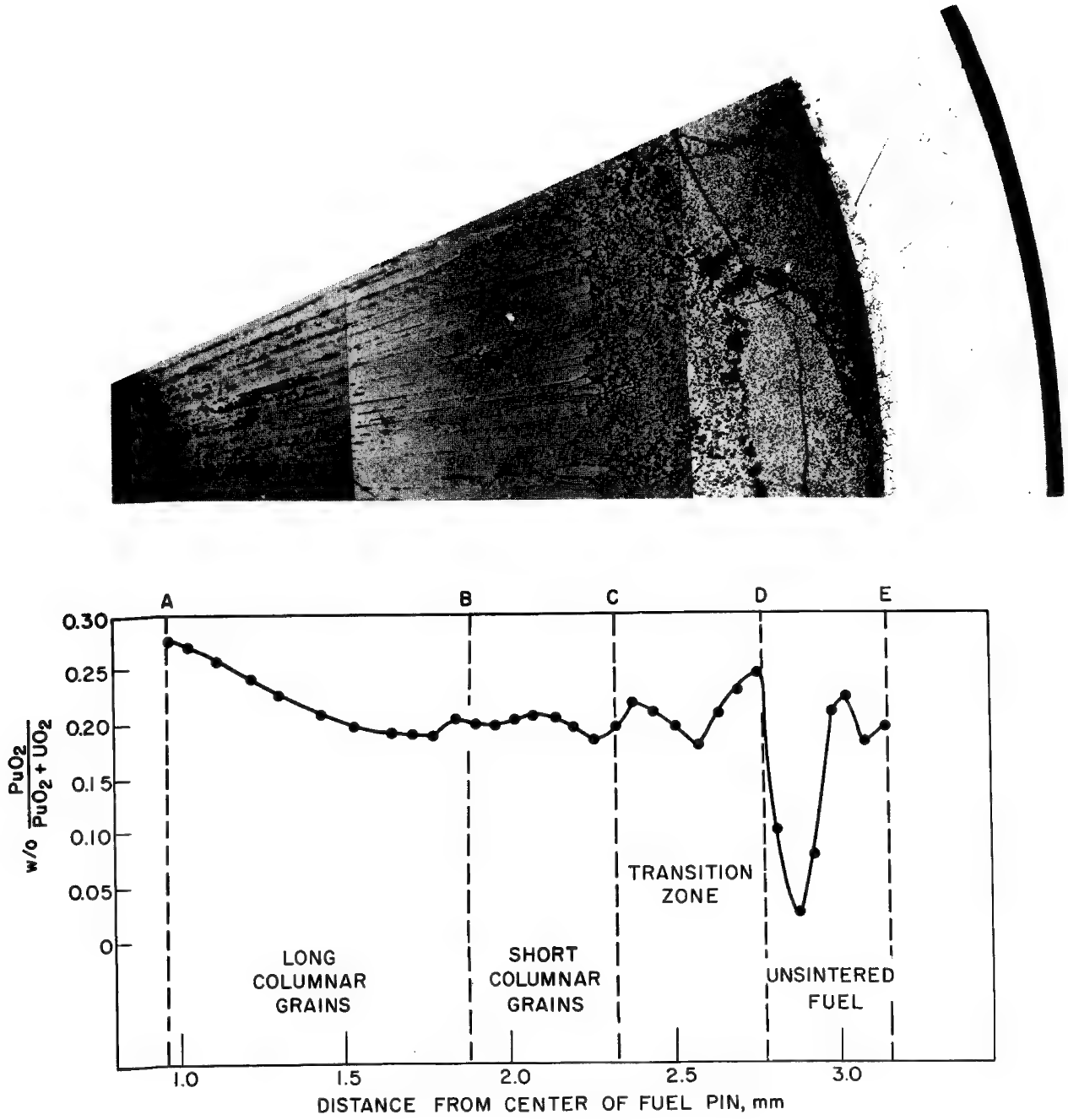

Fig. 1. Radial distribution of plutonium and uranium in UO_2-20wt.% PuO_2 (2.9 at % burnup).

ELECTRON PROBE MICROANALYSIS OF ALKALI METALS IN GLASSES

L. F. Vassamillet and V. E. Caldwell

Compositional changes in glasses during analysis have been reported by several investigators.(1,3) The effect has been shown to be most pronounced for monovalent alkali metals and is impeded by the presence of higher valent elements such as Ca, Mg and Al. A mechanism to account for this change has been suggested(4) by which an electron field due to electrons coming to rest within the target develops sufficient strength to attract alkali ions away from the surface. This is a necessary but not sufficient condition. The experiments to be reported on here show that the temperature of the glass in the volume irradiated increases with duration of bombardment by the incident electrons until a critical temperature is reached at which point diffusion of the alkali ions can proceed. For longer irradiation times at high fluxes the x-ray signal from the alkali ion does not simply decrease with time of bombardment, but increases in intensity after an initial decrease.(2)

The intensity of each alkali metal x-ray line has been measured for binary oxide glasses of Na_2O, K_2O and Rb_2O with SiO_2. In one case, a ternary of Na_2O, K_2O and SiO_2 was investigated. The dependent variables were ambient temperature, incident beam current, beam spot diameter and composition. The nature and thickness of the surface conductivity layer could also be changed. The incubation time, i.e., the length of time before diffusion of the ion is detected, becomes evident when the electron flux falls between proper limits.

The effect of temperature on the volume irradiated was followed by heating of the glass sample independently of the electron beam. By means of a tin oxide conductive coating-heating element the surface temperature of the glass specimen could be controlled up to temperatures of approximately 200°C. The variation of incubation time with sample temperature prior to bombardment permits the measurement of the critical temperature, i.e., temperature at which diffusion is detected. Temperatures determined in this way have been compared with estimates of equilibrium temperatures predicted from heat flow considerations.(5,6,7) For example, the incubation time on a 14.3% K_2O-SiO_2 glass bombarded with a 1 m watt electron beam of 17μ diameter was 93 seconds. The critical temperature was 60°C above ambient. This is some 40°C higher than would be expected for the equilibrium temperature assuming the incident energy is dissipated in a hemisphere of equivalent volume.

The effect of the conductive layer on sample temperature directly under the beam is very small for thin layers of the order of 200 Å, and is essentially independent of the layer materials used in this study (C, Cu or Al).

This study raises questions concerning the nature of the process of chemical composition changes in glasses under bombardment of high energy electrons. The mechanism proposed earlier(2) must be modified in the light of these experiments. The possibility of utilizing a microprobe technique for the study of diffusion rates in glasses is considered.

---

1. A. K. Varshneya, A. R. Cooper and M. Cable, JAP, 37, 2199, 1966.

2. M. P. Borom and R. E. Hanneman, JAP, 38, 2406, 1967.

3. A. K. Baird and D. H. Zenger, "Advances in X-Ray Analysis," 9, 487, 1966.

4. J. L. Lineweaver, JAP, 34, 1786, 1963.

5. R. Castaing, Thesis, Paris 1951, ONEAR Publ. No. 55.

6. G. S. Almasi, J. Blair, R. E. Ogilvie and R. J. Swartz, JAP, 36, 1848, 1965.

7. G. A. Friskney and C. W. Haworth, JAP, 38, 3796, 1967.

NEW APPLICATIONS OF ELECTRON MICROPROBE ANALYSIS IN RENAL PATHOLOGY

P. Galle, J. P. Berry and J. Stuve

These studies were carried out using an electron microprobe analyzer combined with an electron microscope.(1) This instrument has two primary uses in medicine. First, it permits the analysis of intra or extra-cellular inclusions to be made on ultrathin sections of tissue; and second, it allows the determination of the chemical composition of certain microcrystals which appear in biological fluids.

Studies on Ultrathin Sections of Renal Tissue. The preparation of ultrathin sections is the same as that used in classical electron microscopy. Our initial results were presented at the Second Conference in Boston. We will describe here three new applications.

Experimental Poisoning by Gold Salts. Aurothiopropanol ($Au-S-CH_2-CHOH-CH_2-SO_3Na$), a gold salt used in human therapy, was given to rats. Sub-cutaneous injection of high doses caused an acute tubular nephritis; repeated injection of smaller doses resulted in lesions which affected exclusively the proximal tubular cells. Microprobe analysis has enabled us to establish the intracellular organelle responsible for the concentration of gold by the kidney and also the way in which this element is excreted. Gold first appears in the mitochondria. They become greatly modified, increase in volume and form rounded vacuoles. (Fig. 1) Secondly, these mitochondria are expulsed into the tubular lumen where high concentrations of gold are subsequently detectable.

Renal Toxicity of Certain Alkaline Powders. Curious deposits of a mineral nature were observed in the renal biopsy of a patient with chronic nephritis. (Fig. 2) Microprobe analysis showed that these deposits contained large amounts of calcium, phosphorus, sulphur and magnesium. From this information the nephritis was traced to its cause: this patient, who suffered for many years from stomach troubles, ingested an alkaline powder made up of magnesium carbonate, magnesium trisilicate and calcium bicarbonate.

Nephrocalcinosis of Parathyroid Origin. The study by electron microscopy and microprobe analysis of different renal calcium deposits has enabled us to classify six individual types of nephrocalcinosis which differ from each other both by the ultrastructure of their deposits and by their chemical composition. The first five varieties have been the subject of earlier communications(2); we will present here a sixth variety.

The injection of parathyroid hormone into an animal causes an appearance of calcium deposits, whose ultrastructure and chemical composition vary according to the localization of the deposit. Certain of these deposits, found in basement membranes, have a concentric form and contain calcium, phosphorus and sulphur. Others, found in the tubular lumen, take various forms, and contain calcium, phosphorus, sulphur and magnesium. Finally, still others,

found within the cytoplasm of the proximal tubular cell, are formed of masses of very fine needles and contain phosphorus and calcium. This latter variety has been observed only in hyperparathyroidism for which it appears very specific. This method could, therefore, be useful in human pathology as a diagnostic tool, to aid in the important and difficult task of establishing the etiology of a nephrocalcinosis. Calcium deposits observed in the kidneys of patients with parathyroid gland adenomas have, in fact, the same ultrastructure and the same chemical composition as the experimental deposits studied here.

Study of Crystals Found in Biologic Fluids. It is known that the elements contained in certain biologic fluids may form crystals. However, apart from the identification of certain crystals of well-known and characteristic form, it is most often difficult, if not impossible, to determine the nature of the observed crystals, especially when they are of very small dimension. Microprobe analysis can perhaps solve this problem. We present here two examples of possible applications, the study of fluid from a joint and the study of a urine sample.

---

1. P. Galle, "Cytochimie sur Coupes Ultrafines par Spectrographie des Rayons X", Sixth International Congress for Electron Microscopy, Kyoto, 1966, p. 79.

2. P. Galle, "Les Néphrocalcinoses: Nouvelles Données d'Ultrastructure et de Microanalyse", Actualités Néphrologiques de l'Hôpital Necker, 1967 (Flammarion, Paris, 1967), pp. 303-315.

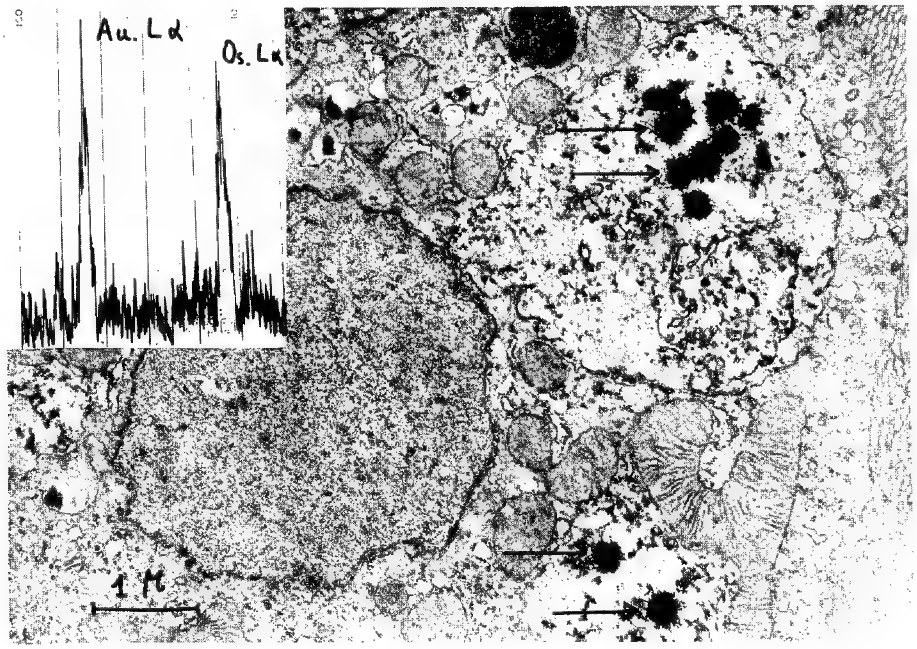

Fig. 1. Experimental poisoning by gold salts. An electron micrograph showing the presence of small dense inclusions (arrow) in a proximal tubule cell of rat kidney. The insert shows the characteristic Lα rays of gold and osmium obtained from these dense inclusions.

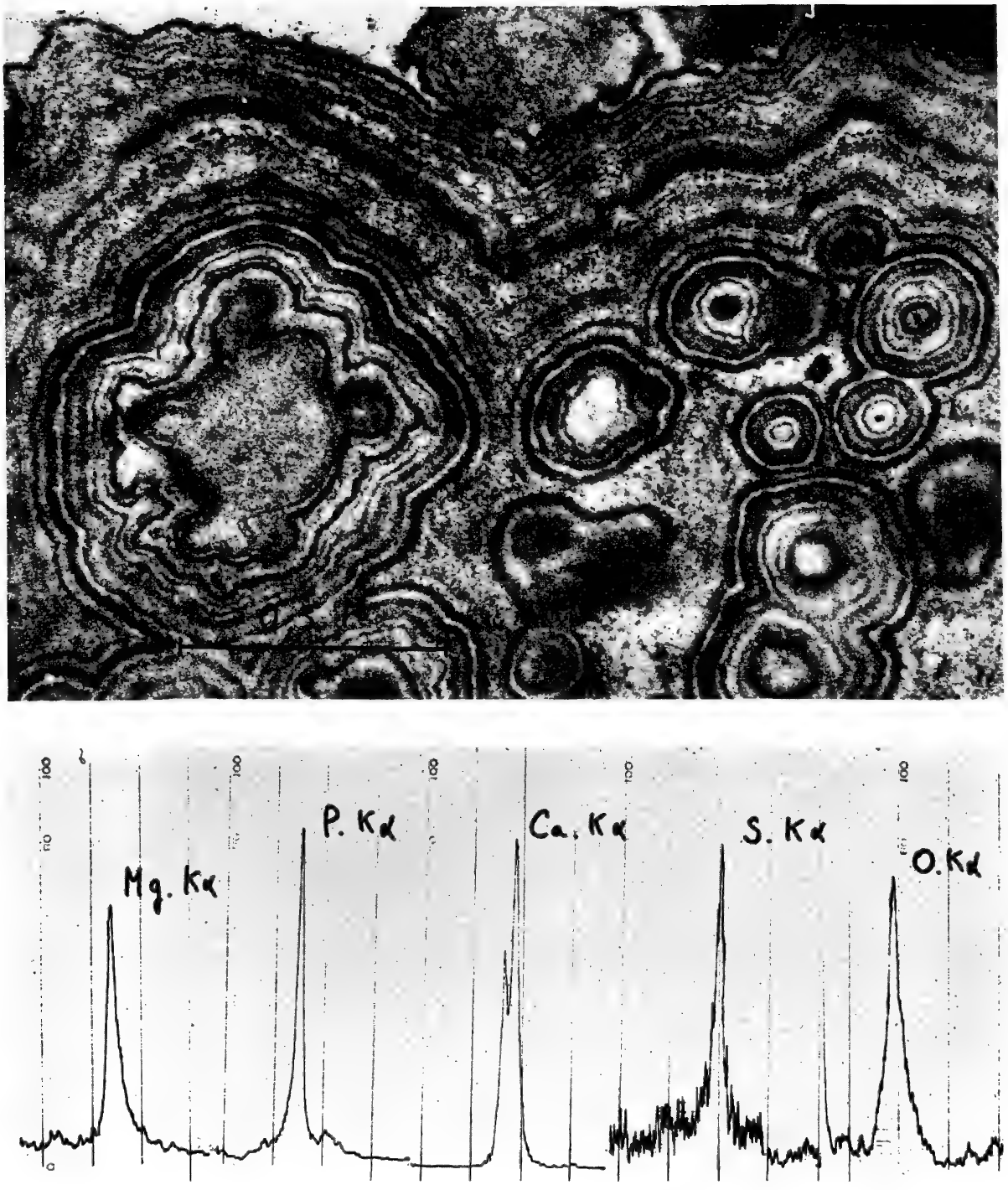

Fig. 2. Abnormal deposits present in a human kidney which contain calcium, phosphorus, sulphur and magnesium.

OBSERVATIONS ON HUMAN BLOOD CELLS

K. G. Carroll and J. L. Tullis

Electron probes make possible detection and measurement of elements within individual cells, and offer the unique opportunity to characterize the chemistry of a single cell, which differentiates it from other seemingly identical cells. This work outlines a continuing study of the chemical composition of white blood cells both normal and abnormal. Originally studies were made of the sodium and potassium content of red cells which led to the discovery of the surprisingly high metal ion content of leucocytes. White cells have now been investigated in whole blood, bone marrow, and lymph nodes and have been found to have chemical compositions in all three sources which correlate with the presence or absence of certain malignancies.

Blood smeared onto silicon substrates has proven to be a simple and effective technique of specimen preparation. In addition to its other obvious advantages, silicon in a polished condition provides a substrate of high reflectivity for light, and its use effectively bridges the gap between the metallurgical microscope necessary in the probe and the biological microscope used in medical research. Probe conditions are usually as follows: accelerating voltage, 30kV; beam diameter, 1 micron; beam current, 10^{-7} amperes. The best monochromator available is quartz (101), bent and ground to the focusing circle in the classical Johannson mounting. Many other crystals can be used, of course, and the observations reported here are not critically dependent upon any of the instrumental variables. Pulse height analysis was performed with an open window accepting amplified pulses from the proportional counter lying between 1 and 10 volts. Because of the strength of the x-ray signal from certain leucocytes, it is not necessary to have ideal conditions of detection to make relevant observations.

The first experiments were done on whole blood smears of a patient with acute leukemia. Strong lines of Ti and Zn K-alpha were observed rather frequently in white cells. It was readily apparent that the two metal ions were situated in the same region of the cell and in a region much smaller than one micron. Further, it appeared that the two ions occurred in a fixed ratio. Rough estimates of this ratio, made by comparison with x-ray lines from metallic Zn. and Ti gave a Zn-Ti atomic ratio of 3 or 4 to 1. Searches of the x-ray spectra of cells also revealed the presence of Fe, K and Ca in some cases. Blood from natural sources rarely, if ever, exhibited the co-occurrence of Ti and Zn. To further characterize this unexpected finding, attention was directed to bone marrow specimens which were richer in leucocytes. Reference 1 gives some quantitative results on six specimens including four normals. The frequency of occurrence of white cells containing Ti and Zn was found to vary from less than one percent in normal specimens to about 20 percent in a case

of lymphoblastic leukemia. The method of counting was to continuously record the x-ray signals from Zn and Ti on a 2-pen recorder during a standard cell count of some 300 leucocytes.

In a further attempt to refine the observations, specimens of pure leucocytes were obtained from surgical biopsies. The white cells were mechanically removed from lymph nodes into saline solution, which was smeared on silicon substrates as before. Table 2 in reference 1 gives the observed frequency of occurrence of Ti and Zn containing cells from lymph nodes, varying from less than one percent in "normals" to about 8 percent in the two malignancies tabulated.

With the recent advent of electron microscope attachments to the present electron probe microanalyzer, resolution is no longer limited to that of the optical microscope; about 1/2 micron. We have applied such an intrument (CAMECA) to the problem of localization of metallic elements within leucocytes. It is necessary to support the cells on an electron-transparent substrate. Evaporated carbon films on copper grids, long used by electron microscopists, serve adequately for the purpose. Many transmission electron microscope images have been made of cells containing Ti and Zn, with simultaneous recording of the x-ray signals from the cells. This data confirms that the metallic elements reside in the cell nuclei and occur in both modular and filamentary form in regions about 0.1 micron in diameter. It should be noted that the finding of Ti in lung tissue cells was first reported by Dr. Tousimis.(2). It would appear likely that, not only is Ti no longer to be regarded as a biologically inactive element, but that an understanding of its synergistic effects with other metallic ions will help to clarify important biological problems of long standing.

---

1. Carroll, K. G. and Tullis, J. L., Nature, Vol. 217, p. 1172 (March 23, 1968).

2. Tousimis, A. J., Eastern Analytical Symposium, New York, November 1967.

AN ELECTRON PROBE AND ELECTRON MICROSCOPE INVESTIGATION OF ASBESTOS BODIES IN LUNG SPUTUM

A. P. von Rosenstiel and H. B. Zeedijk

Typical asbestos-initiated tumors--pleura and peritoneum mesothelioma--have been found at an unusually high frequency in shipyard workers. Only slight asbestos exposure had taken place in these cases. On the other hand the persons involved had been exposed to high concentrations of iron oxide (flame cutters and welders). Corpuscles similar to asbestos bodies, amorphous iron oxide and asbestos fibres were found in the lungs. It has been suggested that these corpuscles might be pseudoasbestos bodies or ferruginous bodies.

Electron probe analysis showed the presence of iron, calcium, phosphorus, oxygen and silicon. However, identification by means of electron diffraction failed to show any results due to the amorphous protein coating of these "asbestos bodies."

With the aid of a micromanipulator and by special etching techniques, the protein layers were partly stripped off from the actual core. Iron, silicon and oxygen were found by electron beam microanalysis. In agreement with the results of the microanalysis, the particles were identified by means of electron microscopy and electron diffraction as amphibole asbestos (silicon-iron asbestos).

Out of twenty-seven fibres investigated, seventeen were uncoated asbestos fibres of the tubular chrysotile type (magnesium-silicon asbestos) whereas the cores of ten stripped asbestos bodies were all analyzed as amphibole asbestos (iron-silicon asbestos).

ELECTRON MICROPROBE ANALYSIS OF THE SILVER AMALGAM--TOOTH INTERFACE

S. H. Y. Wei and M. J. Ingram

Silver amalgam is one of the most widely used filling materials in dentistry. One of the inherent disadvantages of silver amalgam is that it becomes tarnished in the oral environment and tends to discolor the tooth substance with age. This discoloration is commonly believed to be due to the penetration of metallic ions, principally mercury into the tooth substance.(1) On the other hand, other spectrographic analyses(2,3) have shown that the discolored tooth substance contained mainly tin, with traces of silver, copper and zinc but no mercury. The electron microprobe, therefore, was used in this study to determine the distribution of metallic elements at the amalgam--tooth interface and in the tooth substance so as to find out which element(s) is responsible for the tooth discoloration.

Six, freshly extracted molars with large silver amalgam restorations showing discoloration of the enamel and dentin were selected. The roots were removed and the crowns were cleaned and then dehydrated through serial alcohol and embedded in a hard mix of Epon. The embedded specimens were sectioned longitudinally with a diamond wheel so that large areas of amalgam to enamel and dentin interface were exposed. The specimens were then hand polished using fine abrasive paper down to Linde grade 4 paper followed by polishing on metallurgical wheels using fine grain silicon carbide and aluminum oxide until a mirror finish was obtained. Carbon was evaporated onto the sample surface using a vacuum evaporator prior to placement in the electron microprobe.

Microprobe analyses were carried out on an ARL-EMX Electron Microprobe. X-ray scans for silver, mercury and tin were obtained. In addition, a graphic display of the concentration of each element was also obtained using a linear graphic display technique on the Enhancitron. The Enhancitron is a 1026 channel data storage device which is used to construct a graph of the x-ray intensity over a line scan. The probe was operated at 25 kV and 0.05μA for all scans and the average spot size was approximately 1μ.

Slides will be shown at the meeting to demonstrate the results.

In all the scans of amalgam--tooth interface it was noticed that tin was rather unevenly distributed and large numbers of "hot spots" or localized high tin concentrations were seen in the amalgam. There was a high concentration of tin at the interfacial area. Further, tin was found to have consistently migrated from the amalgam restoration into the enamel and dentin. The amount of tin in dentin was higher than in enamel. The results of enhancitron tracings confirmed that tin migrated from the amalgam to the tooth substance.

The electron probe image for silver of the same interfacial area showed that silver in amalgam was also inhomogeneously distributed but the distribution of silver did not correspond to that of tin. Areas which were void of silver were found to exhibit a high tin concentration. No apparent migration of silver into the enamel or dentin had occurred, nor was there a high concentration at the interfacial area.

The distribution of mercury in amalgam, in contrast to tin and silver, was much more homogeneous. There was no migration of mercury in the tooth substance or into the interface and a sharp border between the amalgam and the tooth surface was usually observed. This result was confirmed by the enhancitron tracings.

Paffenbarger(4) explains that most silver amalgams consist of three phases, namely a silver-tin phase (Ag_3Sn), a silver-mercury phase (Ag_2Hg_3) and a tin-mercury phase (Sn_7Hg or Sn_8Hg). The order of corrosion of these three phases, from the greatest to the least, is tin-mercury phase, the silver-tin phase and the silver mercury phase. The different phases with their differing electrode potentials form a corrosion cell with saliva as the electrolyte. Skinner and Phillips(1) suggests that the product of corrosion of this nature is principally tin deposition with traces of silver and copper. The results of this investigation confirmed the above theory and the discoloration of tooth substance by old amalgam fillings is related to the migration of tin ions into the tooth substance. This is in contradiction to the commonly held concept that mercury is the main element responsible for tooth discoloration.

---

1. Skinner, E. W. and Phillips, R. W, The Science of Dental Materials, 6th Edition, Chapters 19-22, pp. 287-357, W. B. Saunders Co., Philadelphia, 1967.

2. Fields, L. B. and Charles, G. W., A Spectrographic Investigation of Trace Elements In Human Teeth. Proc. Oklahoma Acad. Sci., 31: 47-48, 1950.

3. Schoonover, I. C. and Souder, W., Corrosion Of Dental Alloys. J. A. D. A., 28: 1278-1291, 1941.

4. Paffenbarger, G. C., Recent Advances In U. S. A. On Dental Amalgams And Possible Applications, Int. Dent. Journal, 16: 450-465, 1966.

A STUDY OF HIGH TEMPERATURE REACTIONS IN STRONTIUM ZIRCONATE BY CATHODOLUMINESCENCE

N. A. Richard and D. I. Phalen

Variations in the cathodoluminescent emissions of $SrZrO_3$ have been used as an aid in the study of the high temperature reactions of this material with oxygen, hydrogen and tungsten. While luminescence emission analysis is qualitative, the sensitivity to small variations in composition greatly exceeds that attainable by normal electron probe analysis.

The instrumentation used in collecting the luminescence data in this study differs only in detail from that previously described(1,2); light emitted by the specimen is collected by the reflecting objective of the light microscope and is directed through a small quartz prism spectrometer into a photomultiplier detector. The photomultiplier tube current, being proportional to the incident light intensity, may be recorded as a function of wavelength or as a function of the position of the electron probe on the specimen surface. The amplified photomultiplier signal may also be displayed on the oscilliscope in a manner similar to that of the specimen current or electron backscatter image.

Cathodoluminescence emission is produced as a result of transitions between conduction-band electrons and valence-band holes or by the decay of excitons at impurity or defect centers. In oxide insulators under electron excitation, the formation and decay of excitons is believed to be predominant. Therefore, it follows that the spectral distribution of the luminescent emission is dependent upon the electronic states of the atoms in the crystal lattice and is potentially a sensitive indicator of small chemical and structural changes. As the structure of $SrZrO_3$ is an oxygen dominated lattice, the observed variations in the spectral distributions are believed to be related to the content and distribution of oxygen in the lattice. Observations made on a variety of samples appear to be best explained, however, on the basis that the cathodoluminescent emission arises from cation defects. The effect of oxygen upon the spectral distribution may then be considered a secondary effect, which results from perturbations of the crystal field about the adjacent cations.

In general, two types of spectral distributions were observed from $SrZrO_3$: the first has a maximum intensity at about 420mμ with a slight asymmetry on the long wavelength side of the peak while the second is more symetrical with a peak intensity at about 500mμ. The emission band with a peak intensity at 420mμ arises from stoichiometric or Zr-rich $SrZrO_3$, while the emission peak at 500mμ is produced from Sr-rich $SrZrO_3$.

Vacuum degassing of $SrZrO_3$ bodies at 1950°C resulted in the formation of a porous surface layer of ZrO_2. The absence of a diffusion gradient in association with this surface layer suggests that SrO(g), Sr(g) and O(g) were liberated at the

$ZrO_2/SrZrO_3$ interface and permeated the porous ZrO_2 layer at a very high rate. In an attempt to reduce the vaporization of Sr and still remove excess oxygen, specimens were heat treated at 1950°C in hydrogen. The growth of the ZrO_2 layer after 8 hours in hydrogen was found to be about 2 1/2 times that observed for 8 hour vacuum-treated specimens. While no concentration gradients were observed by electron probe analysis, the luminescent spectra of the hydrogen treated material showed two peaks with the intensity of the 500mμ peak diminishing toward the center of the body. From these observations it is concluded that hydrogen has acted to internally reduce the $SrZrO_3$, producing a Sr gradient within the body below the ZrO_2 layer, with excess Sr near the surface.

Heat treatment of outgassed specimens of Sr-rich $SrZrO_3$ in oxygen at 1950°C resulted in the formation of two discrete materials near the outer surface, one resembling grains of the bulk body with an emission peak at 500mμ and the second resembling a grain-boundary phase which produced an emission peak at 425mμ. The "grain-boundary phase" is believed to result from the oxidation of the Sr-rich $SrZrO_3$ and the thickness of the zone represents the depth of oxygen penetration. The diffusion rate of oxygen into Sr-rich $SrZrO_3$, based on these observations is $10^{-8}cm^2/sec$ at 1600°C and $10^{-6}cm^2/sec$ at 1950°C and are in general agreement with values of $4 \times 10^{-7}cm^2/sec$ at 1500°C and $3 \times 10^{-6}cm^2/sec$ at 1950°C which were obtained from electrical conductivity measurements.

Tungsten diffusion has been studied in a diffusion couple composed of tungsten metal and $SrZrO_3$ fired 1 hour at 1500°C in vacuum. After a diffusion anneal of 1 hour at 1950°C in vacuum, the bulk of the $SrZrO_3$ body was white but with a green discoloration, characteristic of WO_3, around the tungsten foil. Electron probe analysis has shown the tungsten concentation gradient to be 4 wt% at a distance of 12 mils. This distance is considerably less that that (36 mils) in which the green discoloration was produced. Extrapolation of the tungsten concentration curve to coincide with the limit of discoloration would indicate that a concentration of about 10 ppm of WO_3 is sufficient to produce the discoloration. The intensity of the luminescent emission at 410mμ was measured as a function of distance from the $W/SrZrO_3$ interface and was found to increase exponentially through the zone of discoloration and similarly, though at a lesser rate, beyond the zone to a distance of 90 mils from the interface. The latter slope is believed to indicate an oxygen gradient resulting from degassing of the body during the diffusion anneal. A second diffusion couple composed of previously degassed $SrZrO_3$ was given an identical diffusion anneal. In this couple no diffusion gradients were observed and no discoloration of the $SrZrO_3$ occurred. Based upon these observations, the high penetration rate of tungsten in the initial diffusion couple is believed to be the result of excess oxygen in the $SrZrO_3$ body and the calculated diffusion rate of $4 \times 10^{-7}cm^2/sec$ represents tungsten ion migration.

The authors wish to thank A. E. Austin and D. A. Vaughan for their advice and encouragement in this investigation.

This work was supported by Air Force Materials Laboratory, Research and Technology

Division, Wright-Patterson Air Force Base, Contract Number AF-33(516)-5249.

---

1. K. F. J. Heinrich, "Oscilloscope Readout of Electron Microprobe Data," Advances in X-ray Analysis, Vol. 3, University of Denver, Plenum Press, New York, 1962, pp. 291-300.

2. R. T. Greer and E. W. White, "Microprobe Attachment for Quantitative Studies of Cathodoluminescence," Second National Conference on Electron Microprobe Analysis, Boston, 1967.

NEW DATA ON NATURAL PHASES IN THE SYSTEM AG-TE

E. F. Stumpfl and J. Rucklidge

The Ag-Te system has been the cause of much controversy in recent years and electron probe microanalyses of a great number of natural Ag-Te phases has been performed in order to clarify some aspects. Silver telluride minerals are an important source of silver and a potential source of tellurium, which has many applications in the electronics and semiconductor industries.

These investigations were performed with an ARL-EMX instrument using both synthetic alloys and pure element standards. One author (Rucklidge 1967) wrote a FORTRAN correction calculation program for the IBM 7094 computer.

Analytical data obtained on hessite, Ag_2Te, agreed well with its theoretical composition and indicated that the gold contents quoted in the literature are probably due to microscopic inclusions of Au-bearing minerals.

Distinctly diverging views have been expressed by a number of authors as to the composition and nomenclature of other Ag-Te phases, particularly with regard to the minerals empressite and stuetzite. The former has been defined, consecutively, as AgTe, $Ag_{2-x}Te_{1+x}$, and $Ag_{5-x}Te_3$; the latter, as Ag_4Te and Ag_5Te_3 (Cabri 1965, Fleischer 1966, Honea 1964, Sindeeva 1964, Thompson et al. 1951). Cabri (1965) states that the mineralogy of silver tellurides "is still far from completely understood."

Part of our data were obtained during an investigation of the type of empressite found at the Empress Josephine Mine, Colorado, and which was originally described by Thompson et al. (1951.) In reflected light, not one but two optically distinct phases are present. The white phase corresponds very closely to the composition AgTe while the gray phase has the formula $Ag_{5-x}Te_3$, with $x = 0.24 - 0.36$. These findings are difficult to reconcile with experimentally determined phase relations in the Ag-Te system (Cabri et al. 1965) because AgTe has so far not been synthesized. These observations seem to suggest that laboratory production of natural processes may not always be possible.

Even though the recent definition of empressite as AgTe (Fleischer 1966) is now supported by electron probe data, the authors feel that stuetzite would better be defined as $Ag_{5-x}Te_3$, and not as Ag_5Te_3 because none of the natural phases analyzed by the electron probe correspond to a composition Ag_5Te_3.

AgTe apparently has similar semiconducting properties as Ag_3AuTe_2, its composition changing from 44.9% Ag, 55.8% Te to 48.9% Ag, 50.8% Te after three minutes exposure to the electron beam.

$Ag_{5-x}Te_3$ has, in some cases, been found to coexist with a member of the Au-Ag-Te system, sylvanite. On the basis of experimental data, the temperature of formation of the respective mineral associations can be determined from electron probe analysis. Sylvanite rarely contains as much Ag as is demanded by the ideal formula, $AuAgTe_4$, and in most instances Au substitutes for Ag. However, this does not apply when sylvanite coexists with $Ag_{5-x}Te_3$. In those cases the composition of sylvanite, as shown by electron probe analyses, comes very near to its stoichiometric ratio. On the basis of these considerations it has been possible to suggest a temperature of formation of about 230°C for ores from the Red Cloud Mine, Boulder Co., Colorado, and of about 300°C for ores from Lindquist Lake, British Columbia.

Slides illustrating microscopic textures of the phases discussed and tabulations of 15 quantitative electron probe analyses will be shown.

Cabri, L. J., 1965, Am. Mineral., 50, 795-801.
Fleischer, M., 1966, Am. Mineral., 51, 1247-1357.
Honea, R. M., 1964, Am. Mineral., 49, 325-338.
Kracek, F. C., et al. 1966, Am. Mineral., 51, 14-28.
Thompson, R. M., et al. 1951, Am. Mineral., 36, 458-470.
Rucklidge, J., 1967, Jour. Geol., 75, 217.
Sindeeva, N. D., 1964, Mineralogy and Types of Deposits of Selenium and Tellurium, Interscience Publishers, New York-London-Sidney, 363 pp.

QUANTITATIVE ANALYSIS WITH A NEWLY DESIGNED ELECTRON PROBE

F. W. Warnaars

Dissatisfaction with the light optics of most of the available electron probes has led to the construction of a new electron probe (Fig. 1). An important part of this instrument is a Leitz polarization microscope mounted outside the vacuum system and used with transmitted and reflected light. The axis of the electron optical system is mounted at 45^{o} to the specimen. A miniature electromagnetic lens, made at the Institute of Applied Physics (T.P.D.) in Delft (the Netherlands) under supervision of J. B. le Poole, is used as an objective lens. A small glass plate is mounted between the light optics and the specimen chamber without changing the optical view of the sample. The specimens in the vacuum can be translated and rotated independently and the axis of rotation at all times coincides with the light optical axis.

When the angle (γ) of the incident electron beam is decreased, the mean depth of direct x-ray production is reduced; a larger portion of the generated radiation reaches the surface. This requires a change of the factor χ in the Philibert formula. It has been suggested (Swindells, 1962; Macres, 1963) that χ becomes μ/ρ cosec θ sin γ. This adaptation has been criticized by Green (1964) and Bishop (1965). The latter proposed $(1-0.5 \cos^2\gamma)$ instead of sin γ.

These different approaches have been checked by the analyses of 35 different minerals which are of simple composition or had been analyzed by wet chemical methods and by a Norelco EPMA, which has an electron beam with an angle of incidence of 90^{o}. For the silicate minerals we obtained better results with sin γ than with $(1-0.5 \cos^2\gamma)$. These better results are only apparent when the values of $F(\chi)$ of the standard and the specimen differ notably, otherwise the difference is hardly worthwhile.

Because of the low take-off angle (15^{o}) x-ray absorption with the new probe is still considerable. As we generally use the same standards for all kinds of minerals the values of $F(\chi)$ can differ appreciably. The first step in the absorption correction is to assume a composition for the unknown mineral. The assumed composition is based upon the count ratios, but these can sometimes be so different from the final corrected values, that the assumed composition is often highly in error and a repetition of the correction procedure is necessary.

For a better determination of the assumed composition it is practical to estimate the $F(\chi)$ expected in the umknown mineral. Therefore, several

F (χ) vs. χ diagrams were made for the elements of different series of rock forming minerals. Variations in mineral composition of a series are indicated in the diagrams. Information about the composition of a sample is obtained by optical methods and from the host rock chemistry. The diagrams can be made only for those series of minerals in which there is one variable, for example: the olivines (Fig. 2), the orthopyroxenes (Fig. 3), the clinopyroxenes, the plagioclases (Fig. 4), the cummingtonites and the cordierites. With the pyroxenes an allowance is made for some alumina which is generally present. The diagrams can be applied only to a constant operating voltage and a fixed take-off angle.

H. E. Bishop, Proc. Phys. Soc., 85, 855-66, 1965.

V. G. Macres, Geometrical Considerations Involving Electron Beam, Unpublished manuscript, 1963.

N. Swindells, J. Inst. Metals, 90, 167-71, 1962.

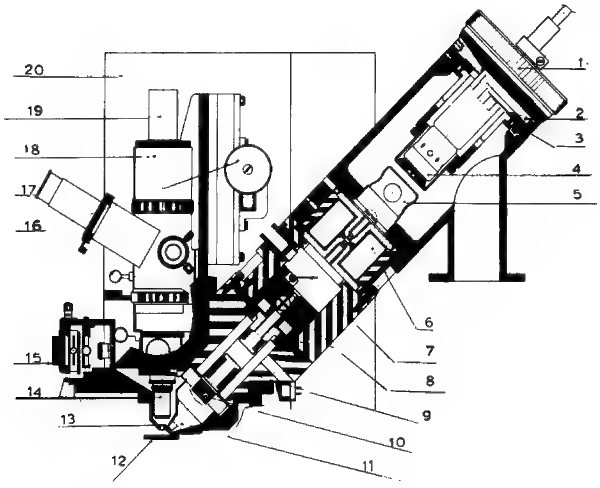

Fig. 1. T.P.D. Electron Probe X-ray Microanalyzer.

1. filament height control
2. filament centering
3. gun centering
4. electron gun
5. anode
6. condenser lens
7. intermediate screen
8. 3 aperature holder
9. scanning coils
10. stigmator
11. miniature lens
12. specimen
13. glass plate
14. objective lens
15. illumination
16. height control
17. binocular
18. Leitz microscope
19. camera tube
20. spectrometer (Norelco)

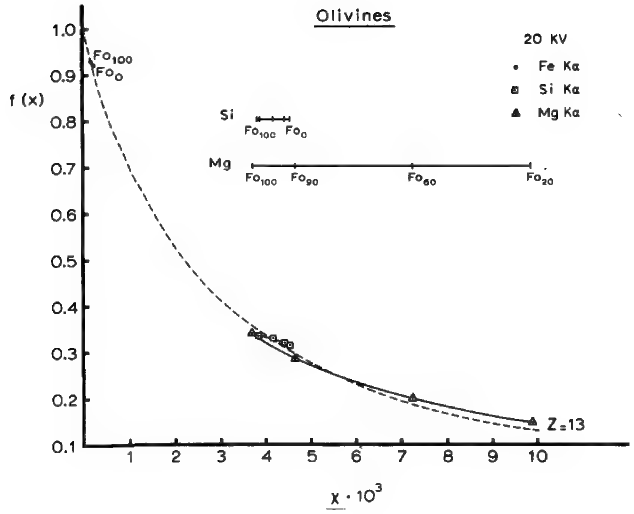

Fig. 2. F (χ) vs. χ diagram of the elements of olivines.

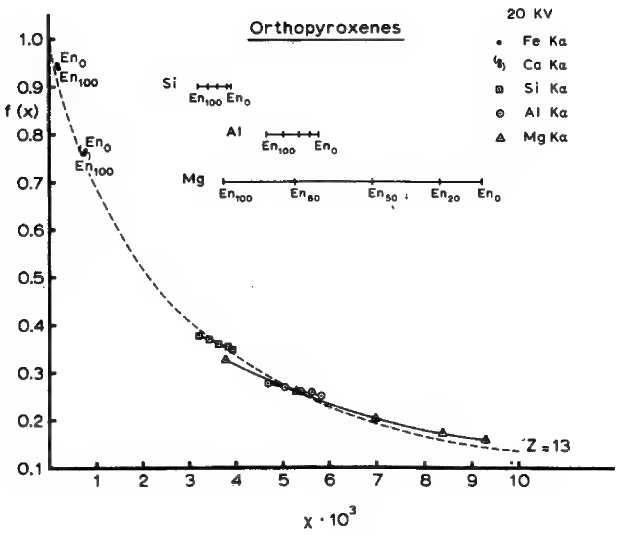

Fig. 3. F (χ) vs. χ diagram of the elements of orthopyroxenes.

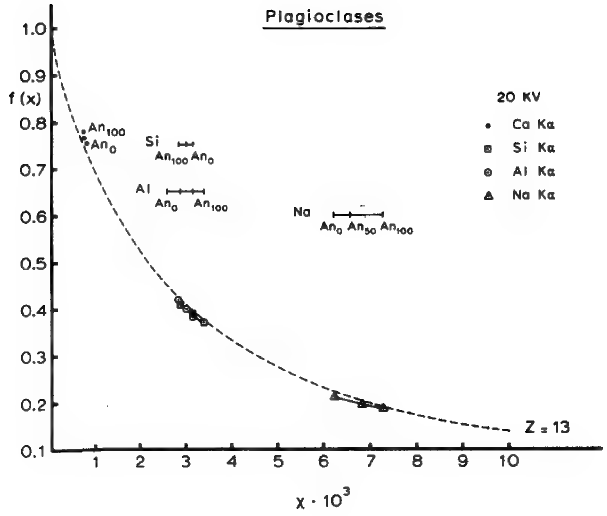

Fig. 4. F (χ) vs. χ diagrams of the elements of plagioclases.

REPORT ON THE ACTIVITIES OF THE NEW YORK METROPOLITAN PROBE USERS GROUP

H. Schreiber, Jr. and G. L. Fisher

The New York Metropolitan Probe Users Group, which was organized over three years ago, has shown continual membership growth. There are now over thirty active members representing private industry, government laboratories and the academic community. Five meetings were held last year to discuss recent developments in microprobe analysis and to present the results of our analyses of microprobe standards. The group was able to analyze two different microprobe standards this year: a set of four Fe-Ni alloys distributed round robin fashion and a GaAs-GaP standard.

The results of the Fe-Ni round robin plus previous results from the same alloys sent individually to each member were used to evaluate two well-known correction procedure computer programs. These two computer programs, J. D. Brown's(1) and J. W. Colby's(2), are used extensively by members of the group. The results of this evaluation are shown in Table I and Fig. 1. Table I shows the average corrected composition for each alloy obtained by correcting the same relative intensities using Brown's and Colby's programs. The chemical analysis of each alloy is also given.

Fig. 1 is a plot of the % deviation of the computer corrected compositions from the chemical composition vs. the percent nickel in the standard. Starting with the 5% Ni standard, where the correction is almost entirely for absorption, the deviations of the computer corrected values are <1%. Notice that the deviations of the values given by Colby's program are less than those given by Brown's. As one moves to higher nickel levels, this continues to be true. Brown's program overcorrects for the secondary fluorescence of Fe Kα by Ni Kα while simultaneously overcorrecting for Ni Kα absorption. Therefore, when using Brown's program, the Fe corrected compositions will be lower and the Ni corrected composition higher than the chemical composition. Values given by Colby's program lie within a deviation of about 1% of the chemical composition up to about 70% Ni. At this point an undercorrection for secondary fluorescence of Fe Kα by Ni Kα causes an increase in the % deviation of the iron values.

Results of the analysis of the GaAs-GaP standard will also be presented. Some difficulties were experienced with this standard because of an interaction between it and the electron beam.

---

1. J. D. Brown, Anal. Chem., Vol. 38, No. 7, pp. 890-894.

2. J. W. Colby, Advances in X-ray Analysis, Vol. 11, 1967, to be published.

TABLE I

Average Corrected Compositions of Microprobe Standards

Computer Program	Average Composition - Weight %							
	Std #1		Std #2		Std #3		Std #4	
	Ni	Fe	Ni	Fe	Ni	Fe	Ni	Fe
Brown's	89.40	10.15	64.12	36.23	57.67	42.48	5.15	94.02
Colby's	89.85	11.04	63.50	37.69	57.16	43.80	5.08	94.30
Chemical Analysis	89.94	10.60	62.8	37.0	56.4	43.7	5.10	94.90

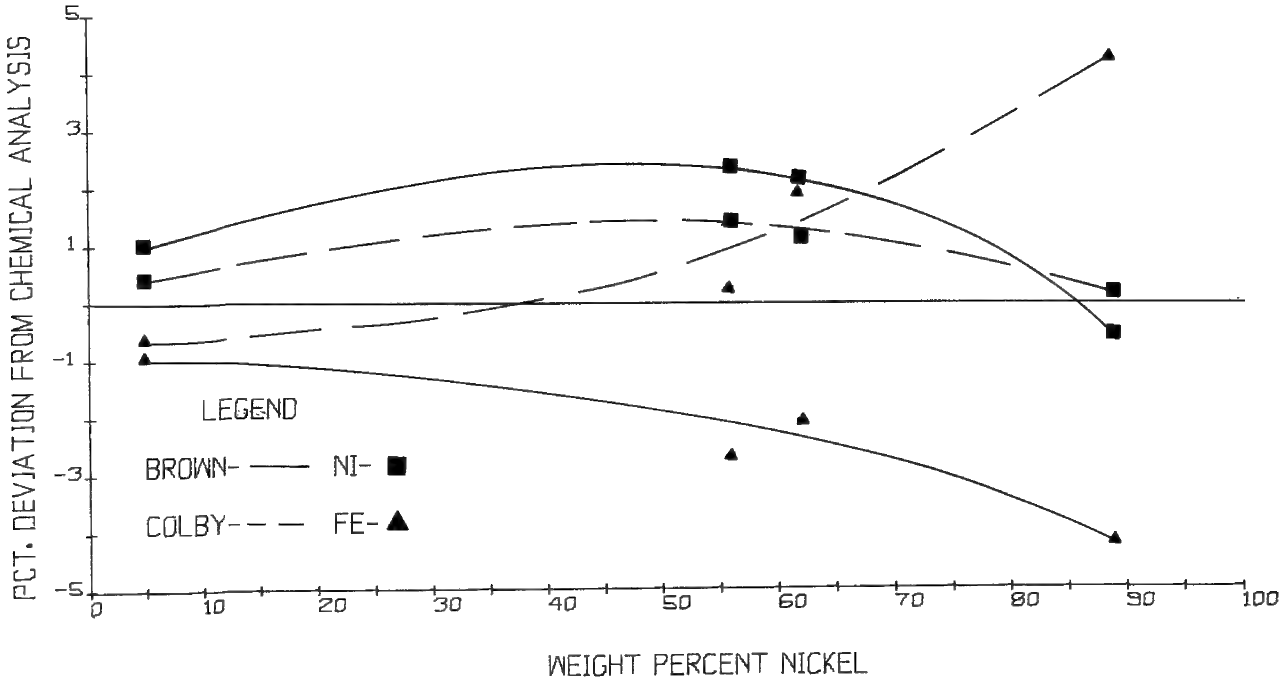

Fig. 1. Evaluation of two correction procedure computer programs.

REPORT ON THE ACTIVITIES OF THE MIDWEST ELECTRON PROBE USERS GROUP

D. R. Beaman and T. P. Schreiber

During the past year the members of the Midwest Electron Probe Users Group have performed quantitative analysis on the following materials of known composition: Ti-Nb, Fe-C, Cr-Co-Mo and polyvinyl chloride (PVC).

The Nb-35 wt% Ti alloy is a particularly interesting one in which to apply quantitative corrections because the Ti is subject to absorption and atomic number effects while the Nb is subject to atomic number effects in the presence of a small absorption correction. Fig. 1 is a plot of the experimental Nb x-ray intensity ratio (k) vs. the take-off angle. The experimental precision ($\pm 1\sigma$) in k is indicated; the number adjacent to the experimental points indicate the number of instruments used in determining the mean k value; the solid lines are curves calculated using the indicated techniques. All of these curves include a negligible (<0.12% Nb) fluorescence contribution, due to the fluorescence of NbLα by TiKα, which was calculated using the Reed technique. A good fit to the experimental data is provided by the following techniques: the Duncumb and Reed(1) atomic number correction used in conjunction with the Philibert(2), Duncumb and Shields(3), or Andersen and Wittry(4) absorption corrections; the Ziebold(5) atomic number tables used with the Duncumb and Shields(3) absorption correction. The best fit to the Ti data was provided by the same techniques that excelled for Nb. Heinrich's(6) mass absorption coefficients were used in the computations.

An Fe-0.62 wt% C sample was manufactured, mounted with standards, polished, coated and checked for homogeneity by one laboratory. The sample was then circulated and examined on eight 52.5° and three 18° take-off angle instruments at 10 kV. The C$k\alpha$ x-ray probe intensity ratios obtained using diamond as the standard were 0.41± 0.11 wt% C on the former and 0.14 wt% C on the latter. All operators took precautions to minimize C contamination (moved sample, extrapolated C intensity to zero time, used cold plates or molecular sieves). These ratios were corrected for absorption and atomic number effects using a variety of correction procedures and mass absorption coefficients. The .41% corrected to .49% and .93% C for $(\mu/\rho)_{Fe}^{Ck\alpha}$ values of 11,000 and 25,000 respectively when using the modified Tong(7) correction procedure.

Table I is a very condensed summary of the quantitative work done by the Group. The data presented therein is for instruments with 52.5° take-off angles only since the largest amount of data has been collected on such instruments. Similar data for other take-off angles will be presented. The precision in the measured probe ratios (σ_k/k) generally lies between ±1 and ±3% and the relative error in the corrected concentration between 0 and 3%. Samples and complete experimental results are available to other user groups wishing them.

The Group has attempted to establish a scheme for measuring homogeneity. Twenty intensity measurements are made on one spot on the alloy with optical refocusing between each measurement. Then one intensity measurement is made in each of twenty random locations, again with optical refocusing. Probe x-ray intensity ratios are calculated for each of the measured intensities using the pure element standard. The variance for each set of twenty probe ratios is determined; S_1^2 is the variance for the fixed position measurements and S_{20}^2 is the variance for the random position measurements. A statistical F test is applied and if $S_{20}^2/1^2 > 2.12$ the sample is assumed to be inhomogeneous and the variance due to inhomogeneity, S_h, is given $S_h^2 = S_{20}^2 - S_1^2$. If $S_{20}^2/S_1^2 < 2.12$ and $\sigma_k/\bar{k} < 1.5\%$ the homogeneity is assumed to be sufficiently good to warrant group investigation. This criterion is arbitrary because there is a high probability that the variances are unequal even though $S_{20}^2/S_1^2 < 2.12$. Thus some samples where minor inhomogeneity exists will be accepted as homogeneous.

Deadtime measurements have been made using a variety of techniques on twenty instruments. Most investigators have used the Heinrich et al.(8) technique; found τ to be between 1.5 and 3 μseconds; failed to detect any intensity or energy dependence; and used sealed detectors. Four investigators have used the Short(9) technique; detected intensity sensitivity; and found the dead-time to be zero below intensity levels which varied from 4,000 to 14,000 cps.

---

1. P. Duncumb and S. J. B. Reed, Tube Investments Research Laboratory Technical Report No. 221, 1967.
2. J. Philibert, in X-ray Optics and X-ray Microanalysis, H. Pattee, V. Cosslett and A. Engstrom,eds., Academic Press, New York and London, 1963, p. 379.
3. P. Duncumb and P. K. Shields, in The Electron Microprobe, T. D. McKinley, K. F. J. Heinrich and D. B. Wittry, eds., John Wiley and Sons, New York, 1966, p. 284.
4. C. A. Andersen and D. B. Wittry, to be published in Brit. J. Appl. Phys.
5. T. O. Ziebold, in The Electron Microanalyzer and its Applications, Lecture notes for summer program at the Massachusetts Institute of Technology, Suppl., 1966.
6. K. F. J. Heinrich, in The Electron Microprobe, T. D. McKinley, K. F. J. Heinrich and D. B. Wittry, eds., John Wiley and Sons, New York, 1966, p.296.
7. J. Ruberol, M. Tong and C. Conty, paper presented at the Groupement pour l'Advancement des Methodes Spectroscopiques (G.A.M.S.) Conference in Paris, France, June 8, 1966.
8. K. F. J. Heinrich, D. Vieth and H. Yakowitz, Advances in X-ray Analysis, Vol. 9, Plenum Press, New York, 1965, p. 208.
9. M. A. Short, Rev. Sci. Inst., 31, 618, 1960.

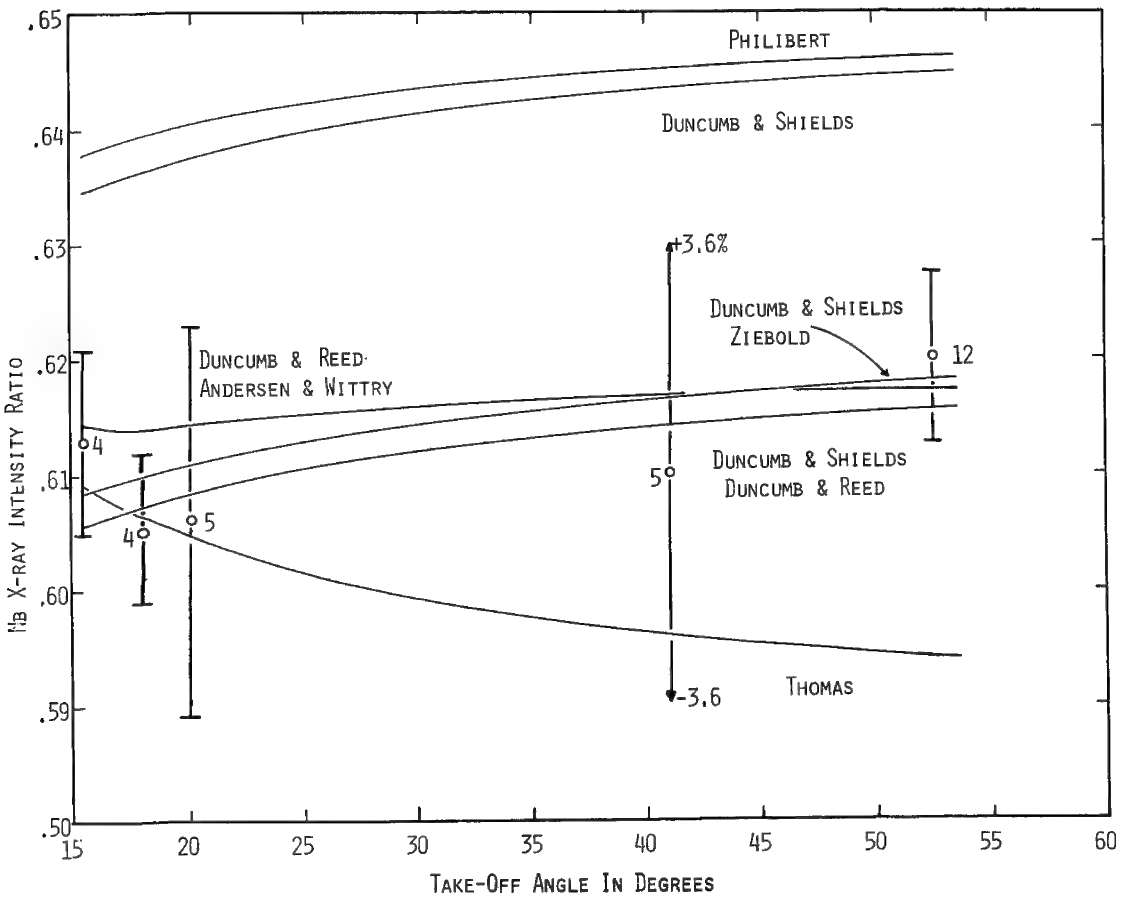

ALLOY	Fe-Ni		Cu-Zn		Ti-Nb		Cr-Co-Mo			Fe-C
ANALYZED ELEMENT	Fe	Ni	Cu	Zn	Ti	Nb	Cr	Co	Mo	C
X-RAY LINE	Kα	Kα	Kα	Kα	Kα	Lα	Kα	Kα	Lα	Kα
kV	25	25	25	25	20	20	20	20	20	10
No. OF INSTRUMENTS	12	12	10	10	11	11	7	7	7	7
$\bar{K}$	49.4	52.5	73.8	27.2	32.6	62.0	11.7	79.9	7.7	0.41
$\pm\sigma_K$	1.3	1.4	0.7	0.5	1.0	0.7	0.3	0.6	0.5	0.11
$\sigma_K/\bar{K}$	2.6	2.7	0.9	1.8	3.1	1.1	2.6	0.8	6.5	27
CHEMICAL CONCENTRATION...C_T	43.6	56.6	72.9	27.1	35.0	65.0	9.9	80.6	9.4	0.62
CALCULATED CONCENTRATION...C_{CALC}	44.7	56.7	72.0	27.1	35.3	65.5	9.9	81.0	9.9	0.49
$(K-C_T)/C_T$	13	-7	1	0	-7	-5	18	-1	-18	-34
$(C_{CALC}-C_T)/C_T$	2.6	0.3	-1.2	0	0.9	0.8	0	0.5	5.3	-21

*THE LAST SEVEN ROWS ARE PERCENTAGES.

Table 1. Analytical results obtained on 52.5° probes. The last seven rows are percentages.

INDEX OF AUTHORS

AND

THEIR AFFILIATIONS

INDEX OF AUTHORS AND THEIR AFFILIATIONS

INDEX OF AUTHORS AND THEIR AFFILIATIONS

INDEX OF AUTHORS AND THEIR AFFILIATIONS

INDEX OF AUTHORS AND THEIR AFFILIATIONS

INDEX OF AUTHORS AND THEIR AFFILIATIONS

INDEX OF AUTHORS AND THEIR AFFILIATIONS